University of the Basque Country

PhD Thesis - 2016

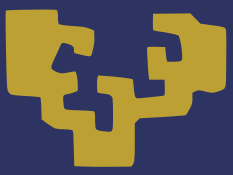

LOWER BOUNDS ON QUANTUM METROLOGICAL PRECISION

Author:
Iagoba Apellaniz

Director:
Géza Tóth

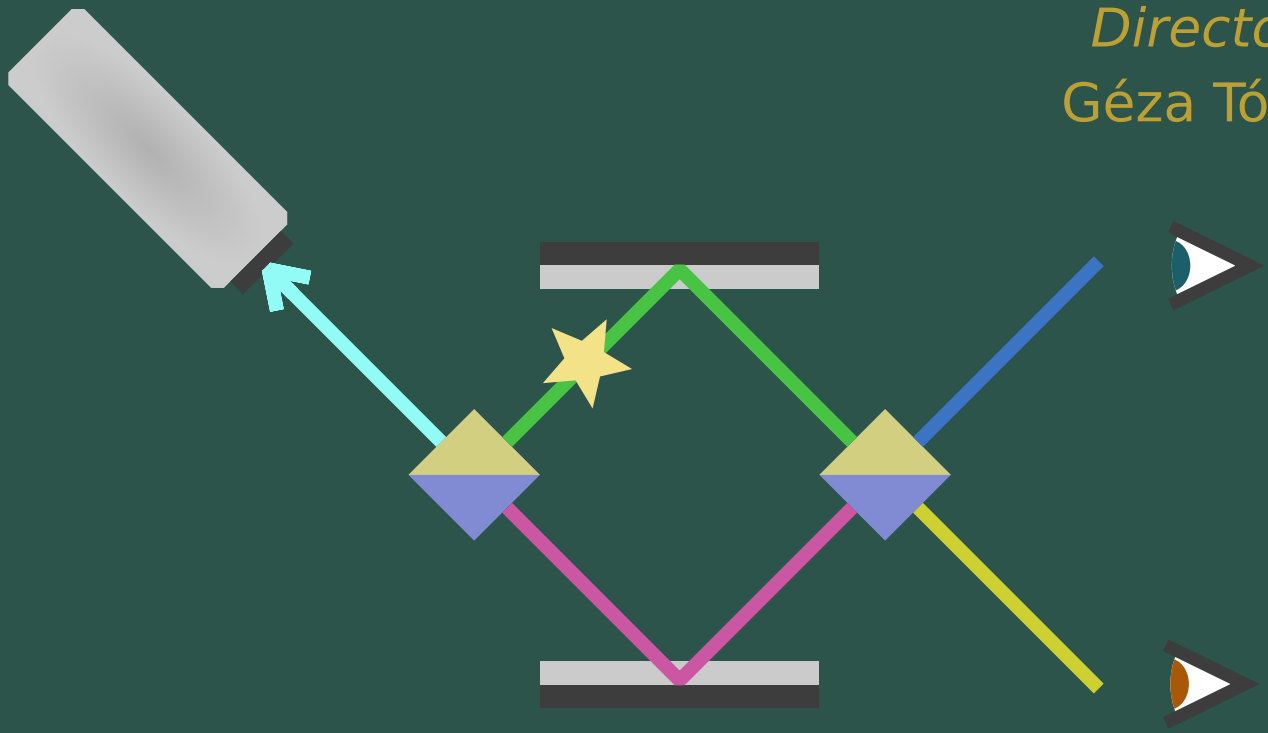

This document was generated with the 2015 distribution of LaTeX.

Prologue

This work is part of the doctoral project on quantum information which I started on the sumer of 2013. This work collects part of the research I have done on these previous years. I will try to be clear throughout all the thesis such that make it readable for a wider audience as it is possible. This way I hope it will be readable by any person with a bachelor in science, particularly in physics or at least with a partial knowledge in quantum mechanics. With that in mind the first and the second chapters will be used to introduce the reader into the context on which this thesis was written as well as the basic notions of quantum metrology, the enveloping field of the present work. Even though I write this thesis for a broad audience in mind, a basic notion on quantum physics and statistics is needed to follow it properly as I said before. For instance, I will assume among other things that the reader knows what probability is and which are its properties, or what a quantum state is and what it represents. I will give references where to find such complementary material when I think is necessary.

This research I publish in a thesis form is part of the work done within the Research Group in qantum information in which Prof. Géza Tóth is the group leader and principal investigator. I have to mentions the rest of the members of the group Dr. Philipp Hyllus, Dr. Giuseppe Vitagliano, Dr. Iñigo Urizar-Lanz, Dr. Zoltán Zinborás and Dr. Matthias Kleinmann at the time I was working on the projects of this thesis. Some of them may still be part of the group and some not. Apart from the group of Géza Tóth based in Bilbao, Spain, this thesis also collects some work done in collaboration with the Theoretical Quantum Optics, TQO, group lead by Prof. Otfried Gühne at the University of Siegen, Germany, and the group of Prof. Carsten Klempt at the Leibniz University in Hannover,

based also in Germany. The last one is an experimental group specialized on the creation of exotic quantum states with very many particles with a variety of applications in quantum technology.

First, we investigate the metrological usefulness of a family of states known as the unpolarized Dicke states, which have boosted the sensitivity of magnetometry when lots of particles are used in the sense that quantum enhancements play a very important role to achieve such a precision. Second, we investigate possible lower bounds on the quantum Fisher information, a quantity that characterizes the usefulness of a state for quantum metrology, using the theory of Legendre transforms such that we obtain thight lower bounds based on few measurements of the initial quantum state that will be used for metrology. And last but not least, we investigate the gradient magnetometry, i.e., we develop a theory to study the capablilities of some states to sense the change in space of the magnetic field and we apply that theory to some known states.

Before the thesis work the reader can find the present prologue, the list of publications, the table of contents, and a list of abbreviations, figures and tables. Then, the thesis starts. On the first pages one can find a brief dedicatory and acknowledgments followed by the chapters. The content of the chapters is organized as follows. First, I start with an introduction to describe the current situation of quantum information especially quantum metrology and I write about the basics of quantum metrology and how it emerges from statics and quantum mechanics. Second, I present the reader our works in characterizing the family of states known as the unpolarized Dicke states, in optimizing the lower bound for the quantum Fisher information when some expectation values of the states are known and our work in gradient quantum metrology.

Iagoba Apellaniz

Bilbao, January 9, 2017

Publications

Géza Tóth and Iagoba Apellaniz. *Quantum metrology from a quantum information science prespective.* Journal of Physics A: Mathematical and Theoretical, **47** 424006, 2014.

Iagoba Apellaniz, Bernd Lücke, Jan Peise, Carsten Klempt and Géza Tóth. *Detecting metrologically useful entanglement in the vicinity of Dicke states.* New Journal of Physics, **17** 083027, 2015.

Preprints

Iagoba Apellaniz, Matthias Kleinmann, Otfried Gühne and Géza Tóth. *Optimal detection of metrologically useful entanglement.* arXiv:1511.05203.

Out of the scope of this thesis

Giuseppe Vitagliano, Iagoba Apellaniz, Iñigo Luis Egusquiza and Géza Tóth. *Spin squeezing and entanglement for arbitrary spin.* Physical Review A, **89** 032307, 2014.

Giuseppe Vitagliano, Iagoba Apellaniz, Matthias Kleinmann, Bernd Lücke, Carsten Klempt and Géza Tóth. *Entanglement and extreme spin squeezing of unpolarized states* arXiv:1605.07202.

Contents

Abbreviations, figures and tables

Abbreviations

BEC	–	Bose-Einstein condensate
FI	–	Fisher information
GHZ	–	Greenberger-Horne-Zeilinger
HS	–	Heisenberg scaling
HL	–	Heisenberg limit
PDF	–	Pobability distribution function
PI	–	Permutationally invariant
POVM	–	Positive-operator valued measure
QFI	–	Quantum Fisher information
SNS	–	Shot-noise scaling
SNL	–	Shot-noise limit

Figures

Tables

University of the Basque Country

PhD Thesis

Lower bounds on quantum metrological precision

Author:
M. Sc. Iagoba Apellaniz

Director:
Prof. Géza Tóth

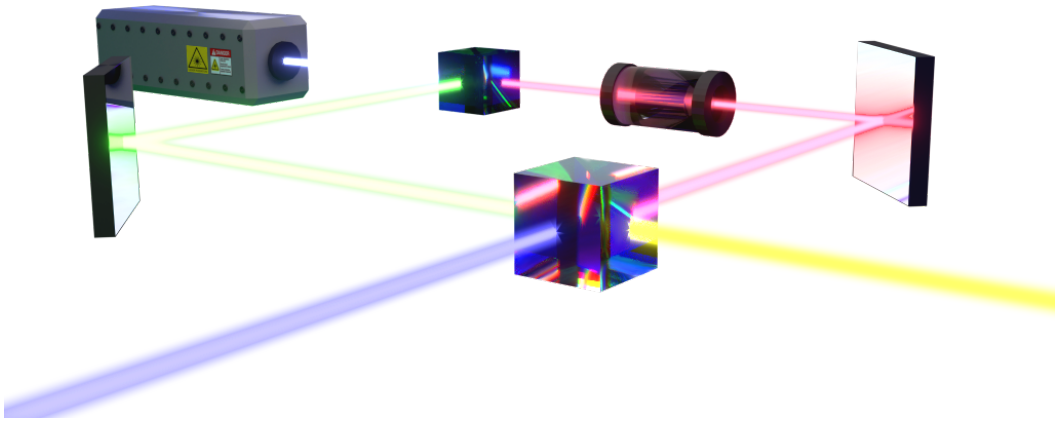

January 9, 2017

To my parents, my family

and to all the people

I have had around those years.

Acknowledgments

I want to thank the people that has supported me in this endeavor. Especially, I want to acknowledge my office and discussion mates, Giuseppe Vitagliano and Iñigo Urizar-Lanz as well as Phillip Hyllus, Matthias Kleinmann and Zoltán Zimborás. A special thank to my director Géza Tóth for all the offered support, without whom my work at hand would not be possible. I also want to thank more people from the department I belong to at the University of the Basque Country, the Department of Theoretical Physics and the History of Science. I appreciate the effort done by people like Iñigo L. Egusquiza in promoting the Ph.D. program of the Department of Theoretical Physics, which has successfully promote plenty of researchers now immersed in wonderful and leading edge research projects world wide. Also I want to acknowledge the Ph.D. students from different departments for the friendship atmosphere one can enjoy working there at this *our* university.

I have been visiting several research groups during those years and I don't forget them, they have accept me as one more between them. So I want to thank a very especial research group for me, the Theoretical Quantum Optics group at the University of Siegen. I would really like to mention the names of all of them but I think it would be quite heavy for the average reader of this thesis. Thank you guys! Also I want to thank people from the group QSTAR at Florence, Italy.

On the other hand I also felt very comfortable at my university, the University of the Basque Country, but I want to thank especially the people that make me grow in all ways as person.

1 Introduction

Metrology plays an important role in many areas of physics and engineering [1]. With the development of experimental techniques, it is now possible to realize metrological tasks in physical systems that cannot be described well by classical physics instead quantum mechanics must be used for their modeling. Quantum metrology [2–5] is the novel field that is concerned with metrology using such quantum mechanical systems.

In quantum metrology, the quantumness of the system plays an essential role [6, 7]. Quantum metrology can find bounds on the highest achievable precision of a metrological setup in which the theory of quantum Fisher information (QFI) has played a crucial role [8–11]. There have been efforts recently connecting quantum metrology to quantum information science, in particular, to the theory of entanglement [12]. Entanglement which is a feature of quantum mechanics that lies in the heart of many problems has attracted an increasing attention in recent years.

There are now efficient methods to detect entanglement with a moderate experimental effort [13, 14]. However, in spite of intensive research, many of the intriguing properties of entanglement are not fully understood. One of such puzzling facts is that, while entanglement is a sought after resource, not all entangled states are useful for some particular quantum information processing task. For instance, it has been realized recently that entanglement is needed in very general metrological tasks to achieve high precision [15]. Remarkably, this is true even in the case of millions of particles,

which is especially important for characterizing the entanglement properties of cold atomic ensembles [16–21]. However, there are highly entangled pure states that are useless for metrology [22].

In the light of these results, beside verifying that a quantum state is entangled, we should also show that it is useful for metrology. One of the basic tasks of quantum metrology is magnetometry with an ensemble of spin-j particles. Magnetometry with a state completely polarized works as follows. The total spin of the ensemble is rotated by a homogeneous magnetic field perpendicular to it. We would like to estimate the rotation angle or phase θ based on some measurement. Then, the phase can be used to determine the strength of the magnetic field. See Figure 1.1.a.

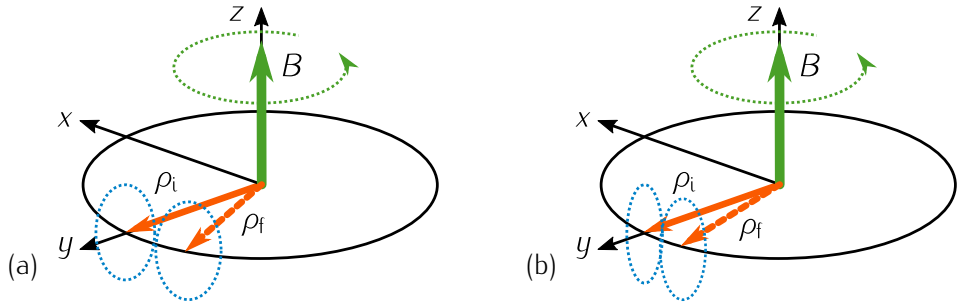

Figure 1.1: (a) The initial state ρ_i is pointing in the y-direction. (blue-dashed-circle) They denote the uncertainty ellipse of the polarization perpendicular to the main spin. The state is rotated according to the strength of the magnetic field B. Hence, the magnetic field can be estimated from the final state ρ_f. (b) When the uncertainty ellipse is reduced in one direction perpendicular to the polarization, the state is called a spin-squeezed state. If the direction in which the uncertainty is reduced coincides with the direction of the rotation, then it is easier to distinguish the final state from the initial state. Which turns into a better precision for the estimation of the magnetic field.

In recent years, quantum metrology has been applied in many scenarios, from atomic clocks [16, 23, 24] and precision magnetometry [25–31] to gravitational wave detectors [32–34]. There have been many experiments with fully polarized ensembles [5, 25, 27, 29, 30, 35, 36], in which the collective spin of the particles is rotated as in Figure 1.1.a and the angle of rotation is estimated by collective measurements. It has also been verified experimentally that spin squeezing can result in a better precision compared to fully polarized states [5, 18, 25, 36–41] since the spin-squeezed states are characterized by a reduced uncertainty in a direction orthogonal to the mean spin [42–45], see Figure 1.1.b.

Besides almost fully polarized states, there are also unpolarized states considered for quantum metrology. Prime examples of such states are Greenberger-Horne-Zelinger (GHZ) states [46], which have already been realized experimentally many times [47–54]. Recently, new types of unpolarized states have been considered for metrology, such as the singlet state [55, 56] and the symmetric unpolarized Dicke states realized in cold gases [20, 57, 58].

In the present thesis we study how large precision can be achieved for realistic noisy systems [59, 60]. We also study how such states can be characterized with few measurements which reduce the experimental efforts considerably. And finally, we discuss the multi-parameter estimation problem. It turns out that some previously not useful states for homogeneous magnetometry may become useful when we use them for differential magnetometry, which is one of the most fundamental two-parameter estimation tasks.

2 Background in quantum metrology

"In the real world, doing real experiments, statistics began to matter"
Roger J. Barlow

In this chapter, we will study the basics of quantum metrology, which stands for the study of metrology enhanced by quantum phenomena. First of all, metrology, as the science of measuring, has played an essential role in the development of science and technology. Metrology studies several aspects of the estimation process, for example, which strategy to follow in order to improve the precision of the estimation. Metrology also covers all intermediate processes, from the design aspects of a precise measuring device, to the most basic mathematical concepts that arise from the formulation of the different problems, which lead at the end to a more complete picture of what metrology is.

Historically, with the discovery of quantum theory and the subsequent development of quantum mechanics, new opportunities emerged for advances in metrology in the early decades of the twentieth century. Later in the last decades of the twentieth century, together with the arrival of concepts like *qubit* and *quantum cryptography*, quantum theory embraced the so-called quantum information theory, which merges the notions of theory of information and computer science with quantum mechanics. Pushed by the developments of quantum technologies, quantum information attracted much attention from the scientific community. Moreover, those emerging fields rapidly became into very interesting interdisciplinary playgrounds of science with many scientists as well as resources involved.

At this point, we want to mention that the role of entanglement, an exclusive feature of quantum

mechanics which cannot be described using classical probabilistic theories, is essential in this context. Said this, entanglement is also at the center of the theory of quantum metrology. Throughout the thesis we will focus mainly on the achievable precision for different systems and schemes.

On the other hand, another very important field of science must be mentioned. We are talking about statistics, without which many descriptions of the actual and past physical findings would lack the rigorous interpretation needed. It basically helps to analyze raw data to make it readable from the human perspective.

This chapter is organized as follows. In Section 2.1, we introduce the basic concepts of statistics and estimation theory at the same time we go deeper in the concepts invoked in this thesis. In Section 2.2, we present the necessary tools of quantum mechanics used throughout the text. Finally in Section 2.3, we arrive at the main set of tools used in the quantum metrology framework and by extension in the present work.

2.1 Background in statistics and theory of estimation

In this section, we will enumerate the basic concepts of statistics as well as the estimation process. As we said, the main mathematical tools used by metrology belong to statistics. Moreover, we are especially interested in estimation theory which shows how to properly estimate some quantity based on some data sample. The data can be from a set of different heights of a, let us say, basketball team, to the outcomes of a coin toss, or even the wavelength of photons coming out of some radioactive sample. The aim of this section is to give the reader sufficient material to follow this thesis and make it comprehensible since the beginning*.

2.1.1 Probability, data samples, average and variance

The probability indicates the relative chance of an event to happen. For instance, if there is a box with ten red balls and five blue balls, considering that the balls of the same color are indistinguishable and that we extract one randomly, we have $\frac{5}{10+5} = \frac{1}{3}$ of probability to obtain a blue ball and $\frac{2}{3}$ to obtain a red ball. The reader may notice many properties a probability should have, such as that the probability of any event to happen is always given by a number in between zero and one.

When someone has a data sample at hand, it might come from diverse sources and might be represented using multiple forms such as numbers or words (for instance, a table of names of people). The first thing one tries to accomplish is to analyze the data to extract the relevant properties from

* For a more detailed material, see Refs. [61, 62]

it. A data sample always come from a population sample, i.e., the data sample might not be complete (one could lose some in the process, or the population might be huge in comparison with what one can handle), or might carry some error (a measuring device always has an error when estimating a continuous magnitude, e.g., the height of people), or both at the same time. Hence, the data sample comes attached with a probability for each data element. In the subsequent paragraphs, we will describe these relations between the data samples and probabilities and we will enumerate the most useful properties and formulas.

First of all, we will explain our notation which follows mainly the one used in Ref. [61]. A probability function gives the probability of an event x to happen when measuring some random variable X, and it is denoted by $\Pr(X = x)$. Second, due to the random nature of the measurements, the N elements of a data sample are considered outputs of N different random variables with their corresponding N values $\{X_i = x_i\}_{i=1}^{N}$, or $\boldsymbol{X} = \boldsymbol{x}$ for short. The joint probability of those random variables is in general not separable. This is due to the fact that the data sample elements could depend on the rest of outcomes or some other more complex relation that makes the most general case to be not separable from the probabilistic point of view. Therefore we define the probability distribution function (PDF) as an N variable function

$$\Pr(\boldsymbol{X} = \boldsymbol{x}) \equiv \Pr(X_1 = x_1, X_2 = x_2, \ldots, X_N = x_N). \tag{2.1}$$

In the case of separable probabilities, this is written as

$$\Pr(\boldsymbol{X} = \boldsymbol{x}) = \prod_{i=1}^{N} \Pr(X_i = x_i) \tag{2.2}$$

which is the case in many relevant situations.

When some indirect property of the system is defined as a function that depends on the measured random variables, the result is also a new random variable with another assigned PDF. For example, we measure the position of a body at some moment. If the system was at rest at the origin when $t = 0$ and assuming that the acceleration is constant, then from the measured final position one could infer the value of the acceleration by using $A = 2X/t^2$, where X denotes the final position at instant t and A the acceleration. If X is a random variable, which is the general case when measuring the position of some physical system, then the probability assigned for A is computed by

$$\Pr(A = a) = \left.\frac{\mathrm{d}X}{\mathrm{d}A}\right|_{A=a} \Pr(X = x) = \frac{2}{t^2}\Pr(X = x). \tag{2.3}$$

In general, for the multiple random variable, we must require the following identity

$$|\Pr(\boldsymbol{X} = \boldsymbol{x})\, \mathrm{d}x_1 \mathrm{d}x_2 \ldots \mathrm{d}x_N| = |\Pr(\boldsymbol{Y} = \boldsymbol{y})\, \mathrm{d}y_1 \mathrm{d}y_2 \ldots \mathrm{d}y_N|, \tag{2.4}$$

for any set of random variables. This leads to some interesting formulas we will discuss later.

We now stick to the simplest case in which the data is a collection of values of the same random variable describing the same physical one-dimensional data population. Moreover, if the probabilities are independent from each other, the PDF takes the form of Eq. (2.2). Some definitions reasonable to mention in this thesis arise for those kind of data samples: the average, variance, moments and central moments. The arithmetic average (there are other types of average one can find in the textbooks) is computed by

$$\overline{x} = \frac{1}{N} \sum x_i. \tag{2.5}$$

The variance is related to the spread of the data and computed by

$$\sigma^2 = \frac{1}{N} \sum (x_i - \overline{x})^2, \tag{2.6}$$

where σ is the standard deviation. Different moments are computed by $\overline{x^r} = \frac{1}{N} \sum x_i^r$ while central moments, i.e., statistical moments that are invariant under the translation of the system, are of the form of $c_r = \frac{1}{N} \sum (x_i - \overline{x})^r$. Note that the variance is the second central moment of the data samples. For completeness, when each element of the data consists of more than a single number, e.g., (x_i, y_i) where x_i could be the velocity and y_i the acceleration in a experiment to estimate the friction caused by a fluid, the co-variance between two data kinds is obtained by

$$V_{X,Y} = \frac{1}{N} \sum_{i=1}^{N} (x_i - \overline{x})(y_i - \overline{y}). \tag{2.7}$$

Note that we grouped the elements of the data sample into pairs while kept distinctions between both kinds X and Y.

We will try to keep this distinction between data sample and data population as clear as possible. The data population is represented in most cases by the probability distribution function. In general, the mean values of any function $g(x)$ over the data sample are denoted with a bar over a lowercase variable, e.g., $\overline{x^r}$ for the r-th moment over the data sample or $\overline{g(x)}$ for the average of $g(x)$ itself. On the other hand, the mean values of any function applied to the data population $g(X)$ is denoted following some textbooks by $\mathrm{E}[g(X)]$, e.g., the r-th moment over the data population is $\mathrm{E}[X^r]$. One clearly may distinguish two cases when we talk about data populations. While the data sample is always consist

of discrete data elements, the data population can be represented by a PDF for discrete values or it can be represented by a PDF for values that can take any real number. For completeness, here are expressed the two definitions for the mean value over the data population, i.e., represented by a PDF, of a function $g(\boldsymbol{X})$ by

$$\mathrm{E}[g(\boldsymbol{X})] = \begin{cases} \displaystyle\int g(\boldsymbol{x})\mathrm{Pr}(\boldsymbol{X}=\boldsymbol{x})\,\mathrm{d}^N\boldsymbol{x}, \\ \displaystyle\sum_{i,j,\ldots} g(\boldsymbol{x})\mathrm{Pr}(\boldsymbol{X}=\boldsymbol{x}). \end{cases} \tag{2.8}$$

At this point, one more straight forward definition needs our attention, the variance of a function $g(X)$ over the data population is denoted by $\mathrm{V}[g(X)] \equiv \mathrm{E}[g(X)^2] - \mathrm{E}[g(X)]^2$.

2.1.2 Frecuentist vs. bayesian approach

2.1.3 Estimators and Fisher information

Let us suppose that the data sample has encoded some desired parameters $\boldsymbol{a} \equiv (a_1, a_2, \ldots)$. The underlying probability, in general also unknown, may be conditioned by the real values of the parameters $\boldsymbol{a}$. The probability of the data sample is therefore written as

$$\mathrm{Pr}(\boldsymbol{X}=\boldsymbol{x}|\boldsymbol{a}), \tag{2.9}$$

where "$|\boldsymbol{a}$" indicates its dependency on these parameters. At this point, note that an estimate of one of the desired parameters must be based on the data sample elements. A function of this type is called the *estimator* and it is connected with the PDF of the data population. Hence as mentioned before, an estimator of a, one of the unknown parameters, is denoted by $\hat{a}$ and the PDF associated to it is computed from the PDF of the data population as

$$\mathrm{Pr}(\hat{a}|\boldsymbol{a})\,\mathrm{d}\hat{a} = \mathrm{Pr}(\boldsymbol{x}|\boldsymbol{a})\,\mathrm{d}x_1\mathrm{d}x_2\ldots\mathrm{d}x_N. \tag{2.10}$$

For short, we have omitted writing "$\boldsymbol{X}=$", thus the conditional joint probability of N random variables $\boldsymbol{X}$ is written simply as $\mathrm{Pr}(\boldsymbol{x}|\boldsymbol{a})$.

As we said, an estimator is defined to be a function of the data sample. For example, one of such estimators is the estimator of the mean value of the population, in general unknown. The mean value of the data population, which in general we do not have access to, is denoted usually by μ. Note that μ is in general different from the mean value of the data sample $\overline{x}$. A valid estimator for the mean value μ would be the mean itself of the data sample, i.e., $\hat{\mu} = \overline{x}$.

An important notion of an estimator is its *efficiency*. The smaller the variance of the estimator the more efficient it is. Remember than an estimator is considered a random variable so it must have a variance when our knowledge about the population is incomplete, i.e., when we estimate it from the data sample.

Focusing into what it is more interesting for of this thesis, an estimator of any kind has a theoretical lower bound for its variance. For the proof of the previous statement, which we will compute for continuous random variables without losing of generality, we start with the normalization formula of a given PDF

$$\int \Pr(\boldsymbol{x}|\boldsymbol{a})\, \mathrm{d}^N\boldsymbol{x} = 1. \tag{2.11}$$

Next, we compute the partial derivative over a, one of any of the unknown parameters, such that

$$\int \partial_a \Pr(\boldsymbol{x}|\boldsymbol{a})\, \mathrm{d}^N\boldsymbol{x} = \int \partial_a \big(\ln \Pr(\boldsymbol{x}|\boldsymbol{a})\big) \Pr(\boldsymbol{x}|\boldsymbol{a})\, \mathrm{d}^N\boldsymbol{x} = 0, \tag{2.12}$$

where for the second equality we used the identity for logarithmic derivatives. From Eq. (2.8), it turns out that the Eq. (2.12) is the expectation value of $\partial_a(\ln \Pr)$. Finally, if we have an *unbiased* estimator, i.e., an estimator for which the expectation value $\mathrm{E}[\hat{a}]$ coincides with true value a of the unknown parameter, the partial differentiation of $\mathrm{E}[\hat{a}]$ over a must be equal to one. Therefore, we apply similar identities as in Eq. (2.12) to arrive at

$$\begin{aligned} \partial_a \mathrm{E}[\hat{a}] = \partial_a a &= \partial_a \int \hat{a} \Pr(\boldsymbol{x}|\boldsymbol{a})\, \mathrm{d}^N\boldsymbol{x} \\ &= \int \hat{a}\, \partial_a \Pr(\boldsymbol{x}|\boldsymbol{a})\, \mathrm{d}^N\boldsymbol{x} = \int \hat{a}\, \partial_a \big(\ln \Pr(\boldsymbol{x}|\boldsymbol{a})\big) \Pr(\boldsymbol{x}|\boldsymbol{a})\, \mathrm{d}^N\boldsymbol{x} = 1, \end{aligned} \tag{2.13}$$

where we have used the definition of the expectation value for continuous variables Eq. (2.8) and we use the fact that the estimator is not a function of the parameter a.

At this point, we invoke the Schwartz inequality for two real multidimensional functions $g(\boldsymbol{x})$ and $h(\boldsymbol{x})$ such that $(\int gh\, \mathrm{d}^N\boldsymbol{x})^2 \leqslant (\int g^2\, \mathrm{d}^N\boldsymbol{x})(\int h^2\, \mathrm{d}^N\boldsymbol{x})$. With this, we can follow step by step the following recipe to obtain a lower bound for the variance of a general estimator. First the definition of the variance over the data population looks like

$$V[\hat{a}] = E[(\hat{a} - a)^2] = \int (\hat{a} - a)^2 \Pr(\boldsymbol{x}|\boldsymbol{a})\, \mathrm{d}^N\boldsymbol{x}, \tag{2.14}$$

remember that the estimator is assumed to be unbiased. Second, subtracting a times Eq. (2.12) to

Eq. (2.13) the following holds,

$$\int (\hat{a} - a)\partial_a \big(\ln \Pr(\boldsymbol{x}|\boldsymbol{a}) \big) \Pr(\boldsymbol{x}|\boldsymbol{a}) \, \mathrm{d}^N \boldsymbol{x} = 1 \tag{2.15}$$

because a is not a function of $\boldsymbol{x}$. Hence, using the Schwartz inequality we can write

$$\mathrm{V}[\hat{a}] = \int (\hat{a} - a)^2 \Pr(\boldsymbol{x}|\boldsymbol{a}) \, \mathrm{d}^N \boldsymbol{x} \geqslant \frac{1}{\int \left[\partial_a \big(\ln \Pr(\boldsymbol{x}|\boldsymbol{a}) \big) \right]^2 \Pr(\boldsymbol{x}|\boldsymbol{a}) \, \mathrm{d}^N \boldsymbol{x}}, \tag{2.16}$$

which is also known as the Cramér-Rao bound or the Fisher inequality. The denominator in the right hand-side is called generally the Fisher information (FI) or simply information.

With this review of the most interesting properties of "classical" metrology, from the point of view of this thesis, we conclude this section. In the next section, we will discuss some properties of the quantum mechanics and then we will follow with another section which presents the basis of quantum metrology.

2.2 Quantum mechanics from metrology perspective

The ubiquitous probabilistic nature of quantum mechanics makes us to work with probabilities on a regular basis. Moreover, if one studies fields connected to experiments or some short of physical realizations, this probabilistic nature of quantum mechanics becomes even more visible. On the other hand, exotic features such as entanglement arise from quantum mechanics, which is directly connected with the probabilistic notions explained before. The present section is intended to describe quantum systems from the point of view of metrology.

2.2.1 The quantum state, multiparticle state, entanglement

A formal mathematical description of the quantum state is given next. This also allows us to introduce some notation used throughout the thesis. A *state* in quantum mechanics lives in a Hilbert space, $\mathcal{H}$. The state, ρ, has the following properties:

i) It is Hermitian, so it is invariant under the complex transposition, $\rho = \rho^\dagger$ and all its eigenvalues are real.

ii) Its trace is equal to one, $\mathrm{tr}(\rho) = 1$.

iii) It is positive semi-definite, i.e, all its eigenvalues are bigger or equal to zero, $\rho = \sum_\lambda p_\lambda \Pi_\lambda$ where $p_\lambda \geqslant 0$ and $\Pi_\lambda \equiv |\lambda\rangle\langle\lambda|$ is the projector of the eigenstate $|\lambda\rangle$, a vector state satisfying

the following eigenvalue equation $\rho|\lambda\rangle = p_{lambda}|\lambda\rangle$. From (ii), it follows that $\sum_\lambda p_\lambda = 1$.

iv) If all p_λ are zero except one, the state is called a pure state and is equivalent to the projector of such eigenstate $\rho = \Pi_\lambda = |\lambda\rangle\langle\lambda|$.

v) Using the properties (iii) and (iV), it follows that the quantum states form a convex set where the extreme must be pure states.

vi) An expectation value of an observable $\mathcal{O}$ is computed as $\langle\mathcal{O}\rangle = \mathrm{tr}(\mathcal{O}\rho)$. To make a connection with the previous section, the state represents the so-called data population, hence using the notation in Sec. 2.1, $\langle\mathcal{O}\rangle \equiv \mathrm{E}[\mathcal{O}]$.

The composite system of N different parties live in the Hilbert space $\mathcal{H} = \mathcal{H}^{(1)} \otimes \mathcal{H}^{(2)} \otimes \cdots \otimes \mathcal{H}^{(N)}$ or $\mathcal{H} = \bigotimes_{i=1}^{N} \mathcal{H}^{(i)}$ for short, where $\otimes$ stands for tensor product. For instance, this composite Hilbert space could be used to represent a many-particle system, in this case N particles. A *separable* state in this Hilbert space can be written as

$$\rho_{\mathrm{sep}} = \sum_i p_i \rho_i^{(1)} \otimes \rho_i^{(2)} \otimes \cdots \otimes \rho_i^{(N)}, \tag{2.17}$$

where p_i are convex weights that add up to one and are equal to or bigger than zero. If a state cannot be written like Eq. (2.17), the state is said to be *entangled*. We mention it as a formal description of the entanglement [14, 63]. One may note at this moment, that relaxing the requirements of Eq. (2.17), one can lead to different classifications of the states. Concepts like genuine multipartite entanglement, k-producible states, or entanglement depth, among others, arose from weaker constraints than Eq. (2.17) [14, 63].

It is important to describe one of such classifications in order to characterize the different levels or multipartite entanglement followed in this work. We call a state k-producible, if it *can* be written as a mixture of the tensor product of different multipartite states with at most k parties in each,

$$\rho_{k\text{-pro}} = \sum_i p_i \rho_i^{(\alpha,\ldots,\beta)} \otimes \rho_i^{(\gamma,\ldots,\delta)} \otimes \ldots, \tag{2.18}$$

where superscript indexes between parenthesis go from 1 to N and denote to which parties belong to the state, and where each index appears once in each sum element. For instance a separable state like Eq. (2.17) is 1-producible as well as N-producible. If a state cannot be written as k-producible, then it must be $(k+1)$-entangled. This defines the entanglement depth, see Figure 2.1. Later on, these concepts of entanglement and entanglement depth will arise naturally on the metrological framework [64].

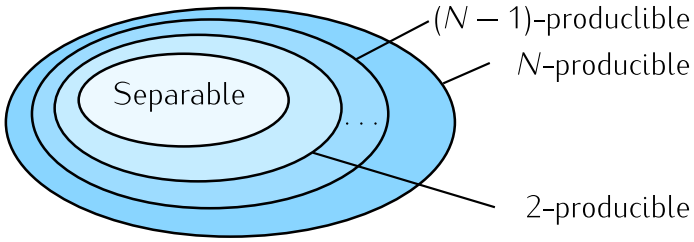

Figure 2.1: k-producible set of states contains $k-1$-producible states. Based on the Eq. (2.18), one can argue that a state that cannot be written as k-producible must be $k+1$-entangled or equivalently has $k+1$ entanglement depth. A separable state can always be written as 1-producible which on the other hand is its original definition.

2.2.2 Angular momentum operators for multipartite systems

Besides those concepts, we present a set of operators that will appear many times in all chapters, namely the angular momentum operators. Again these definitions allow us to introduce much of the notation used on this book. For a single party with discrete d levels, and therefore with a spin $j = (d-1)/2$, the eigenvalue equation for the angular momentum projection operators are

$$j_l^{(n)}|m\rangle_l^{(n)} = m|m\rangle_l^{(n)} \tag{2.19}$$

for $m = -j, \ldots, +j$, where $l = x, y, z$. It is usual to omit the subscript of $|m\rangle_l^{(n)}$ when $l = z$ because it is the preferred direction for many authors and the superscript (n) can also be omitted when the single-particle states are given in an ordered form to build a multiparticle state, i.e., $|\psi\rangle = |m_1\rangle|m_2\rangle \ldots |m_n\rangle$ where we also omitted writing the tensor product operator $\otimes$ in between single-particle states. In many cases, it is also usual to merge all into a single ket state $|\psi\rangle = |m_1 m_2 \ldots m_N\rangle$ for simplicity[†].

The square of the total angular momentum, $\boldsymbol{j}^2 = j_x^2 + j_y^2 + j_z^2$, for a single party (n) acts on any state simply as

$$(\boldsymbol{j}^2)^{(n)}\rho = j_n(j_n+1)\rho, \tag{2.20}$$

where state must be defined in a Hilbert space containing $\mathcal{H}^{(n)}$, the Hilbert space of n^{th} particle and where j_n is the spin number of such a particle. Note that in order to distinguish the spin number j_n and the operators $j_l^{(n)}$ we may use the fact that the operators are attached to a Hilbert space with a superscript or even we can use a "hatted" notation to denote which of them is an operator like $\hat{j}_l$ and which is not.

The collective angular momentum projection operators J_l are defined as the sum of their respective single-party spin operators $j_l^{(n)}$ such that they are extended to the remaining of the Hilbert spaces

[†] This notation is normally used in many-body quantum mechanics, see Refs. [65, 66].

by tensor products of the identity operators defined for the rest of subspaces,

$$J_l = \sum_{i=1}^{N} \mathbb{I}^{(1,\ldots,i-1)} \otimes j_l^{(i)} \otimes \mathbb{I}^{(i+1,\ldots,N)} \equiv \sum_{i=1}^{N} j_l^{(i)}, \tag{2.21}$$

where $\mathbb{I}$ stand for the identity operator and the last formula is the most used since it is easy to note that the single-party operator must be extended in order to sum the correctly. On the other hand, note that the squares of the different projections of total angular momentum are not equal to the sum of the square angular momentum projections of each of the parties. Thus we obtain that

$$J_l^2 = \sum_{i,j}^{N} j_l^{(i)} j_l^{(j)} = \sum_{i=1}^{N} (j_l^2)^{(i)} + \sum_{i \neq j}^{N} j_l^{(i)} j_l^{(j)}. \tag{2.22}$$

Therefore, neither square of the total angular momentum is the sum of the square of all single-party angular momenta but

$$\boldsymbol{J}^2 = \sum_{i}^{N} \boldsymbol{j}^{(i)} + \sum_{l=x,y,z} \sum_{i \neq j}^{N} j_l^{(i)} j_l^{(j)}, \tag{2.23}$$

where we separated the sum into two parts, the first one corresponds to the sum of all single party angular momentum projections squared and the second corresponds to the product of angular momentum projection operators of two distinct subsystems summed for all $l = x, y, z$. Many more combinations of these single-party operators may arise in different contexts. In the Appendix A, we discuss in more detail the different structures that arise from adding the angular momentum operators, e.g., the symmetric subspace or the singlet subspace.

2.2.3 Dynamics of quantum systems

The most basic evolution of the state is represented by unitary evolution operators denoted by U and those are the only ones appearing throughout the thesis. On the other hand, there are other types of dynamics involving particle loss, entropy changes in the system and open quantum systems in general. These transformations are governed by master-equations such as the Lindblad equation [67–69].

For the understanding of this thesis it is enough to present the unitary evolution operators. We also restrict ourselves to the case in which the evolution is constant in time, so are in general the

Hamiltonians of the metrological setups. The unitary evolution operators is defined as

$$U = \exp(-i\alpha G) = \sum_{n=0}^{\infty} \frac{(-i\alpha G)^n}{n!}, \tag{2.24}$$

where we use the matrix exponentiation in the last equality, G represents a Hermitian operator usually called generator and α is the amount of change. When a constant Hamiltonian H acts on an initial state ρ, the state evolves in time as

$$\rho(t) = U\rho U^{\dagger} = e^{-i\frac{tH}{\hbar}}\rho e^{+i\frac{tH}{\hbar}}. \tag{2.25}$$

Note that all information we can extract from the system comes in the form of expectation values of different operators at different times, $\langle\mathcal{O}\rangle(t) = \mathrm{tr}(\mathcal{O}\rho(t))$. When the state evolves in time but the operators are constant the picture of the system is called the Schrodinger-picture. Using the cyclic property of the trace, $\mathrm{tr}(ABC) = \mathrm{tr}(CBA)$, the Heisenberg-picture, a dual interpretation of the same physical system in which the state remains the same while the operators evolve in time, emerges. It is well known that the operators in this picture evolve as $\mathcal{O}(t) = U^{\dagger}\mathcal{O}U$, where $\mathcal{O}$ is the initial operator. One can check different textbooks of quantum mechanics, just to mention some see Refs. [65, 66].

2.3 Quantum metrology

We summarize important recent advances in quantum metrology. Simple metrological setups allow for encoding some desired parameter into the state of the system, thus from the readout of the final state one could infer it. The basic ideas of quantum metrology emerge when one applies the notions of estimation theory to the intrinsic probabilistic nature of quantum mechanics. Merging the probabilistic features of quantum mechanics and the estimation theory is not trivial. Nevertheless, with the initial pioneering works of C. W. Helstrom, W. K. Wootters, and S. L. Braunstein and C. M. Caves, in 1969, 1981 and 1992-1994 respectively [8, 70–72], until the works of V. Giovannetti et al, and M. G. Paris, roughly two decades later [2, 4], the foundations of quantum metrology were stabilized. Later, advanced works in quantum metrology appeared [22, 73–76] together with experimental realizations [20, 29, 35] which raised the interest in this topic. In this section, we will highlight the most important aspects of this field and with this we will conclude this chapter for presenting the background theory in which stands the work developed by the authors.

The most basic scheme for a metrological setup in the present context is the following. First, a state ρ is prepared followed by a general evolution represented by a mapping Λ_θ in which the unknown parameter θ is imprinted into the state. Finally, the outgoing state is characterized by some

measured quantity $\langle M \rangle$, which allows to infer the value of the parameter θ. Figure 2.2 illustrates the main steps of quantum metrology.

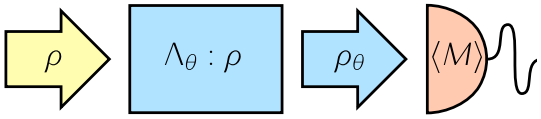

Figure 2.2: Sequence of the different steps for the basics of the estimation process in quantum metrology. First, an input state ρ enters the region in which the unknown parameter θ is imprinted in it, for the most general case, represented with Λ_θ. The state with the encoded parameter θ is measured and θ must be inferred from the measured quantity $\langle M \rangle$.

In the many-particle case, most of the metrology experiments have been done in systems with simple Hamiltonians that do not contain interaction terms. Such Hamiltonians cannot create entanglement between the particles. A typical situation is that we rotate our many particle state by some angle and we want to estimate the rotation angle θ. It has been shown that particles exhibiting quantum correlations, or more precisely, quantum entanglement [14, 63], provide a higher precision than an ensemble with non-entangled particles. The most important question is how the achievable precision of the angle estimation $(\Delta\theta)^2$ scales with the number of particles. Very general derivations lead to, at best,

$$(\Delta\theta)^2 \sim \frac{1}{N} \tag{2.26}$$

for non-entangled particles. The equation above is called *shot-noise* or standard scaling (SNS), the term originating from the shot-noise in electronic circuits, which is due to the discrete nature of the electric charge. On the other hand, quantum entanglement makes it possible to reach

$$(\Delta\theta)^2 \sim \frac{1}{N^2} \tag{2.27}$$

which is called the *Heisenberg* scaling (HS). Note that if the Hamiltonian of the dynamics has interaction terms, then these bounds can be surpassed [63, 77–82].

It is time to mention that the above calculations have been carried out for an ideal situation. When an uncorrelated noise is present in the system, it turns out that for large enough particle number the scaling becomes a SNS [60]. The possible survival of a better scaling under correlated noise, under particular circumstances, or depending on some interpretation of the metrological task, is at the center of attention currently. All these are strongly connected to the question of whether strong multipartite entanglement can survive in a noisy environment.

Finally, note that often, instead of $(\Delta\theta)^2$ one calculates its inverse, which is large for high precision. It scales as $(\Delta\theta)^{-2} \sim N$ for SNS and as $(\Delta\theta)^{-2} \sim N^2$ for the HS.

2.3.1 Quantum magnetometry

Without loss of generality, we present in this section the characterization of the precision of one of the simplest metrological tasks, namely the estimation of a homogeneous magnetic field based on the interaction between the system and the field. In this section, we will mostly study the interaction of a system with a homogeneous field in the z-direction. In the Chapter ??, we will show a different situation in which the magnetic field changes linearly with the position of the system. With the aim of estimating the strength of the magnetic field, a state is used in order to interact with it, coupling the magnetic moment of the state and the external magnetic field. Finally, measuring how the state has changed one could in principle infer on the strength of the magnetic field.

In general, we will say that the magnetic moments of the states come exclusively from the spin angular momentum, neglecting any possible contribution from the orbital angular momentum. This way the physics is simpler. This is justified in the sense that most of the recent experiments in this context have been carried out with ion-traps, Bose-Einstein condensates (BEC) or at most cold atomic ensembles, which have indeed a negligible orbital angular momentum.

Beside this considerations, the interaction Hamiltonian can be written as

$$H = -\boldsymbol{\mu} \cdot \boldsymbol{B} \tag{2.28}$$

up to some constant factor. Now in the simplest case we will choose the magnetic field to be pointing to some fixed direction, for instance, the z-direction. So the magnetic field vector can be written as $B = B\boldsymbol{k}$, where $\boldsymbol{k}$ is the unitary vector pointing to the z-direction. This way the estimation problem is much simpler, since one does not need to determine the direction of the magnetic field.

The magnetic moment of the system is proportional to the spin angular momentum, $\boldsymbol{\mu} = -\mu_B g_s \hbar^{-1} \boldsymbol{J}$, where μ_B and g_s are the Bohr magneton and anomalous gyromagnetic factor respectively. Finally, one can rewrite the interaction Hamiltonian as

$$H = \gamma B J_z, \tag{2.29}$$

where $\gamma = \mu_B g_s \hbar^{-1}$ and we have used the fact that $\boldsymbol{J} \cdot \boldsymbol{k} = J_z$. Finally, the unitary operator leading the evolution of the system can be written as

$$U = \exp(-i\theta J_z), \tag{2.30}$$

where the magnetic field strength is encoded into the phase-shift $\theta = -\mu_B g_s t B/\hbar$. Here μ_B stands

for the Bohr magneton and g_s for the giro-magnetic constant for the spin angular momentum, and t is the evolution time.

We have to mention as well that for large particle ensembles, typically only collective quantities can be measured in order to characterize the state on different phases of the metrological sequence, see Figure 2.2. Such collective quantities are in this case the angular momentum components defined in Eq. (2.21) and their combinations. More concretely, we can measure the expectation values of any direction

$$J_{\boldsymbol{n}} := \sum_{l=x,y,z} n_l J_l, \tag{2.31}$$

where $\boldsymbol{n} = (n_x, n_y, n_z)$ is a unit vector describing the direction of the component.

2.3.2 Metrology with almost polarized states, including spin-squeezed states

Let us present one of the basic approaches to calculate the metrological precision of a quantum setup. In order to estimate the phase-shift θ we measure the expectation value of a Hermitian operator, which we will denote by M in the following. If the evolution time is a constant then estimating θ is equivalent to estimating the magnetic field strength B in Eq. (2.29). The precision of the estimation can be characterized with the error propagation formula as

$$(\Delta\theta)^2 = \frac{(\Delta M)^2}{|\partial_\theta \langle M\rangle|^2}, \tag{2.32}$$

where $\langle M\rangle$ is the expectation value of the operator M, and we used the assumption that $\langle M\rangle$ is a random variable and that it has a PDF that can relate $\Pr(\langle M\rangle|\theta)$ with a PDF as a function of the estimator $\Pr(\hat{\theta}|\theta)$, see the Section 2.1.3, and for a recent review discussing this approach in detail, see Ref. [75]. Thus, the precision of the estimate depends on how sensitive $\langle M\rangle$ is to the change of θ, and also on how large the variance of M is. Based on the formula Eq. (2.32), one can see that the larger the slope $|\partial_\theta\langle M\rangle|$, the higher the precision. On the other hand, the larger the variance $(\Delta M)^2$, the lower the precision. Figure 2.3 helps to interpret the quantities appearing in Eq. (2.32).

We focus on multi-partite systems of spin-$\frac{1}{2}$ particles, widely known in the field as qubits, for homogeneous magnetometry in order to simplify the discussion. For this, let us start with an almost polarized state. We present the state totally polarized along the l-direction as

$$|+j\rangle_l^{\otimes N} \equiv |+j\rangle_l^{(1)}|+j\rangle_l^{(2)}\cdots|+j\rangle_l^{(N)}, \tag{2.33}$$

since it plays a very important role in quantum metrology when $l = y$. It is almost all the times one

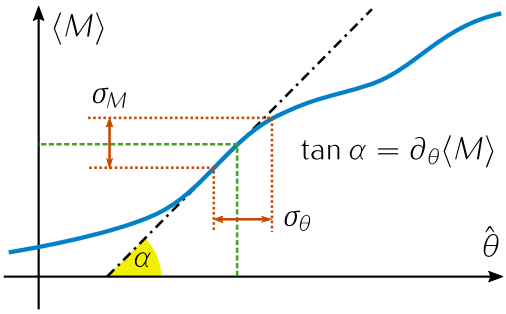

Figure 2.3: (Blue solid) Functional relation between the expectation value $\langle M\rangle$ and the estimator of the wanted parameter $\hat{\theta}$. (Green dashed) One to one correspondence when the estimator $\hat{\theta}$ is based on $\langle M\rangle$. (Red dotted) Obtaining the error of the estimate is based on Eq. (2.32). The slope of the curve at that point, denoted with $\tan\alpha$, directly relates the uncertainty σ_M on the measured quantity $\langle M\rangle$ and the error on the estimation σ_θ.

of the states that reaches the shot-noise scaling Eq. (2.26) and saturates the shot-noise limit, which will appear later in this section. In this case, the spin-vector of the ensemble, originally pointing into the y-direction, will be rotated. The rotation after the evolution is used to estimate the strength of the magnetic field. A way to measure the rotation suffered by the system is to measure the expectation value $\langle J_x\rangle$, which is zero at the beginning.

For small angles of θ and using the Eq. (2.32) after substituting M by J_x, we arrive at

$$(\Delta\theta)^{-2} = \frac{|\partial_\theta\langle J_x\rangle|^2}{(\Delta J_x)^2}, \tag{2.34}$$

for a state almost completely polarized along the y-axis. Next, we have to compute these values for small angles of θ.

To compute them we use the Heisenberg picture of the operator J_x, that after applying the unitary operator Eq. (2.30), is written as

$$J_x(\theta) = U^{i\theta J_z} J_x U^{-i\theta J_z} = \mathrm{c}_\theta J_x - \mathrm{s}_\theta J_y, \tag{2.35}$$

where we also introduced a notation for trigonometric functions since they will appear many times in this work, $\mathrm{c}_x \to \cos(x)$, $\mathrm{s}_x \to \sin(x)$ and $\mathrm{t}_x \to \tan(x)$. Thus, the square of J_x is simply

$$J_x^2(\theta) = \mathrm{c}_\theta^2 J_x^2 - 2\mathrm{c}_\theta\mathrm{s}_\theta\{J_x, J_y\} + \mathrm{s}_\theta^2 J_y^2, \tag{2.36}$$

where $\{A, B\} = AB + BA$ is the anti-commutator, since the operators may not commute in general and in this particular case it is not an exception. Finally we compute the derivative with respect to

θ of $\langle J_x \rangle$ as

$$\partial_\theta \langle J_x \rangle(\theta) = \partial_\theta \mathrm{c}_\theta \langle J_x \rangle - \partial_\theta \mathrm{s}_\theta \langle J_y \rangle = -\mathrm{s}_\theta \langle J_x \rangle - \mathrm{c}_\theta \langle J_y \rangle, \tag{2.37}$$

where we used the linearity of the trace to compute the expectation value and the linearity of the derivative.

Hence, assuming that we are in the small angle limit to compute the Eq. (2.34), we may take the terms proportional to $\sin(\theta)$ as zero. Therefore, when we measure $\langle J_x \rangle$ to estimate the angle θ, the precision of the estimation is given by

$$(\Delta\theta)^{-2} = \frac{|\mathrm{c}_\theta \langle J_y \rangle|^2}{\mathrm{c}_\theta^2 \langle J_x^2 \rangle - (\mathrm{c}_\theta \langle J_x \rangle)^2} = \frac{\langle J_y \rangle^2}{(\Delta J_x)^2}. \tag{2.38}$$

For the state totally polarized along the y-axis, the initial expectation values $\langle J_x \rangle$, $\langle J_x^2 \rangle$ and $\langle J_y \rangle$ needed to compute the precision are

$$\begin{aligned} \langle J_x \rangle_{\mathrm{tp}} &= 0, \\ \langle J_x^2 \rangle_{\mathrm{tp}} &= \tfrac{N}{4}, \\ \langle J_y \rangle_{\mathrm{tp}} &= \tfrac{N}{2}. \end{aligned} \tag{2.39}$$

Thus, we obtain a precision that scales linearly with N,

$$(\Delta\theta)_{\mathrm{tp}}^{-2} = \frac{N^2/4}{N/4} = N. \tag{2.40}$$

Note that the totally polarized state Eq. (2.33) is a separable pure state with all particles pointing into the y-direction. We obtained the shot-noise scaling, even with very simple, qualitative arguments

A way of improving the precision is considering that the variances of the angular momentum components are bounded by the Heisenberg uncertainty relation [42]

$$(\Delta J_x)^2 (\Delta J_z)^2 \geqslant \frac{1}{4} |\langle J_y \rangle|. \tag{2.41}$$

Due to decreasing $(\Delta J_x)^2$, our state fulfills

$$(\Delta J_x)^2 < \frac{1}{2} |\langle J_y \rangle|, \tag{2.42}$$

where the main spin points along the y-axis and for totally polarized states $(\Delta J_x)^2 = \frac{1}{2}|\langle J_y \rangle|$ hold. Such states are called *spin-squeezed* states [42–45] and they can in principal overcome the SNS.

Next, we can ask, what the best possible phase estimation precision is for the metrological task considered in this section. For that, we have to use the following inequality based on general principles of angular momentum theory

$$\langle J_x^2 + J_y^2 + J_z^2 \rangle \leqslant \frac{N(N+2)}{4}. \tag{2.43}$$

Note that Eq. (2.43) is saturated only by symmetric multiparticle states, see Appendix A. Together with the identity connecting the second moments, variances and expectation values

$$(\Delta J_l)^2 + \langle J_l \rangle^2 = \langle J_l^2 \rangle, \tag{2.44}$$

Eq. (2.43) leads to a bound on the uncertainty in the anti-squeezed direction, in this case z-direction, for the variance

$$(\Delta J_z)^2 \leqslant \frac{N(N+2)}{4} - \langle J_y \rangle^2 = \frac{N}{2} + \frac{N^2}{4}\left(1 - \frac{\langle J_y \rangle^2}{J_{\max}^2}\right), \tag{2.45}$$

where $J_{\max}$ is the maximum value a angular momentum component can take, i.e., $N/2$. This leads to a bound in the precision when measuring $\langle J_x \rangle$ as

$$(\Delta\theta)^{-2} = \frac{\langle J_y \rangle^2}{(\Delta J_x)^2} \leqslant 4(\Delta J_z)^2 \leqslant 2N + N^2\left(1 - \frac{\langle J_y \rangle^2}{j_{\max}}\right), \tag{2.46}$$

which indicates that the precision is limited for almost completely polarized states to the shot-noise scaling. The bound above is not optimal, as for the fully polarized state we would expect N and we obtain $2N$.

2.3.3 The quantum Fisher information

In this section, we review the theoretical background of the Fisher information, the Cramér-Rao bound and we introduce the quantum Fisher information.

First of all, we have already shown the Fisher information and the Cramér-Rao bound in the Section 2.1.3. The formula Eq. (2.16) tells us that if we measure an operator, say M, and we know its probability distribution function $\Pr(\langle M \rangle|\theta)$, we can bound the achievable precision. In quantum mechanics the PDF of a state ρ_θ when measuring the operator M is given by

$$\Pr(m|\theta) = \mathrm{tr}(\Pi_m \rho_\theta), \tag{2.47}$$

where Π_m are the projector operators or the eigenstates on which M is expanded, $M = \sum m\Pi_m$.

Following arguments found on Refs. [2, 4], one can arrive at a universal bound valid for any kind of measurements. This bound is called the quantum Cramér-Rao bound given as

$$(\Delta\theta)^{-2} \leqslant \mathcal{F}_{\mathrm{Q}}[\rho, J_z], \tag{2.48}$$

where $\mathcal{F}_{\mathrm{Q}}[\rho, J_Z]$ denotes the quantum Fisher information for the initial state ρ and the unitary evolution generated by J_z. In principle, it might be difficult to find the operator that leads to the best estimation precision just by trying several operators. Fortunately, the Eq. (2.48) gives us that upper bound that is valid for any choice on the measurement [9, 83].

As a direct consequence, based on Eq. (2.32) for any given M, we have that

$$\mathcal{F}_{\mathrm{Q}}[\rho, J_z] \geqslant \frac{|\partial_\theta \langle M\rangle|^2}{(\Delta M)^2} \tag{2.49}$$

is an upper bound for concrete bounds based on the measurement scheme. For example, when the rotation of the system is estimated by measuring $\langle J_x\rangle$ the quantum Fisher information is bounded from below by [15]

$$\mathcal{F}_{\mathrm{Q}}[\rho, J_z] \geqslant \frac{\langle J_y\rangle^2}{(\Delta J_x)^2}, \tag{2.50}$$

as it is directly infer from Eq. (2.38).

The quantum Fisher information can be computed by closed formulas such as

$$\mathcal{F}_{\mathrm{Q}}[\rho, J_z] = 2\sum_{\lambda,\nu} \frac{(p_\lambda - p_\nu)^2}{p_\lambda + p_\nu} |\langle\lambda|J_z|\nu\rangle|^2, \tag{2.51}$$

$$\mathcal{F}_{\mathrm{Q}}[\rho, J_z] = \inf_{p_k, \psi_k} 4\sum_k p_k (\Delta J_z)^2_{\psi_k}, \tag{2.52}$$

for the case of unitary evolution Eq. (2.30) and where the state can be decomposed in its eigenbasis as $\rho = \sum_\lambda p_\lambda |\lambda\rangle$ in the first case, or where it is any arbitrary convex decomposition like $\rho = \sum_k p_k |\psi_k\rangle\langle\psi_k|$, used the later in the second case. The first one is based on the eigen-decomposition of the state whereas the second is the convex-roof of $4(\Delta J_z)^2$ [4, 84, 85]. Both formulas yield to the same expression for pure states

$$\mathcal{F}_{\mathrm{Q}}[|\psi\rangle, J_z] = 4(\Delta J_z)^2, \tag{2.53}$$

since the convex-roof over a pure state is computed on the state itself, and using first the identity $(a-b)^2 = (a+b)^2 - 4ab$ and second that $p_\lambda = \delta_{\lambda,1}$ (we choose the pure state to be $|1\rangle$ without loss

of generality) in Eq. (2.51) we arrive at the result

$$\begin{aligned}\mathcal{F}_{\mathrm{Q}}[|\psi\rangle, J_z] &= 2\sum_{\lambda,\nu}\left(p_\lambda + p_\nu - \frac{4p_\lambda p_\nu}{p_\lambda + p_\nu}\right)|\langle\lambda|J_z|\nu\rangle|^2 \\ &= 4\,\mathrm{tr}(J_z\rho) - 8\sum_{\lambda,\nu}\frac{p_\lambda p_\nu}{p_\lambda + p_\nu}|\langle\lambda|J_z|\nu\rangle|^2 \\ &= 4(\Delta J_z)^2.\end{aligned} \tag{2.54}$$

Some interesting properties of the quantum Fisher information emerge from these expressions:

i) The QFI is convex on states, as it is directly shown in Eq. (2.52) while it can be proven if one starts from Eq. (2.51),

$$\mathcal{F}_{\mathrm{Q}}[p\rho_1 + (1-p)\rho_2, J_z] \leqslant p\mathcal{F}_{\mathrm{Q}}[\rho_1, J_z] + (1-p)\mathcal{F}_{\mathrm{Q}}[\rho_2, J_z]. \tag{2.55}$$

ii) Recently, it has been shown due to Eq. (2.52), that the quantum Fisher information is the largest convex function that fulfills (i) [84, 85].

iii) For pure states $\mathcal{F}_{\mathrm{Q}}[|\psi\rangle, J_z] = 4(\Delta J_z)^2$, as it has been already mentioned.

iv) For all states, the QFI is smaller or equal to four times the variance in all cases,

$$\mathcal{F}_{\mathrm{Q}}[\rho, J_z] \leqslant 4(\Delta J_z)^2_\rho. \tag{2.56}$$

.

The main relation between the quantum Fisher information and the variance, which analogously to Eq. (2.52) can be proven that it is the concave-roof of the variance [84], can be summarized as follows. For any decomposition $\{p_k, |\Psi_k\rangle\}$ of a state ρ we have

$$\frac{1}{4}\mathcal{F}_{\mathrm{Q}}[\rho, J_z] \leqslant \sum_k p_k(\Delta J_z)^2_{\Psi_k} \leqslant (\Delta J_z)^2_{\Psi_k}, \tag{2.57}$$

where the upper bound and the lower bound are both tight in the sense that there are decompositions that saturate the first inequality, and there are others that saturate the second one.

After the discussion relating the quantum Fisher information to the variance, and examining its convexity properties, we list some further useful relations for the QFI. In this case, we substitute the generator of the phase shift J_z by some more general Hermitian operators. From Eq. (2.51), we can obtain directly the following identities:

i) The formula Eq. (2.51) does not depend on the diagonal elements of the generator on the

eigenbasis of the state. Hence,

$$\mathcal{F}_{\mathrm{Q}}[\rho, A] = \mathcal{F}_{\mathrm{Q}}[\rho, A + D], \tag{2.58}$$

where D is an arbitrary matrix that is diagonal in the eigenbasis of the state, i.e., $[\rho, D] = 0$.

ii) The following identity holds for all unitary dynamics U as it could be expected from the Schrodinger vs Heisenberg pictures,

$$\mathcal{F}_{\mathrm{Q}}[U\rho U^{\dagger}, A] = \mathcal{F}_{\mathrm{Q}}[\rho, U^{\dagger}AU]. \tag{2.59}$$

In particular the QFI does not change for unitary dynamics of the type $U = e^{-iB}$ when $[A, B] = 0$.

iii) The quantum Fisher information is additive under tensor product as

$$\mathcal{F}_{\mathrm{Q}}[\rho^{(1)} \otimes \rho^{(2)}, A^{(1)} \otimes \mathbb{I}^{(2)} + \mathbb{I}^{(1)} \otimes A^{(2)}] = \mathcal{F}_{\mathrm{Q}}[\rho^{(1)}, A^{(1)}] + \mathcal{F}_{\mathrm{Q}}[\rho^{(2)}, A^{(2)}]. \tag{2.60}$$

For N-fold tensor product of the system, we obtain an N-fold increase in the quantum Fisher information

$$\mathcal{F}_{\mathrm{Q}}[\rho^{\otimes N}, \textstyle\sum_{n=1}^{N} A^{(n)}] = N\mathcal{F}_{\mathrm{Q}}[\rho, A], \tag{2.61}$$

for all $A^{(n)} = A$.

iv) The quantum Fisher information is additive under a direct sum too [86]

$$\mathcal{F}_{\mathrm{Q}}[\textstyle\bigoplus_k p_k\rho_k, \bigoplus_k A_k] = \displaystyle\sum_k p_k \mathcal{F}_{\mathrm{Q}}[\rho_k, A_k], \tag{2.62}$$

where $\sum_k p_k = 1$. The above equation is relevant, for instance, for experiments where the particle number variance is not zero, and the ρ_k corresponds to density matrices with a fixed particle number [22, 73].

Entanglement and the quantum Fisher information

The quantum Fisher information is strictly related to entanglement. In this section, we discuss now this relation and we review some important facts concerning it. We will show that entanglement is needed to overcome the shot-noise sensitivity in very general metrological tasks. Moreover, not only entanglement but multipartite entanglement is necessary for a maximal sensitivity. All these statements will be derived in a very general framework, based on the quantum Fisher information. We will also briefly discuss the question whether inter-particle entanglement is an appropriate notion

for our systems.

Let us first examine the upper bounds on the QFI for general quantum states and for separable states. Due to the Cramér-Rao bound Eq. (2.48), these are also bounds for the sensitivity of the phase estimation. Entanglement has been recognized as an advantage for several metrological tasks (see, e.g., Refs. [44, 87]). For a general relationship for linear interferometers, we ca take advantage of the properties of the quantum Fisher information discussed above. Since for pure states the quantum Fisher information equals four times the variance, for pure product states we can have at most

$$\mathcal{F}_{\mathrm{Q}}[\rho, J_z] = 4(\Delta J_z)^2 = 4\sum_{n=1}^{N}(\Delta j_z^{(n)})^2 \leqslant N. \tag{2.63}$$

For the second equality, we used the fact that for a product state the variance of a collective observable is the sum of the single-particle variances. Due to the convexity of the QFI, this upper bound is still valid for all separable states of the form Eq. (2.17) and we obtain [15]

$$\mathcal{F}_{\mathrm{Q}}[\rho, J_z] \leqslant N, \tag{2.64}$$

a bound for not entangled states. All states violating Eq. (2.64) are entangled. The entangled states make it possible to surpass this bound, the shot-noise limit (SNL), and some might be more useful than separable states for the metrological tasks at hand.

The maximum achievable precision for general states, called the Heisenberg limit (HL), can be obtained evaluating the Eqs. (2.51) or (2.52) for pure states only. Therefore, similarly we have

$$\mathcal{F}_{\mathrm{Q}}[\rho, J_z] = 4(\Delta J_z)^2 \leqslant N^2, \tag{2.65}$$

which is a valid bound still for mixed states. Note that such a bound has the Heisenberg scaling Eq. (2.27). Note that our derivation is very simple, and does not require any information about what operator we measure to estimate θ. Equation (2.64) has been used already to detect entanglement based on the metrological performance of the quantum states in Refs. [20, 58].

At this point one might ask if all entangled states can provide a sensitivity larger than the SNL. This would show that entanglement is equivalent to metrological usefulness. Concerning linear interferometers, it has been proven that not all entangled states violate the SNL Eq. (2.64)., even allowing local unitary transformations. Thus not all entangled states are useful for phase estimation [22]. It has been shown that there are even highly entangled pure states that are not useful. Hence, the presence of entanglement seems to be rather a necessary but not sufficient condition.

The quantum Fisher information can be used to define a entanglement parameter that characterizes the metrological usefulness as

$$\chi = \frac{\mathcal{F}_{\mathrm{Q}}[\rho, J_z]}{N}, \tag{2.66}$$

which is one or less for separable states and where it can take at most the value of N as is deduced from Eq. (2.65).

On the other hand, for k-producible states the QFI is bounded from above, similarly as we did in Eqs. (2.64) and (2.65), by [73, 88]

$$\begin{aligned} \chi &\leqslant \frac{sk^2 + (N - sk)^2}{N}, \\ &\overset{k \ll N}{\lesssim} k, \end{aligned} \tag{2.67}$$

where s is the integer part of $\frac{N}{k}$ and we write the case on which $k \ll N$. It is instructive to write the equation above for the case in which N is exactly divisible by k as

$$\chi \leqslant k. \tag{2.68}$$

Thus, the bounds reachable by k-producible states are distributed linearly in k.

It is also instructive to define a QFI averaged over all possible directions. Simple calculations show that

$$\operatorname*{avg}_{\boldsymbol{n}} \mathcal{F}_{\mathrm{Q}}[\rho, J_{\boldsymbol{n}}] \equiv \int_{\boldsymbol{n}=(\mathrm{c}_\varphi \mathrm{s}_\vartheta, \mathrm{s}_\varphi \mathrm{s}_\vartheta, \mathrm{c}_\vartheta)} \mathcal{F}_{\mathrm{Q}}[\rho, J_{\boldsymbol{n}}] \sin(\vartheta)\, \mathrm{d}\varphi \mathrm{d}\vartheta = \frac{1}{3} \sum_{l=x,y,z} \mathcal{F}_{\mathrm{Q}}[\rho, J_l], \tag{2.69}$$

where we used the spherical coordinates, where φ and ϑ are the azimuthal and polar angles respectively, for the definition of the averaged QFI and the Eq. (2.31) for $J_{\boldsymbol{n}}$. Therefore, bounds similar to Eqs. (2.64) and (2.65) for separable and general states can be obtained for the average quantum Fisher information,

$$\operatorname*{avg}_{\boldsymbol{n}} \mathcal{F}_{\mathrm{Q}}[\rho, J_{\boldsymbol{n}}] \leqslant \frac{2}{3} N, \tag{2.70}$$

$$\operatorname*{avg}_{\boldsymbol{n}} \mathcal{F}_{\mathrm{Q}}[\rho, J_{\boldsymbol{n}}] \leqslant \frac{1}{3} N(N+2). \tag{2.71}$$

Similar to Eq. (2.66) an entanglement criterion can be constructed for the averaged QFI.

Finally, we also mention that bound entangled states can also be detected with the entanglement criteria based on the quantum Fisher information. Bound entanglement is a weak type of entanglement, which is not distillable with local operations and classical communication [13, 14]. Ref. [73]

presented states that were detected as bound entangled based on the criterion for the average QFI Eq. (2.69). Ref. [89] presented states that violate the criterion based on a bound for the quantum Fisher information similar to Eq. (2.66).

3 Metrology in the vicinity of Dicke states

"An experimentalist should not be unduely inhibited by theoretical untidyness"
Robert H. Dicke

In this chapter we will present recent results regarding the metrological usefulness of a family of unpolarized states. Such states can be used as trial states to estimate the homogeneous magnetic field strength, see Section 2.3.1 for references about magnetometry. It turns out that unpolarized states are the most adequate states to reach the Heisenberg limit, as it was shown in the Section 2.3. Hence, these states have attracted considerable interest.

One of the figures of merit of these states is the so-called unpolarized Dicke state [90] in an arbitrary l-direction, which consists of an equal number of qubits pointing in the l-direction and pointing opposite direction while the whole state is symmetrized, and where $l = x, y, z$. It can be written as

$$|\mathrm{D}_N\rangle_l \equiv |\mathrm{D}_{N,\frac{N}{2}}\rangle_l := \binom{N}{N/2}^{-\frac{1}{2}} \sum_{k\in\sigma_s} \mathcal{P}_k \left(|1\rangle_l^{\otimes N/2}|0\rangle_l^{\otimes N/2}\right), \tag{3.1}$$

where k are elements of the set of all possible unique permutations of N elements of 2 kinds, σ_s, see Appendix A for more information about the notation used in Eq. (3.1). Note that in Eq. (3.1) we omit the subscript giving the number of $|1\rangle$'s which is the notation we will follow in this chapter. Such a state is known to be highly entangled [? ?] and can reach Heisenberg scaling when used for

magnetometry [**?**].

One of the characteristics of state Eq. (3.1) is that it is an eigenstate of the collective operator J_l with corresponding eigenvalue equal to zero. At the same time, it lives in the subspace where the collective total spin is maximum, i.e, $\langle \boldsymbol{J}^2 \rangle = N(N+2)/4$. Based on these and the fact that the state is unpolarized, we can see that has a very large uncertainty for the collective spin operators perpendicular to J_l.

For metrology, we chose the magnetic field to be pointing in the z-axis. Hence, the Dicke state we choose must an eigenstate of a perpendicular component of the angular momentum operator such as J_x. Hence, we will consider a scheme in which the state is rotated around the z-direction and the rotation angle must be estimated based on collective measurements. A criterion to detect the metrological usefulness of states of this type has been derived in Ref. [91].

In this chapter, we present a condition for metrological usefulness for the case when the second moment of a total angular momentum component is measured to obtain an estimate for the rotation angle. Our method is expected to simplify the experimental determination of metrological sensitivity since it is much easier to measure the collective operators of the state than carrying out the metrological procedure and measure directly the sensitivity. We also test our approach using the experimental results of Refs. [20, 58], which realize parameter estimation with a Dicke state. Thus, our work is expected to be useful for similar experiments in the future.

The chapter is organized as follows. In Section 3.1, we review some important concepts behind the theory of metrology with unpolarized states. In Section 3.2, we present our criterion. In Section 3.3, we compare findings to sensitivity bounds obtained from the quantum Fisher information. In Section 3.4, we show how to apply our criterion to experimental results.

3.1 Unpolarized Dicke states for magnetometry

The use of unpolarized states for magnetometry has been shown useful in Eq. (2.46). While the quantum Fisher information would give us directly the performance of the state, we typically cannot compute it because a complete knowledge of the state would be necessary, see Eq. (2.51). On the other hand, we can use the error propagation formula Eq. (2.32) to obtain a bound on the achievable precision which at the same time bounds the QFI.

As one can see in Figure 3.1, a pure Dicke state of 16 qubits, initially an eigenstate of the J_x operator, is rotated around the z-axis. The state is unpolarized so the expectation value of any component of the total angular momentum remains zero. It turns out that measuring the evolution

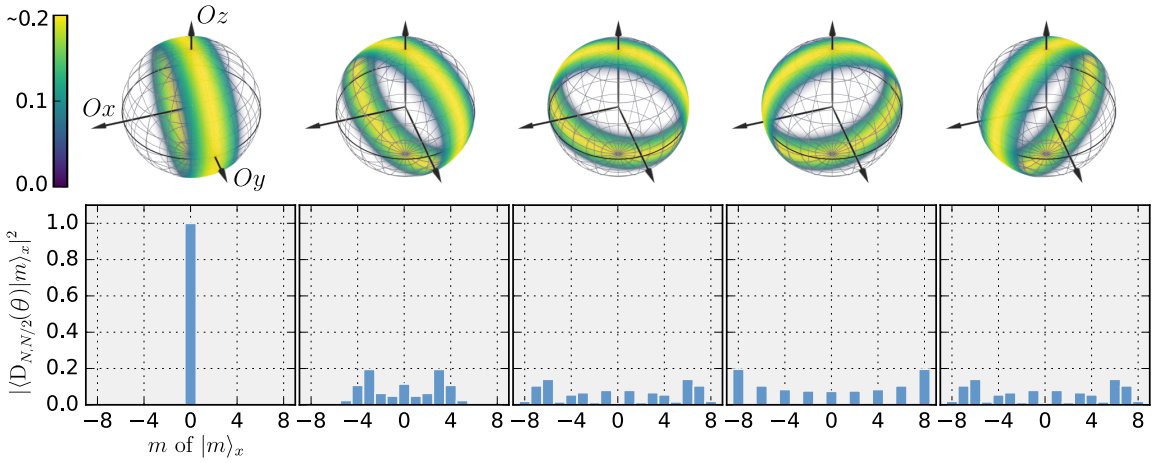

Figure 3.1: Sequence of the evolution of an unpolarized Dicke state of 16 qubits for $\theta = \{i\pi/6\}_{i=0}^{4}$. Bloch spheres representing the Husimi quasi-probabilistic distribution of the state, and below PDF of the J_x positive-operator valued measure (POVM) for each step of the sequence

of the second moment of J_x allows the estimation of rotation angle θ, and therefore, the magnetic field. The expectation value $\langle J_x^2 \rangle$ is initially zero for a pure unpolarized Dicke state, and it increases rapidly as it can be seen in the Figure 3.1. Another observation is that for $\theta = \pi/2$ the value of $\langle J_x^2 \rangle$ will be at its maximum proportional to $\langle \boldsymbol{J}^2 \rangle$ or equivalently to $\mathcal{J}_{N/2}$, see Eq. (A.3). Hence, the change in the second moment over the phase shift must be in this case proportional to N^2. We lead to the conclusion that one only needs to measure the second moment of the collective spin J_x to achieve Heisenberg scaling for the estimation.

In certain situations, it is better to use Eq. (2.32) rather than Eq. (2.48) for calculating the achievable precision, since it gives the precision for a particular operator to be measured in an experimental setup. This is reasonable, since in a typical experiment, only a restricted set of operators can be measured. In this work, we will consider many-particle systems in which the particles cannot be accessed individually, and only collective quantities can be measured. As we said, measuring the second moment of J_x is a valid choice to estimate the rotation angle. In the following equation, we show the error propagation formula when measuring the second moment of the J_x total angular momentum component,

$$(\Delta\theta)^{-2} = \frac{|\partial_\theta \langle J_x \rangle|^2}{(\Delta J_x^2)^2}. \tag{3.2}$$

Since Eq. (3.2) is always smaller than $\mathcal{F}_{\mathrm{Q}}$, and as a consequence of Eq. (2.66), if

$$\frac{|\partial_\theta \langle J_x \rangle|^2}{(\Delta J_x^2)^2} \geqslant N \tag{3.3}$$

holds, then the system is entangled. Hence again, entanglement is required for a large metrological precision. Based on Eq. (2.67), we can bound the entanglement depth from below of the systems as follows. Similarly to the previous paragraph, if for a quantum state

$$\frac{|\partial_\theta \langle J_x \rangle|^2}{(\Delta J_x^2)^2} \geqslant kN \tag{3.4}$$

holds, then it is at least $(k+1)$-entangled.

3.2 Evolution of the expectation values

With the aim of obtaining the precision, Eq. (3.2), we will compute the dependence on θ of the expectation value of the operator J_x and higher order moments. We will use the Heisenberg picture, where the operators evolve in time while the state remains the same. The operator J_x can be written as a function of θ in the following way,

$$J_x(\theta) = e^{i\theta J_z} J_x(0) e^{-i\theta J_z} = J_x(0)\mathrm{c}_\theta - J_y(0)\mathrm{s}_\theta, \tag{3.5}$$

where $J_l(0)$ for $l = x, y, z$ are the collective angular momentum operators at time equal zero. We will denote them by J_l from now on. The notation for the trigonometric functions c_θ and s_θ was introduced in Section 2.3.2.

We need to compute the second and the fourth moments of J_x as it is required by the Eq. (3.2). But before any calculation we will make a simplifying assumption which turns out to be true in the most common situations. The assumption is that both expectation values are even functions of θ, so

$$\begin{aligned} \langle J_x^2(\theta) \rangle &= \langle J_x^2(-\theta) \rangle, \\ \langle J_x^4(\theta) \rangle &= \langle J_x^4(-\theta) \rangle \end{aligned} \tag{3.6}$$

holds. This way we can omit the terms that are odd in θ. In Section 3.4, we will see that unitary dynamics of some experimentally prepared states have this property. The assumption Eq. (3.6) is needed to obtain a closed formula for the precision of the phase estimation.

The square of J_x in the Heisenberg picture is written as

$$J_x^2(\theta) = J_x^2 \mathrm{c}_\theta^2 + J_y^2 \mathrm{s}_\theta^2 - (J_x J_y + J_y J_x)\mathrm{c}_\theta \mathrm{s}_\theta. \tag{3.7}$$

Hence, due to the first constraint of Eq. (3.6) and Eq. (3.7), we require that

$$\langle \{J_x, J_y\} \rangle = 0, \tag{3.8}$$

where $\{\ ,\ \}$ stands for the anticommutator. Apart for been simpler to compute the Eq. (3.8) is based also on initial expectation values of the state. We will see that as we said before this is easily guarantied for most important cases.

As we have done with the expectation value of the square of J_x, now we do the same for J_x^4. This way one will be able to distinguish which other expectation value of combination of operators must vanish in order to have Eq. (3.6) guarantied. The fourth power of J_x can be written in the Heisenberg picture as

$$\begin{aligned} J_x^4(\theta) = J_x^4 \mathrm{c}_\theta^4 + J_y^4 \mathrm{s}_\theta^4 + (J_x^2 J_y^2 + J_x J_y J_x J_y + J_x J_y^2 J_x + J_y J_x J_y J_x + J_y J_x^2 J_y + J_y^2 J_x^2) \mathrm{c}_\theta^2 \mathrm{s}_\theta^2 \\ - (J_x^3 J_y + J_x^2 J_y J_x + J_x J_y J_x^2 + J_y J_x^3) \mathrm{c}_\theta^3 \mathrm{s}_\theta - (J_x J_y^3 + J_y J_x J_y^2 + J_y^2 J_x J_y + J_y^3 J_x) \mathrm{c}_\theta \mathrm{s}_\theta^3. \end{aligned} \tag{3.9}$$

And again assuming that the expectation value of $J_x^4(\theta)$ must be an even function of θ, we see that the terms multiplied by $\mathrm{c}_\theta^3 \mathrm{s}_\theta$ and $\mathrm{c}_\theta \mathrm{s}_\theta^3$, respectively, must be zero. So, the expectation value of $(J_x^3 J_y + J_x^2 J_y J_x + J_x J_y J_x^2 + J_y J_x^3)$ and $(J_x J_y^3 + J_y J_x J_y^2 + J_y^2 J_x J_y + J_y^3 J_x)$ must vanish. Hence, the second constraint of the Eq. (3.6) can be fulfilled if

$$\begin{aligned} \langle \left\{ J_x^2, \{J_x, J_y\} \right\} \rangle = 0, \\ \langle \left\{ J_y^2, \{J_x, J_y\} \right\} \rangle = 0. \end{aligned} \tag{3.10}$$

Finally, we can write the evolution of second and fourth moments of the J_x operator as

$$\langle J_x^2(\theta) \rangle = \langle J_x^2 \rangle \mathrm{c}_\theta^2 + \langle J_y^2 \rangle \mathrm{s}_\theta^2 \tag{3.11}$$

$$\begin{aligned} \langle J_x^4(\theta) \rangle = \langle J_x^4 \rangle \mathrm{c}_\theta^4 + \langle J_y^4 \rangle \mathrm{s}_\theta^4 \\ + \langle \{J_x^2, J_y^2\} + \{J_x, J_y\}^2 \rangle \mathrm{c}_\theta^2 \mathrm{s}_\theta^2. \end{aligned} \tag{3.12}$$

From here, we are able to write the evolution of the variance of the second moment when Eq. (3.6) is

fulfilled. We obtain

$$\begin{aligned}(\Delta J_x^2(\theta))^2 &= \langle J_x^4(\theta)\rangle - \langle J_x^2(\theta)\rangle^2 \\ &= \langle J_x^4\rangle \mathrm{c}_\theta^4 + \langle J_y^4\rangle \mathrm{s}_\theta^4 + \langle \{J_x^2, J_y^2\} + \{J_x, J_y\}^2\rangle \mathrm{c}_\theta^2 \mathrm{s}_\theta^2 - \left(\langle J_x^2\rangle \mathrm{c}_\theta^2 + \langle J_y^2\rangle \mathrm{s}_\theta^2\right)^2 \\ &= \left(\langle J_x^4\rangle - \langle J_x^2\rangle^2\right)\mathrm{c}_\theta^4 + \left(\langle J_y^4\rangle - \langle J_y^2\rangle^2\right)\mathrm{s}_\theta^4 + \left(\langle \{J_x^2, J_y^2\} + \{J_x, J_y\}^2\rangle - 2\langle J_x^2\rangle\langle J_y^2\rangle\right)\mathrm{c}_\theta^2 \mathrm{s}_\theta^2 \\ &= (\Delta J_x^2)^2 \mathrm{c}_\theta^4 + (\Delta J_y^2)^2 \mathrm{s}_\theta^4 + \left(\langle \{J_x^2, J_y^2\} + \{J_x, J_y\}^2\rangle - 2\langle J_x^2\rangle\langle J_y^2\rangle\right)\mathrm{c}_\theta^2 \mathrm{s}_\theta^2.\end{aligned} \tag{3.13}$$

In order to compute the Eq. (3.2), we also need the modulus square of the derivative of the second moment of the J_x operator. Using Eq. (3.11) for the expression of the evolution of the second moment, the numerator of Eq. (3.2) follows

$$\begin{aligned}|\partial_\theta \langle J_x^2(\theta)\rangle|^2 &= |-2\langle J_x^2\rangle \mathrm{c}_\theta \mathrm{s}_\theta + 2\langle J_y^2\rangle \mathrm{c}_\theta \mathrm{s}_\theta|^2 \\ &= 4\langle J_y^2 - J_x^2\rangle^2 \mathrm{c}_\theta^2 \mathrm{s}_\theta^2.\end{aligned} \tag{3.14}$$

From the equations above directly follows expression for the precision of θ,

$$\begin{aligned}(\Delta\theta)^2 &= \frac{(\Delta J_x^2)^2 \mathrm{c}_\theta^4 + (\Delta J_y^2)^2 \mathrm{s}_\theta^4 + \left(\langle \{J_x^2, J_y^2\} + \{J_x, J_y\}^2\rangle - 2\langle J_x^2\rangle\langle J_y^2\rangle\right)\mathrm{c}_\theta^2 \mathrm{s}_\theta^2}{4\langle J_y^2 - J_x^2\rangle^2 \mathrm{c}_\theta^2 \mathrm{s}_\theta^2} \\ &= \frac{(\Delta J_x^2)^2 \mathrm{t}_\theta^{-2} + (\Delta J_y^2)^2 \mathrm{t}_\theta^2 + \langle \{J_x^2, J_y^2\} + \{J_x, J_y\}^2\rangle - 2\langle J_x^2\rangle\langle J_y^2\rangle}{4\langle J_y^2 - J_x^2\rangle^2}.\end{aligned} \tag{3.15}$$

To this calculations further computations follows mainly regarding to the following expectation value $\langle \{J_x^2, J_y^2\} + \{J_x, J_y\}^2\rangle$. This calculus is left for the Appendix efapp:simplification-of-4th-moments. Finally, the expression Eq. (3.15) can be written as

$$(\Delta\theta)^2 = \frac{(\Delta J_x^2)^2 \mathrm{t}_\theta^{-2} + (\Delta J_y^2)^2 \mathrm{t}_\theta^2 + 4\langle J_y^2\rangle - 3\langle J_z^2\rangle - 2\langle J_x^2\rangle(1 + \langle J_y^2\rangle) + 6\langle J_x J_y^2 J_x\rangle}{4\langle J_y^2 - J_x^2\rangle^2}. \tag{3.16}$$

We have verified the correctness of our analytic formula Eq. (3.16) comparing it with a numerical simulation of the Eq. (3.2) for the ground-state of $H = J_x^2 + J_y$ for 6 qubits, $|\mathrm{GS}\rangle$. We computed the evolution of the expectation values of the second and the fourth moments of the operator J_x for $\theta \in [0, \pi]$, for thousand of equidistant points, from which we obtained the bound, see Figure 3.2 (a). Finally, we have also checked that the constraints assumed at the beginning of this section are fulfilled. For that, we considered the range $\theta \in [-\pi, \pi]$ and we have computed the expectation values, see Figure 3.2 (b). We can conclude saying that our formula Eq. (3.16) reproduces exactly the evolution of the error propagation formula, Eq. (3.2).

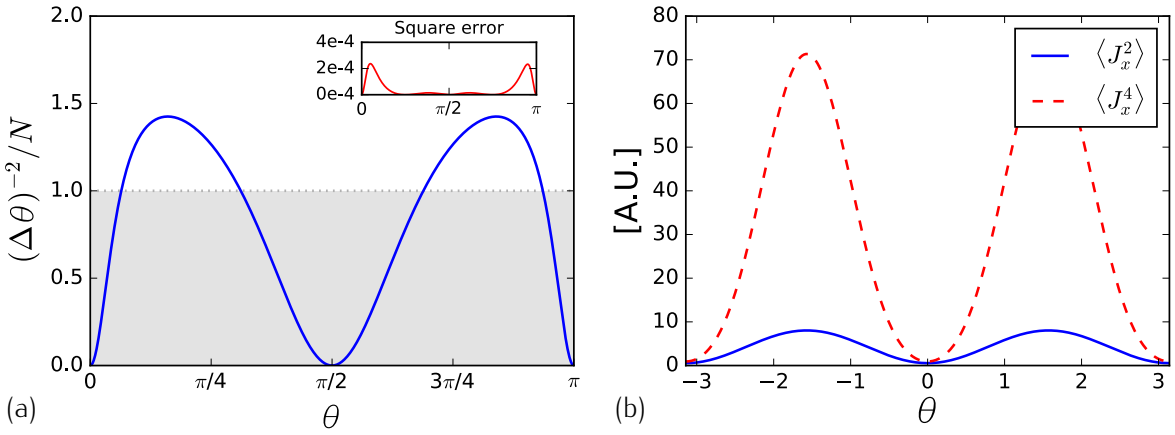

Figure 3.2: (a) Evolution of the precision $(\Delta\theta)^{-2}/N$ for 6 qubits based on the simulation of the system $|\mathrm{GS}\rangle$ and its expectation values. The agreement with the Eq. (3.16) is shown in the inset plot where the square of the difference between two approaches are plotted, the analytically obtained result and the simulation. The difference is more or less two orders of magnitude below the actual value for the relevant points, which is mainly because of computing the derivative near the points on which the value of the expectation value $\langle J_x^2 \rangle$ and the value of the $(\Delta J_x^2)^2$ are both close to zero. (b) With the system at hand, we verified the parity with respect to θ of the expectation values of the second and the fourth moment, so to fulfill the constraint Eq. (3.6).

3.2.1 The optimal precision

First of all, note that all the dependence on the phase shift θ is in the first two terms of the numerator of Eq. (3.16). Hence, one can minimize the sum on the first two terms in order to find where the precision is best. So it follows that for the optimal angle

$$\tan^2(\theta_{\mathrm{opt}}) = \sqrt{\frac{(\Delta J_x^2)^2}{(\Delta J_y^2)^2}} \tag{3.17}$$

holds. By substituting Eq. (3.17) into Eq. (3.16), we obtain the optimal bound as

$$(\Delta\theta)^2_{\mathrm{opt}} = \frac{\sqrt{(\Delta J_x^2)^2(\Delta J_y^2)^2} + 4\langle J_y^2 \rangle - 3\langle J_z^2 \rangle - 2\langle J_x^2 \rangle(1 + \langle J_y^2 \rangle) + 6\langle J_x J_y^2 J_x \rangle}{4\langle J_y^2 - J_x^2 \rangle^2}. \tag{3.18}$$

.

We conclude this section checking our bound for pure unpolarized Dicke state aligned with the x-axis, $|\mathrm{D}_N\rangle_x$, whose precision bound is well known using the QFI for pure states Eq. (2.53),

$$\mathcal{F}_{\mathrm{Q}}[|\mathrm{D}_N\rangle_x, J_z] = 4(\Delta J_z)^2_{|\mathrm{D}_N\rangle_x} = \frac{N(N+2)}{2}. \tag{3.19}$$

With this aim we compute all the expectation values needed for the Eq. (3.18) which almost all of them are trivial, $\langle J_x J_y^2 J_x \rangle = \langle J_x^4 \rangle = \langle J_x^2 \rangle = 0$ since the state is an eigenstate of J_x with an eigenvalue zero. The last expectation value is obtained as

$$\langle J_y^2 \rangle = \langle J_z^2 \rangle = \frac{N(N+2)}{8}. \tag{3.20}$$

Note that for the Eq. (3.20) we use that the state is invariant under rotations over the x-axis, the sum of all the second moments must give $\langle \boldsymbol{J}^2 \rangle = \frac{N(N+2)}{4}$, and $\langle J_x^2 \rangle = 0$. Hence, the Eq. (3.20) holds.

From the equation above and using the expression for the optimal precision Eq. (3.18), one arrives at the following formula for the precision of the phase shift for a pure unpolarized Dicke state,

$$(\Delta\theta)^2_{\text{opt}} = \frac{2}{N(N+2)}, \tag{3.21}$$

which coincides exactly with the inverse of the quantum Fisher information for such state Eq. (3.19) [20]. Hence for the ideal Dicke state, the Cramér-Rao bound Eq. (2.48) is saturated, which means that estimating the phase shift θ using the measurement of $\langle J_x^2 \rangle$ is optimal. Based on Eq. (3.17), we add that the optimal angle for the ideal Dicke state is $\theta_{\text{opt}} = 0$.

3.3 Testing the formula against some known states

In this section, we will compare our criteria based on few expectation values against the corresponding quantum Fisher information obtained for some known states. We find that our formula gives a good lower bound on the quantum Fisher information, which is the best achievable precision when any measurement is allowed. However note that the Cramér-Rao bound might be impractical.

Let us consider first the spin-squeezed states. Those states will be defined as the ground states $|\text{GS}\rangle_\lambda$ of the following Hamiltonian, called the spin-squeezing Hamiltonian

$$H_\lambda = J_x^2 - \lambda J_y, \tag{3.22}$$

see Appendix E. For $\lambda > 0$, the ground state is unique, and it is in the symmetric subspace. Hence, we can restrict our attention to this subspace for our computations, and hence we can model larger systems. For $\lambda \to \infty$, the ground state is the totally polarized state in the y-direction Eq. (2.33). And for $\lambda \to 0^+$, it is the Dicke state Eq. (3.1). Note that for $\lambda = 0$ the eigenvalue is degenerate, so there are more than one ground states. On the other hand, we still can use limit in which λ tends to zero from the positive axis to arrive at the Dicke state. Figure 3.3 (a) shows the sensitivity we

obtained together with the QFI for the same states. Our bound is close to the QFI when the state is well polarized. It also coincides with the bound in the $\lambda \to 0^+$ limit, when the ground state is close to the unpolarized Dicke state.

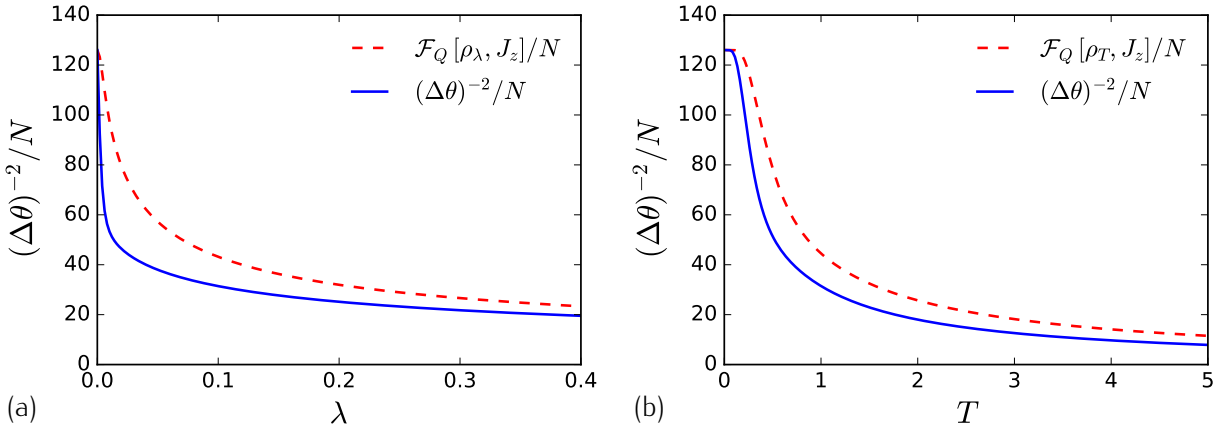

Figure 3.3: Comparison between our formula for the precision and the QFI for different states. (a) Comparison for ground states of H_λ. (b) Comparison with gaussian mixture of Dicke states.

The second family of states we use to test our formula are the Gaussian mixture of Dicke states around the unpolarized Dicke state, which have the following form as function of T as

$$\rho_T \propto \sum_{m=0}^{N} e^{-\frac{(m+N/2)^2}{T}} |D_{N,m}\rangle_x \langle D_{N,m}|_x \tag{3.23}$$

for even N, where $|D_{N,m}\rangle$ is defined in Eq. (A.5). It can be used to model a noisy or thermal unpolarized Dicke state. For $T = 0$, we obtain the pure unpolarized Dicke state. For $T > 0$, other symmetric Dicke states in the vicinity of the unpolarized one are also populated. The result can be seen in Figure 3.3-(b). Again, our bound seems to be quite close to the corresponding QFI.

Note also that in Figure 3.3, based on Eq. (2.67), if the bound turns to be greater than k integer, then a metrologically useful $(k+1)$-particle entanglement is detected in the system. Note that this is true whenever k is a divisor of N, or $k \ll N$.

Although showing how the optimal precision formula behaves compared with the quantum Fisher information for those two families of states, we will now prove that they indeed they fulfill the constraints appearing in Eq. (3.6). Hence, we compute the Eq. (3.6) for the spin-squeezed states $|GS\rangle_\lambda$. For that it is enough to know that since those states are non-degenerate eigenvalue must preserve the symmetries of the Hamiltonian. In this case, the Hamiltonian Eq. (3.22) is invariant under $x \leftrightarrow -x$ and $z \leftrightarrow -z$, thus it must be invariant under $n\pi$ angle rotations under the y-axis for

n integer, for more references about symmetries in quantum mechanics see Refs. [65, 66]. Hence, we can write for the evolution of the expectation value of any power of the J_x that

$$\mathrm{tr}(e^{+i\theta J_z} J_x^m e^{-i\theta J_z} \rho_\lambda) = \mathrm{tr}(e^{+i\theta J_z} J_x^m e^{-i\theta J_z} e^{-in\pi J_y} \rho_\lambda e^{+in\pi J_y}), \tag{3.24}$$

where $\rho_\lambda = |\mathrm{GS}\rangle\langle\mathrm{GS}|_\lambda$. If the equation above holds, then for the case $n = 1$, we can use the cyclic property of the trace to arrive at

$$\begin{aligned} \mathrm{tr}(e^{+i\pi J_y} e^{+i\theta J_z} J_x^m e^{-i\theta J_z} e^{-i\pi J_y} \rho_\lambda) &= \mathrm{tr}(e^{+i\theta(-1)J_z} (-1)^m J_x^m e^{-i\theta(-1)J_z} \rho_\lambda) \\ &= \mathrm{tr}(e^{-i\theta J_z} (-1)^m J_x^m e^{+i\theta J_z} \rho_\lambda), \end{aligned} \tag{3.25}$$

or equivalently

$$\langle J_x^m(\theta)\rangle_{\rho_\lambda} = \langle (-1)^m J_x^m(-\theta)\rangle_{\rho_\lambda}, \tag{3.26}$$

which implies that for even m, and specially for $m = 2, 4$, the expectation values are an even function of θ, and that for odd m the expectation values are odd functions of θ, which proves the Eq. (3.6) for the present case.

On the other hand for the thermal state ρ_T, we have that its eigenstates are simultaneously eigenstates of J_x, and hence the state invariant under rotations around the x-axis. Which still holds for the entire state, since it is a statistical mixture of states invariant under rotations around the x-axis. Moreover, it is also invariant for the case in which the state is rotated around the x-axis by π angle. Hence, we have for the evolved expectation values of J_x^m that

$$\mathrm{tr}(e^{+i\theta J_z} J_x^m e^{-i\theta J_z} \rho_T) = \mathrm{tr}(e^{+i\theta J_z} J_x^m e^{-i\theta J_z} e^{-i\pi J_x} \rho_T e^{+i\pi J_x}) \tag{3.27}$$

for any m. Finally, using again the cyclic properties of the trace, we flip the signs of the of angular momentum components orthogonal to J_x, so in this case $J_y \to -J_x$ and $J_z \to -J_z$, and we arrive at

$$\mathrm{tr}(e^{+i\pi J_x} e^{+i\theta J_z} J_x^m e^{-i\theta J_z} e^{-i\pi J_x} \rho_T) = \mathrm{tr}(e^{-i\theta J_z} J_x^m e^{+i\theta J_z} \rho_T). \tag{3.28}$$

We conclude that for this case all the moments of the J_x operator are even functions of θ for the thermal state, i.e., $\langle J_x^m(\theta)\rangle_{\rho_T} = \langle J_x^m(-\theta)\rangle_{\rho_T}$, which proves that the Eq. (3.6) holds for this case too.

3.4 Using our method with real experimental data

In reference [92], a state is produced in the laboratory with the proper characteristics of an unpolarized Dicke state, small variance in one direction, say x, and a very large variance in the perpendicular

directions to the x-axis. In the cited experiment with N qubits, it is possible to determine the operator J_x as the population imbalance of the two levels as

$$J_z = \frac{1}{2}(N_+ - N_-), \tag{3.29}$$

where N_m is the number of particles in the state $|m\rangle$, in this case either $|+\rangle$ or $|-\rangle$. Hence, measuring the population imbalance and collecting the statistics of the measurements, the expectation values of all moments of J_x can be obtained. In practice, it is possible to measure the lower order moments like $\langle J_x^2\rangle$ and $\langle J_x^4\rangle$, while higher order moments need too many repetitions of the experiment to collect enough statistics.

The other two global operators J_y and J_z are obtained by rotating the system using a $\frac{\pi}{2}$ microwave coupling pulse before the measurement of the population imbalance. Whether J_y or J_z is obtained depends on the relation between the microwave phase and the phase of the initial BEC. The condensate phase represents the only possible phase reference in analogy to the local oscillator in optics. Intrinsically, it has no relation to the microwave phase, such that it homogeneously average over all possible phase relations. From another point of view, one can also say that the fluctuation of the magnetic field results in a random rotation of the spin around the z-axis. Hence, what is obtained in this case is

$$J_\alpha = \sin(\alpha)J_y + \cos(\alpha)J_z, \tag{3.30}$$

where α is an angle, and we need to consider the average over all possible angles. Effectively, the state has the following form

$$\rho = \frac{1}{2\pi}\int e^{-i\alpha J_x}\rho_0 e^{i\alpha J_x}\,\mathrm{d}\alpha, \tag{3.31}$$

where ρ_0 is what we would obtain if we would have access to the phase reference. Note that the integration over the rotation angle α does not create entanglement. If the state ρ is entangled then ρ_0 has to be also entangled.

Let us see the consequences of our state having the form Eq. (3.31). For the density matrix ρ, since it is invariant under rotations around the x-axis, we have

$$\langle J_\alpha^m\rangle = \langle J_y^m\rangle = \langle J_z^m\rangle \tag{3.32}$$

for all m. Hence the expectation values of $\langle J_y^m\rangle$ and $\langle J_z^m\rangle$ can be obtained from the statistics of measuring J_α. Moreover, for states of the form Eq. (3.31) the unitary dynamics will fulfill the condition Eq. (3.6).

There is a single remaining term in the expression for the achievable precision Eq. (3.18), the

expectation value for $\langle J_x J_y^2 J_x \rangle$, which can be bounded as

$$\begin{aligned}\langle J_x J_y^2 J_x \rangle &= \frac{\langle J_x (J_y^2 + J_z^2) J_x \rangle}{2} = \frac{\langle J_x (J_x^2 + J_y^2 + J_z^2) J_x \rangle - \langle J_x^4 \rangle}{2} \\ &\leqslant \frac{N(N+2)}{8} \langle J_x^2 \rangle - \frac{\langle J_x^4 \rangle}{2},\end{aligned} \tag{3.33}$$

where the last inequality is due to that for all states $\langle \boldsymbol{J}^2 \rangle \leqslant \mathcal{J}_N/2$, see Eq. (A.3), while symmetric states saturate the inequality in Eq. (3.33). Note that obtaining $\langle J_x J_z^2 J_x \rangle$ can be hard experimentally. In any case, this simplification can only make our estimation of the precision worse while for symmetric states the equality holds. Hence, the lower bound for the achievable precision can be written as

$$(\Delta\theta)^2_{\text{opt}} \leqslant \frac{\sqrt{(\Delta J_x^2)^2 (\Delta J_y^2)^2} + \langle J_y^2 \rangle + \frac{3N(N+2)-8}{4} \langle J_x^2 \rangle - 2 \langle J_x^2 \rangle \langle J_y^2 \rangle - 3 \langle J_x^4 \rangle}{4 \langle J_y^2 - J_x^2 \rangle^2}, \tag{3.34}$$

where some terms were reordered and further simplified.

It is worth to study the case appearing in Ref. [58] and apply our methods such that we obtain conclusions about the metrological usefulness of the state. The system under consideration has around $N = 7900$. Note that using the expectation value of the particle number, in our case $\langle N \rangle = 7900$, cannot overestimate any lower bound on the precision. For a discussion about entanglement criteria in systems with particle number fluctuations see Ref. [93]. The measured data for the system yields

$$\begin{aligned}\langle J_x^2 \rangle &= 112 \pm 31, & \langle J_y^2 \rangle &= 6 \times 10^6 \pm 0.6 \times 10^6, \\ \langle J_x^4 \rangle &= 40 \times 10^3 \pm 22 \times 10^3, & \langle J_y^4 \rangle &= 6.2 \times 10^{13} \pm 0.8 \times 10^{13}.\end{aligned} \tag{3.35}$$

Hence, we obtain the maximum precision as

$$\frac{(\Delta\theta)^{-2}_{\text{opt}}}{N} \geqslant 3.7 \pm 1.5. \tag{3.36}$$

The statistical uncertainties of Eqs. (3.35) and (3.36) have been obtained through bootstraping, while the direct substitutions of expectation values would yield to 3.3 of gain over the shot-noise limit $(\Delta\theta)^{-2} = N$. Based on Eq. (2.66), this proves the presence of metrologically useful entanglement [15]. Based on Eq. (2.67), it even demonstrated that the quantum state had metrologically useful 4-particle entanglement. Assuming an error of a standard deviation, Eq. (3.36) still proves 3-particle entanglement.

Next we plot the value for the precision substituting directly the experimental data into Eq. (3.16),

see Figure 3.4. Since we cannot obtain the expectation value $\langle J_x J_y^2 J_x \rangle$ we approximate it with the

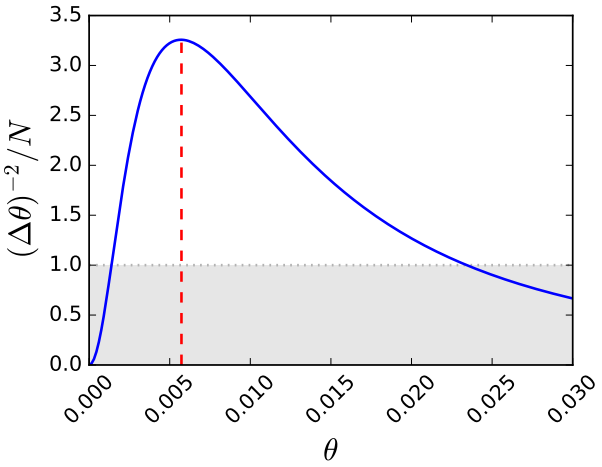

Figure 3.4: (solid) The precision as a function of the parameter θ given by Eq. (3.16) varies through the evolution. Note that for the initial moment the precision is zero. (dashed) We highlight where the precision reaches its maximum at $\theta \approx 0.0057$. (gray-area) It represent the region where the precision is below the shot-noise limit.

right-hand side of Eq. (3.33). With that we underestimate $(\Delta\theta)^{-2}$.

Thus, we could detect metrological usefulness by measuring the second and fourth moments of the collective angular momentum components. For future applications of our scheme, it is important to reduce further the number of quantities we need to obtain a lower bound for the precision. In practice, one can easily avoid the need for determining $\langle J_y^4 \rangle$. Note that if we measure J_y then the distribution of the values obtained is strongly non-Gaussian. The values $\pm N/2$ appear most frequently, and the value 0 appears least frequently [20]. See also the distribution of a pure Dicke state when $\theta = \pi/2$ in the Figure 3.1. The state has more overlap with the eigenstates of the edges than in the middle. Based on $\langle AB \rangle \leqslant \lambda_{\max}(A)\langle B \rangle$, where $\lambda_{\max}(A)$ is the largest eigenvalue of A, for two commuting positive-semidefinite observables,

$$\langle J_y^4 \rangle \leqslant \frac{N^2}{4}\langle J_x^2 \rangle. \tag{3.37}$$

Since even for a noisy Dicke state $\langle J_y^2 \rangle$ is very large, the above equation is a very good upper bound. Substituting it into the Eq. (3.18), we will underestimate $(\Delta\theta)^{-2}$.

It is also possible to approximate $\langle J_x^4 \rangle$ with $\langle J_x^2 \rangle$ in the sense that it is small and that mainly its value comes from technical noise,

$$\langle J_x^4 \rangle \approx \beta \langle J_x^2 \rangle^2. \tag{3.38}$$

This approximation, even if it is not a strict bound on the precision, can be very useful in order to

characterize the metrological usefulness of the state based only on second statistical moments of only two angular momentum components, namely $\langle J_y^2 \rangle$ and $\langle J_x^2 \rangle$. Those two expectation values are related with how thin is the state in one direction and how wide in the perpendicular ones. So in this case we use $\beta = 3$ assuming that the distribution function has a Gaussian shape.

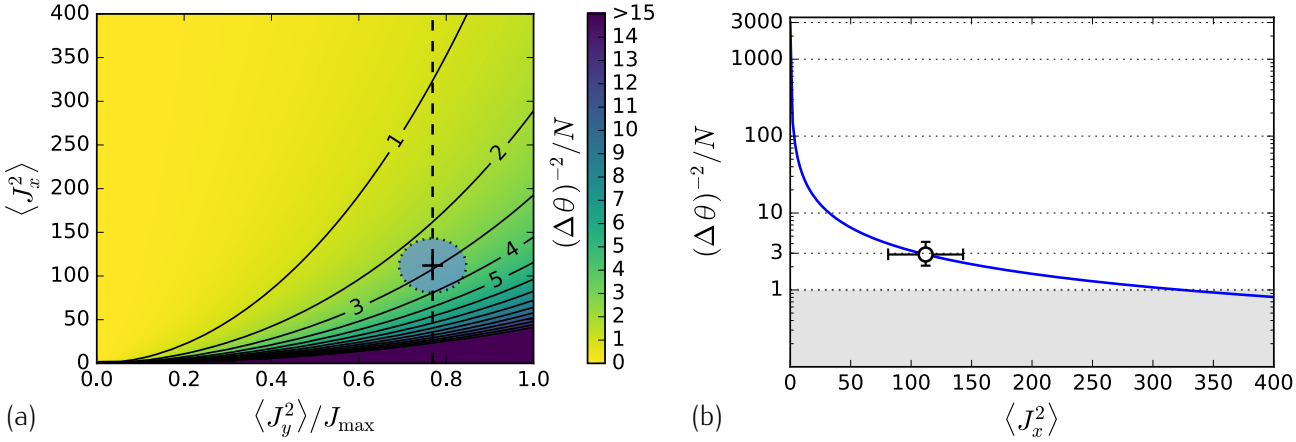

Figure 3.5: (a) Precision bound as a function of $\langle J_y^2 \rangle$ and $\langle J_x^2 \rangle$. The expectation value $\langle J_y^2 \rangle$ is normalized with $J_{\max}$ or equivalently with $\mathcal{J}_{N/2}$. (solid) Different boundaries for metrologically useful entanglement depths are shown with solid lines. (cross) and (blue-ellipse) Those elements stand for the point corresponding to the experimental data and the region with one σ confidence, respectively. (dashed) This corresponds to the constant $\langle J_y^2 \rangle$ cross section plotted next. (b) Constant $\langle J_y^2 \rangle$ cross section for the precision bound. (solid) Precision bound based on the Eq. (3.39). One can see that decreasing further the uncertainty in $\langle J_x^2 \rangle$ can improve the bound significantly. (white-point) Experimental data with the corresponding errors. Even if the point is slightly below the 4-particle entanglement level, we can say that with only two second moments, we characterize the state in such a way that it does not differ very much from the original prediction when fourth moments were also included and 4-particle entanglement was witnessed for the system.

From these considerations we are able to write a second bound with fewer expectation values for the optimal precision such that

$$(\Delta\theta)^2_{\text{opt}} \leqslant \frac{\langle J_y^2 \rangle + \frac{3N(N+2)-8}{4}\langle J_x^2 \rangle + \left(\sqrt{\frac{N^2}{2\langle J_y^2 \rangle} - 2} - 2\right)\langle J_y^2 \rangle \langle J_x^2 \rangle - 9\langle J_x^2 \rangle^2}{4\langle J_y^2 - J_x^2 \rangle^2}. \tag{3.39}$$

We have used this formula to compute the bound for the optimal precision with the measured data shown on Eq. (3.35), $(\Delta\theta)^{-2}_{\text{opt}} \geqslant 2.9N$, see Figure 3.5. It turns out that even this way, 3-particle metrologically useful entanglement is detected. Figure 3.5-(a) shows the two-dimensional plot which is obtained based on these considerations. The regions with various levels of multipartite entanglement ca clearly be identified. The ideal Dicke state corresponds to the bottom-right corner. In Figure 3.5-(b), the cross section of the two-dimensional plot is shown.

4 Witnessing metrologically useful entanglement

"All the truths of mathematics are linked to each other, and all means of discovering them are equally admissible."
Adrien-Marie Legendre

Typically, one has not access to the density matrix of the system been used for metrology or for other quantum process. Moreover, for systems on which the particle number is very large, this is the case when one wants to do metrology with quantum states, the details of the density matrix are forbidden by practical reasons. Since the quantum Fisher information is based on the complete knowledge of the density matrix, shortcuts to avoid the complete tomography must be developed as we have had shown one practical case on the previous chapter. In this chapter, we obtain a general procedure to get an optimal bound for the quantum Fisher information based on as many expectation values of the initial state as one is ready to measure. Two main features are worth to mention again. First, in general this method gives us an optimal tight bound. Last but not least, the bound is based on the expectation values of the initial state only, so it is not necessary to perform an evolution of the state to estimate how well will it behave. This is in contrast to other approaches one can find in the literature, an it is a time saving concept.

The figure of merit of bounds from below for the quantum Fisher information based on expectation

values of the initial state is the following,

$$\mathcal{F}_{\mathrm{Q}}[\rho, J_z] \geqslant \frac{\langle J_x \rangle^2}{(\Delta J_y)^2}. \tag{4.1}$$

where the state is polarized along the x-axis and the variance of the J_y operator is smaller than the standard. On the previous chapter we also have shown one of these bound specifically designed for unpolarized Dicke states.

Homogeneous magnetometry, $\boldsymbol{B} = B\boldsymbol{k}$ where B is constant in time.

Section [REF], see magnetometry, generator J_z.

Quantum Fisher information $\mathcal{F}_{\mathrm{Q}}[\rho, J_z]$.

4.1 Bound from below of a function convex over the states given some arbitrary expectation values

The problem of getting a lower bound for a convex function on the states having already some expectation values of some arbitrary observables was studied by O. Gühne *et al.* and J. Eisert *et al.* in Refs. [94, 95] respectively, mainly from the perspective of entanglement measures. The illustrated techniques are based on the well known Legendre transform for differentiable functions, see Appedix G for more details. We first review in this section the state-of-the-art solution for this problem. And later on, we extend it to the quantum Fisher information. For simplicity in the next subsection, Sec ??, we assume that a single expectation value is given. An extension to the case on which more expectation values are given will follow in the Subsection ??. Finally, we will summarize it with an explicit formula which will be used to compute the bounds.

4.1.1 Estimation of a general convex function based on the expectation value of an arbitrary observable

When a convex function $g(\rho)$ is given together with an expectation value of some operator $w = \mathrm{tr}(\rho W)$, a tight lower bound, $\mathcal{B}_g(w)$, can be obtained as [94–96]

$$\begin{aligned} g(\rho) \geqslant \mathcal{B}_g(w) &:= \sup_r \{rw - \hat{g}(rW)\} \\ &= \{\inf_\rho g(\rho) \,|\, w = \mathrm{tr}(\rho W)\} \end{aligned} \tag{4.2}$$

where $\hat{g}(rW)$ is the Legendre transform of $g(\rho)$ and the second equality expresses the tightness of the bound. The Legendre transform in this context is defined as

$$\hat{g}(rW) = \sup_{\rho}\{\langle rW\rangle_{\rho} - g(\rho)\}, \tag{4.3}$$

where the maximisation is over *all* possible states. This method to obtain the lower bound has been used to compute entanglement measures, as we mentioned before [].

Following the theory one can find that in the case on which the convex function $g(\rho)$ is defined as convex roof over all possible convex decompositions of the state, the optimisation of Eq. (4.3) can be reduced to an optimisation over pure states only, thus simplifying the process []

$$\begin{aligned}
\hat{g}(rW) &= \sup_{\rho}\{\langle rW\rangle_{\rho} - g(\rho)\} \\
&= \sup_{\rho}\Big\{r\langle W\rangle_{\rho} - \inf_{\{p_k,|\phi_k\rangle\}}\big\{\sum_k p_k g(|\phi_k\rangle)\big\}\Big\} \\
&= \sup_{\{p_k,|\phi_k\rangle\}}\Big\{\sum_k p_k\langle rW\rangle_{|\phi_k\rangle} - \inf_{\{p_k,|\phi_k\rangle\}}\big\{\sum_k p_k g(|\phi_k\rangle)\big\}\Big\} \\
&= \sup_{\{p_k,|\phi_k\rangle\}}\Big\{\sum_k p_k\big\{\langle rW\rangle_{|\phi_k\rangle} - g(|\phi_k\rangle)\big\}\Big\} \\
&= \sup_{|\psi\rangle}\big\{\langle rW\rangle_{|\psi\rangle} - g(|\psi\rangle)\big\}.
\end{aligned} \tag{4.4}$$

However, even an optimization over all pure states is feasible numerically only for small systems. We will show later on this section how to circumvent this issue in the case of the QFI. The convex roof construction has the following form

$$g(\rho) = \inf_{\{p_k,\psi_k\}}\sum_k p_k g(|\psi_k\rangle), \tag{4.5}$$

where the mixed state is decomposed into $\rho = \sum_k p_k|\psi_k\rangle\langle\psi_k|$. Among other definitions of the QFI on the literature, there is one that defines it as the convex roof of $4(\Delta J_z)^2$, the variance of the generator, as it has been shown on Ref. [97**?**], we can compute the Legendre transform optimizing for pure states only. Hence, we will be able to use this simplification to apply this method to obtain the lower bound on the QFI. Notice that in this context the QFI is the convex roof of four times the variance of the generator, Eq. (**??**).

4.1.2 Measuring several observables

For some cases, it is interesting to characterise the quantum state not only with a single measurement but with several. For instance, we could want to use, as it is done with the spin-squeezed states the absolute polarisation and the variance of one of the orthogonal components of the angular momentum to detect entanglement and metrological usefulness []. So far, we studied the case on which a single measurement is used. Its extension to several expectation values is indeed straight-forward. We can generalize Eqs. (4.2) and (4.3) for several observables $\{W_i\}_{i=1}^M$ as follows [94]

$$\mathcal{B}_g(w_1, w_2, \dots) := \sup_{\boldsymbol{r}} \left\{ \boldsymbol{r}\boldsymbol{w} - \sup_{\rho} \{ \langle \boldsymbol{r}\boldsymbol{W} \rangle - g(\rho) \} \right\}, \tag{4.6}$$

where $\boldsymbol{a}\boldsymbol{b} = \sum_{k=1}^M a_k b_k$, the usual notation for scalar products of two vectors.

4.1.3 Explicit form of the expression to be optimized

After we have shown how to find a lower bound for a general convex function of the state based on its expectation values and how to simplify that method for the case on which the function is defined as convex roof, now we are in a position to achieve the main goal of this chapter. First of all, we notice that for the quantum Fisher Information the inner maximization, the Legendre transform, is obtained optimizing a quadratic function on expectation values,

$$\begin{aligned} \hat{\mathcal{F}}_{\mathrm{Q}}(rW) &= \sup_{|\psi\rangle} \left\{ r\langle W \rangle_\psi - 4(\Delta J_z)^2_\psi \right\} \\ &= \sup_{|\psi\rangle} \left\{ r\langle W \rangle_\psi - 4\langle J_z^2 \rangle_\psi + 4\langle J_z \rangle^2_\psi \right\} \\ &= \sup_{|\psi\rangle} \left\{ \langle rW - 4J_z^2 \rangle_\psi + \langle 2J_z \rangle^2_\psi \right\}, \end{aligned} \tag{4.7}$$

where we have used the fact that the QFI can be expressed as convex roof of $(\Delta J_z)^2$ and we again fall into the problem of a single parameter for simplicity on the following derivations. Equation (4.7) can be rewritten as an optimization linear in operator expectation values and over a parameter μ as

$$\hat{\mathcal{F}}_{\mathrm{Q}}(rW) = \sup_{|\psi\rangle, \mu} \left\{ \langle rW - 4J_z^2 \rangle_\psi + 8\mu \langle J_z \rangle_\psi - 4\mu^2 \mathbb{I} \right\}, \tag{4.8}$$

which, making use of $\max\{\langle A\rangle\} = \lambda_{\max}[A]$ for any observable, can be reformulated as

$$\begin{aligned}\hat{\mathcal{F}}_{\mathrm{Q}}(rW) &= \sup_{|\psi\rangle}\left\{\lambda_{\max}[rW - 4J_z^2 + 8\mu J_z - 4\mu^2]\right\} \\ &= \sup_{|\psi\rangle}\left\{\lambda_{\max}[rW - 4(J_z-\mu)^2]\right\}\end{aligned} \tag{4.9}$$

where we omitted in writing $\mathbb{I}$ for clarity and $\lambda_{\max}[A]$ stands for the maximum eigenvalue of the operator A. At the extremum, we make the following observation, the derivative with respect to μ must be zero, hence at the optimum $\mu = \langle J_z\rangle_{\mathrm{opt}}$ which represents the expectation value J_z should have considering the optimal state on Eq. (4.7). This also means that we have to test μ values in the interval $-N/2 \leqslant \mu \leqslant N/2$ only for spin-half systems.

The full optimization problem to be solved consists of Eqs. (4.2) and (4.9) substituting $g(\rho)$ by $\mathcal{F}_{\mathrm{Q}}[\rho, J_z]$,

$$\mathcal{B}_{\mathcal{F}}(w) = \sup_r\left\{rw - \sup_{\mu}\{\lambda_{\max}[rW - 4(J_z-\mu)^2]\}\right\}. \tag{4.10}$$

It is crucial that the optimization over r is a concave function, since the theory tells us that $\hat{\mathcal{F}}_{\mathrm{Q}}(rW)$ is a convex function [], even when the multi-parametric case is considered. Thus the optimum can be determined easily with simple methods, e.g., the gradient method, looking for the maximum in r. Based on Eq. (4.2), we can see that even if we do not find the global optimum in r, we obtain a valid lower bound. The extension of this bound to the multi-parametric case is done using the recipie given in Eq. (4.6). On the other hand, the function to be optimized for μ does not have a single maximum in general. Moreover, not finding the optimal μ leads to an overestimating of the bound. Thus, a large care must be taken especilly when optimizing over μ.

We stress again the generality of this findings beyond linear interferometers covered on the following sections. For nonlinear interferometers [], the phase θ must be estimate in an unitary dynamics $U = \exp -iG\theta$, where G is not a sum of single spin operators, hence, is different from the angular momentum components.

Next, we will demonstrate the use of our approach for several experimentally relevant situations. In the many-particle case, often symmetric operators can be used to describe accurately the system, which makes possible to carry out calculations for thousand of particles, as will be presented later on this chapter.

4.2 Examples

In this section, we show how to obtain lower bounds based of the fidelities with respect to the GHZ state and the unpolarized Dicke state as well as with different configurations of powers of collective angular momentum operators, e.g., the set $\{\langle J_y\rangle, \langle J_x\rangle, \langle J_x^2\rangle\}$.

4.2.1 Exploiting symeetries

When making calculations for quantum systems with an increasing number of qubits, we soon run into difficulties when computing the largest eigenvalue of Eq. (4.9). The reason is that for N qubits, we need to handle $2^N \times 2^N$ size matrices, hence we are limited to systems of 10 to 15 qubits.

We can obtain bounds for much larger particle numbers, if we restrict ourselves to the symmetric subspace []. This approach can give optimal bounds for many systems, such as Bose-Einstein condensates of two-level atoms, which are in a symmetric multiparticle state. The bound computed for the syymmetric subspace might be not correct and generally overestimated for general cases.

Finally, it is important to note that if the operators W_k are permutationally invariant (PI) and the eigenstate with the maximal eigenvalue in Eq. (4.9) is non-degenerate. And the resulting maximal eigenvalue is the same ...

We follow presenting the proof of the recently mentioned observation for completeness. Let us denote the ground state of a permutationally invariant Hamiltonian by $|\Psi\rangle$ This is at the same time the $T = 0$ thermal ground state, hence it must be a permutationally invariant pure state. For such states $S_{kl}|\Psi\rangle\langle\Psi|S_{kl} = |\Psi\rangle\langle\Psi|$, where S_{kl} is the swap operator exchanging qubits k and l. Based on this, follows that $S_{kl}|\Psi\rangle = c_{kl}|\Psi\rangle$, and $c_{kl} \in -1, +1$. There are three possible cases to consider:

i) All $c_{kl} = +1$. In this case, for all permutation operator Π_j we have

$$\Pi_j|\Psi\rangle = |\Psi\rangle, \tag{4.11}$$

since any permutation operator Π_j can be constructed as $\Pi_j = \prod_i S_{k_i l_i}$. Equation (4.11) means that the state $|\Psi\rangle$ is symmetric.

ii) All $c_{kl} = -1$. This means that the state is antisymmetris, however this state exists only for $N = 2$ qubits.

iii) Not all c_{kl} are identical to each other. In this case, there must be k_+, l_+, k_-, k_- such that

$$\begin{aligned} S_{k_+,l_+}|\Psi\rangle &= +|\Psi\rangle, \\ S_{k_-,l_-}|\Psi\rangle &= -|\Psi\rangle. \end{aligned} \tag{4.12}$$

Let us assume that k_+, l_+, k_-, l_- are index different from each other. In this case, $|\Psi'\rangle = S_{k_+,k_-}S_{l_+,l_-}|\Psi\rangle$ another ground state of the Hamiltonian H such that

$$\begin{aligned} S_{k_+,l_+}|\Psi'\rangle &= -|\Psi'\rangle, \\ S_{k_-,l_-}|\Psi'\rangle &= +|\Psi'\rangle. \end{aligned} \tag{4.13}$$

Comparing Eqs. (4.12) and (4.13) we can conclude that $|\Psi'\rangle \neq |\Psi\rangle$, while due to the permutational invariance of H we have that $\langle H\rangle_{\Psi'} = \langle H\rangle_{\Psi}$. Thus, $|\Psi\rangle$ is not a non-degenerate ground state. The proof works in an analogous way for the only nontrivial case $k_+ = k_-$, when $S_{k_+,k_-} = \mathbb{I}$.

Hence, if $N > 2$ then only i) is possible and $|\Psi\rangle$ must be symmetric.

4.2.2 Fidelity measurements

Let us consider the case when W is a projector onto a pure quantum state. First, we consider GHZ states [] hence W is the projector $|\mathrm{GHZ}\rangle\langle\mathrm{GHZ}|$ and $\langle W\rangle = F_{\mathrm{GHZ}}$, the fidelity with respect to the GHZ state. Based on knowing F_{GHZ}, we would like to estimate $\mathcal{F}_{\mathrm{Q}}[\rho, J_z]$[‡].

Using Eqs. (??) and (??), we will obtain an analytical tight lower bound on the QFI based on the fidelity F_{GHZ}. The calculation that we have to carry out is computing the bound

$$\mathcal{B}_{\mathcal{F}}(F_{\mathrm{GHZ}}) = \sup_r \left\{ rF_{\mathrm{GHZ}} - \sup_\mu \{\lambda_{\max}[r|\mathrm{GHZ}\rangle\langle\mathrm{GHZ}| - 4(J_z-\mu)^2]\}\right\}. \tag{4.14}$$

We will make our calculations in the J_z orthonormal basis, which is defined with the 2^N basis vectors $b_0 = |00\ldots000\rangle$, $b_1 = |00\ldots001\rangle$, ..., $b_{(2^N-2)} = |11\ldots110\rangle$, and $b_{(2^N-1)} = |11\ldots111\rangle$. It is easy to see that the matrix in the argument of $\lambda_{\max}$ in the Eq. (4.14) is almost diagonal in the J_z basis. To be more specific, the only non-diagonal matrix block comes from $|\mathrm{GHZ}\rangle\langle\mathrm{GHZ}|$, which has non-trivial

[‡] Not a tight lower bounds on the quantum Fisher information based on the fidelity have been presented in [].

matrix elements only in the $\{b_0, b_{(2^N-1)}\}$ basis. Thus, we have to diagonalize the following matrix

$$r|\mathrm{GHZ}\rangle\langle\mathrm{GHZ}| - 4(J_z-\mu)^2 = \begin{pmatrix} \frac{r}{2} - 4(\frac{N}{2}-\mu)^2 & \frac{r}{2} \\ \frac{r}{2} & \frac{r}{2} - 4(\frac{N}{2}+\mu)^2 \end{pmatrix} \oplus D, \tag{4.15}$$

where D is already a $(2^N-2)\times(2^N-2)$ diagonal matrix with $D_k = -4(\langle J_z\rangle_{b_k} - \mu)^2$ negative eigenvalues for $k = 1, 2, \ldots, (2^N-2)$. This means that the Eq. (4.15) can be diagonalized as $\mathrm{diag}[\lambda_+, \lambda_-, D_1, D_2, \ldots, D_{2^N-2}]$, where the two eigenvalues $\lambda_\pm$ are

$$\lambda_\pm = \frac{r}{2} - N^2 - 4\mu^2 \pm \sqrt{16\mu^2N^2 + \frac{r^2}{4}}. \tag{4.16}$$

Next, we show a way that can simplify our calculations considerably. As indicated in Eq. (4.14), we have to look for the maximal eigenvalue and then optimize it over μ. We exchange the order of the two steps, that is, we look for the maximum of each eigenvalue over μ, and then find the maximal one. Clearly based on the fact that the eigenvalues of D are negative an that we can find a μ such that D_k equal zero but not positive. Due to this, the problem can be simplified to the following equation

$$\begin{aligned} \sup_\mu\{\lambda_{\max}[r|\mathrm{GHZ}\rangle\langle\mathrm{GHZ}| - 4(J_z-\mu)^2]\} &:= \max\{0, \sup_\mu(\lambda_+)\} \\ &= \begin{cases} 0, & \text{if } r < 0, \\ \dfrac{r}{2} + \dfrac{r^2}{16N^2} & \text{if } 0 \leqslant r \leqslant 4N^2, \\ -N^2 + r, & \text{if } r > 4N^2, \end{cases} \end{aligned} \tag{4.17}$$

where we did not have to have to look for the maximum of λ_- over μ since clearly $\lambda_+ \geqslant \lambda_-$. Finally, we have to substitute Eq. (4.17) into Eq. (4.14), and carry out the optimization over r, considering $F_{\mathrm{GHZ}} \in [0, 1]$.

This way we arrive at the solution for the lower bound of the QFI base on the fidelity with respect to the GHZ state as

$$\mathcal{B}_{\mathcal{F}}(F_{\mathrm{GHZ}}) = \begin{cases} N^2(1-F_{\mathrm{GHZ}})^2, & \text{if } F_{\mathrm{GHZ}} < 1/2, \\ 0, & \text{if } F_{\mathrm{GHZ}} \leqslant 1/2. \end{cases} \tag{4.18}$$

This equation is plotted in Figure 4.1.a. Note that in the figure the plot is normalized by N^2 and that the resulting semi-parabola is independent of the number of particles. Moreover, the bound is zero for $F_{\mathrm{GHZ}} \leqslant 1/2$. This is consistent with the fact that for the product states $\rho = |111\ldots11\rangle$ or $\rho = |000\ldots00\rangle$ we have $F_{\mathrm{GHZ}} = 1/2$, while $\mathcal{F}_{\mathrm{Q}}[\rho, J_z] = 0$.

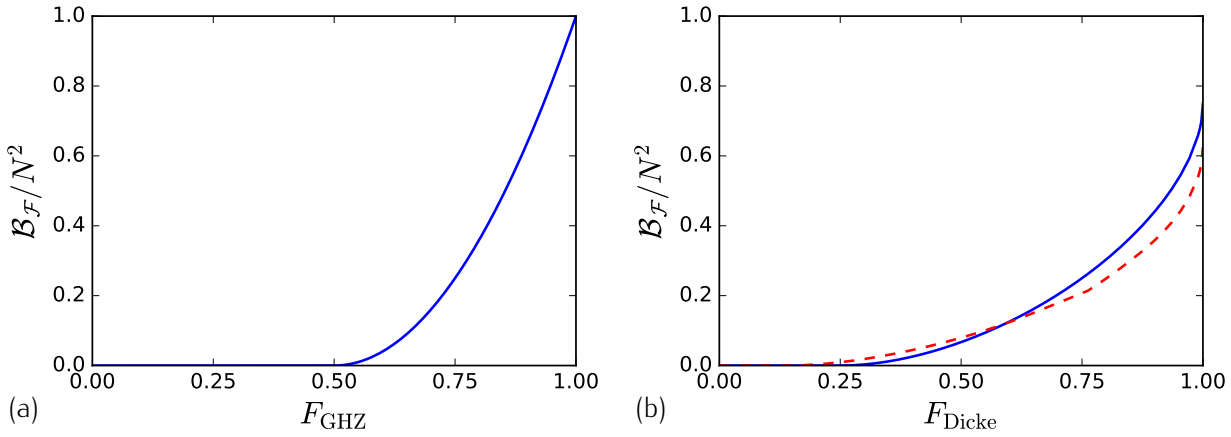

Figure 4.1: (a) Analytical solution of the bound $\mathcal{B}_\mathcal{F}$ for different values of the fidelity with respect to the GHZ state. (b) Numerical results for the minimum quantum Fisher information as a function of the fidelity with respect of unpolarise Dicke states perpendicular to the magnetic field, $|\mathrm{D}_N^0\rangle$. (blue-line) For systems with 4 particles and (red-dashed) for system with 8 particles. One may notice that when the fidelity is at its maximum the bound approaches to 0.5 as it is the quantum Fisher information for large particle number.

Next, let us consider symmetric unpolarized Dicke state with even N particles along the x-direction, which is given by

$$|\mathrm{D}_{N,N/2}\rangle_x = \binom{N}{N/2}^{-\frac{1}{2}} \sum_k \Pi_k(|1\rangle_x^{\otimes N/2}|0\rangle_x^{\otimes N/2}), \tag{4.19}$$

where the summation is over all the different permutations, Π_k, of the product state having $N/2$ particles in $|1\rangle_x$ and the rest $N/2$ in the $|0\rangle_x$ state, the single qubit $j_x^{(n)}$ basis states.

This state is known to be highly entangled [] and allows for Heisenberg limited interferometry []. In the following we will omit the second subscript and we use the notation $|\mathrm{D}_N\rangle_x \equiv |\mathrm{D}_{N,N/2}\rangle_x$, where we even may skip the subscript x since this Dicke state will be always in the center of our attention, the unpolarized Dicke state perpendicular to the magnetic field in this case along the z-direction. The witness operator that can be used for noisy Dicke states is $W = |D_N\rangle\langle D_N|$, hence the expectation value of the witness is just the fidelity with respect to the Dicke state, i.e., $\langle W\rangle = F_{\mathrm{Dicke}}$. In Figure 4.1.b, we plotted the results for symmetric Dicke states of various spin numbers. $F_{\mathrm{Dicke}} = 1$ corresponds to $\mathcal{F}_\mathrm{Q}[\rho, J_z] = N(N+2)/2$. At this point, note that for the examples presented above, the QFI bound scales as $\mathcal{O}(N^2)$ in the asymptotic limit if the quantum state has been prepared perfectly[§].

Note that estimating $\mathcal{F}_\mathrm{Q}[\rho, J_z]$ based on F_{Dicke} was possible for 40 qubits [TD: Ask geza for the data points for 40 particles] for Fig 4.1.b, since we carried out the calculations for the symmetric

[§] $\mathcal{O}(x)$ is the usual Landau notation used to describe the asymptotic behavior for large x [].

subspace. For our case, the witness operator W is permutationally invariant and it has a non-degenerate eigenstate corresponding to the maximal eigenvalue. Hence, based on the arguments of the Section ?? the bound is valid even for general case, i.e., non-symmetric states.

We now compute several quantities for the large N case. We show that if the fidelity with respect to the Dicke state is larger than a bound then $\mathcal{B}_{\mathcal{F}} > 0$, where we omit the arguments for brevity. Moreover, we have seen in Figure 4.1.b that the lower bound on $\mathcal{F}_{\mathrm{Q}}[\rho, J_z]$ as a function of the fidelity F_{Dicke} normalized by N^2 is not the same curve for all N. Next, we will demonstrate by numerical evidence that the lower bound normalized by N^2 collapses to a nontrivial curve for large N.

As a first step, let us consider the completely polarized state along z-direction $|1\rangle_y^{\otimes N}$. This state does not change under rotations around the z-axis, hence $\mathcal{F}_{\mathrm{Q}}[\rho, J_z] = 0$. Its fidelity with respect to the Dicke state, Eq. (4.19), is

$$F_{\mathrm{Dicke}}(|1\rangle_y^{\otimes N}) = \frac{1}{2^N}\binom{N}{N/2} \approx \sqrt{\frac{2}{\pi N}} \tag{4.20}$$

From convexity of the bound on the quantum Fisher information in F_{Dicke}, it immediately follows that for F_{Dicke} smaller than Eq. (4.20) the optimal bound on $\mathcal{F}_{\mathrm{Q}}[\rho, J_z]$ will give zero.

Next, we examine what happens if the fidelity is larger than Eq. (4.20). For that we notice first that $\mathcal{F}_{\mathrm{Q}}[\rho, J_z]$ is the convex roof of $4(\Delta J_z)^2$ []. Hence, if we have a mixed state for which $\mathcal{F}_{\mathrm{Q}}[\rho, J_z]$ is zero, then it can always be decomposed into the mixture of pure states for which $\mathcal{F}_{\mathrm{Q}}[|\Psi\rangle, J_z]$ is zero too. As a consequence, the extremal states of the set of states for which $\mathcal{F}_{\mathrm{Q}}[\rho, J_z] = 0$ are pure states, and we can restrict our search for pure states. The optimization problem we have to solve is given as

$$F_{\mathrm{opt}} = \left\{ \max_{\Psi} |\langle\Psi|\mathrm{D}_N\rangle_x|^2 \,|\, \mathcal{F}_{\mathrm{Q}}[|\Psi\rangle, J_z] = 0 \right\}. \tag{4.21}$$

Pure states $|\Psi\rangle$ that are invariant under $U_\theta = \exp(-iJ_z\theta)$ for any θ. Such states are the eigenstates of J_z. In order to maximize the overlap with the Dicke state $|\mathrm{D}_N\rangle_x$, we have to look for symmetric eigenstates of J_z. These are the symmetric Dicke states in the z-basis $|\mathrm{D}_{N,m}\rangle_z$. Then, using the following identity

$$\sum_{k=0}^{q}\binom{n}{k}\binom{n}{q-k}(-1)^k = \begin{cases}\binom{n}{q/2}(-1)^{q/2}, & \text{for even } q,\\ 0, & \text{for odd } q.\end{cases} \tag{4.22}$$

one finds that the squared overlap is given by

$$|\langle \mathrm{D}_{N,m}|_z|\mathrm{D}_N\rangle_x|^2 = \begin{cases} \frac{\binom{N/2}{m/2}^2\binom{N}{N/2}}{2^N\binom{N}{m}}, & \text{for even } m \text{ and } N, \\ 0, & \text{for odd } m, \end{cases} \tag{4.23}$$

which maximal, in the case of even N, when $m = N$ or $m = 0$, thus the totally or anti-totally polarized states respectively. We skip the case on which N is odd. For detailed calculations of Eq. (4.23) see Appendix D.

Next, we will examine the behavior of our lower bound on $\mathcal{F}_{\mathrm{Q}}[\rho, J_z]$ based on the fidelity F_{Dicke} for large N. In figure **??** [TD: Ask Geza for the data], the calculations up to $N = 500$ present a strong evidence that for fidelity values $F_{\mathrm{Dicke}} = 0.2, 0.5, 0.8$ the lower bound on QFI has a $\mathcal{O}(N^2)$ scaling for increasing N. If this is correct then reaching a fidelity larger than a certain monotonously decreasing bound for large N would imply Heisenberg scaling for the bound on the quantum Fisher information. Note that it is difficult to present a similar numerical evidence for small values of F_{Dicke} since in that case the bound for QFI is nonzero only for large N due to Eq. (4.20).

4.2.3 Spin-squeezed states

In the case of spin squeezing, the quantum state has a large spin in the y-direction, while a decreased variance in the x-direction. By measuring $\langle J_y\rangle$ and $(\Delta J_x)^2$ we can estimate the lower bound for the quantum Fisher Information by Eq. (**??**). However, this formula does not necessarily give the best lower bound for all values of the collective observables. With our approach we can find the best bound.

To give a concrete example, we choose $W_1 = J_y$, $W_2 = J_x^2$ and $W_3 = J_x$ for the operators to be measured. We vary w_1 and w_2 in some interval. We also require that $w_3 = 0$, since we assume that the mean spin points into the y-direction[¶] This is reasonable since in most spin-squeezing experiments we know the direction of the mean spin.

Our result can be seen in Figure 4.2. We chose $N = 4$ particles since for small N the main features of the plot are clearly visible. The hatched area correspond to non-physical conbination of expectation values. States at the boundary can be obtained as ground states of $H^{(\pm)}_{\mathrm{bnd}}(\lambda) = \pm J_x^2 - \lambda J_y$, see Appendix E. In Figure 4.2, the state fully polarized in the y-direction, and initial state for

[¶] Due to symmetries of the problem, when minimizing $\mathcal{F}_{\mathrm{Q}}[\rho, J_z]$ with the constraints on $\langle J_z\rangle$ and $\langle J_x^2\rangle$, we do not have to add explicitly the constraint $\langle J_x\rangle = 0$. Optimization with only the first two constraints will give the same bound (see Section **??**).

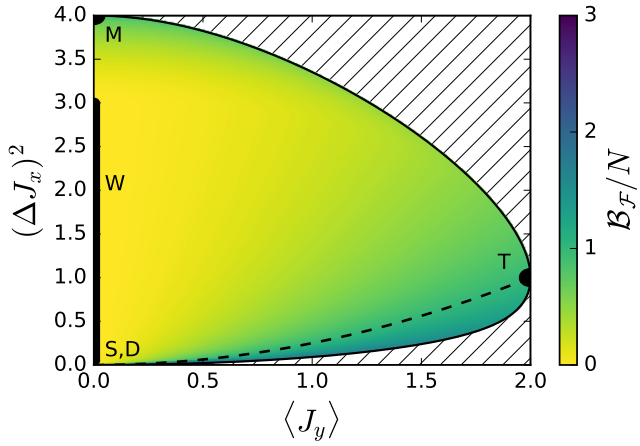

Figure 4.2: We show as a function of the expectation value, $\langle J_y \rangle$, and the variance in the perpendicular direction, $(\Delta J_x)^2$, the minimum sensitivity for a 4-qubit system. (hatched) The physically forbidden region is indicated. (M,T,S,D) Those points indicate where the mixed state (), the totally polarized state (), the single state and the unpolarized Dicke state would be located. (W) on this line sit any of the states which is a mixture between the completely mixed state of the symmetric subspace and the singlet state among others, for instance the completely mixed state of the whole Hilbert space. (dashed) It indicates the shot-noise threshold where below it non-classical sensitivities can be achieved.

spin-squeezing experiments, corresponds to point T. The unpolarized Dicke state along x-direction Eq. (4.19) corresponds to point D. We add that outside the symmetric subspace, there are other states with $\langle J_y \rangle = \langle J_x^2 \rangle = 0$, which also corresponds to point D (in this case denoted by point S). For example, such a state is the multiparticle singlet corresponding to point S. However, usual spin-squeezing procedures remain in the symmetric subspace, thus we discuss only the Dicke state. Spin squeezing makes $(\Delta J_x)^2$ decrease, while $\langle J_y \rangle$ aslo decreased somewhat. Hence, at least for small squeezing it corresponds moving down from point T to point D following the boundary, while the metrological usefulness is increasing. Below the dashed line $\mathcal{F}_Q[\rho, J_z] > N$, hence the state possesses metrologicaly useful entanglement []. The equal mixture of $|000\ldots00\rangle_x$ and $|111\ldots11\rangle_x$ corresponds to point M, with $\mathcal{F}_Q[\rho, J_z] = N$. Finally, the completely mixed state rests on the line W. It cannot be used for metrology, hence $\mathcal{F}_Q[\rho, J_z] = 0$.

We now compare the difference between our bound and L. Pezze and A. Smerzi bound Eq. (2.50). First, we consider the experimentally relevant region for which $(\Delta J_x)^2 \leqslant 1$. We find that for points away from the physical boundary at least by 0.001 on the vertical axis, the difference between the two bounds is smaller than 2×10^{-6}. For points at the boundary, the difference is somewhat larger, but still small, the relative difference is smaller than 2% for 4 particles. [TD: Add part of the appendix] Hence, Eq. (2.50) practically coincides with the optimal bound for $(\Delta J_x)^2 < 1$.

We now consider regions on Figure 4.2 for which $(\Delta J_x)^2 > 1$. The difference between the two

bound is now larger. It is larger at point M, for which the bound Eq. (2.50) is zero. Hence for measurement values corresponding to points close to M, our method improve the formula Eq. (2.50). It is important from the point of view of applying our method to spin-squeezing experiments that the bound Eq. (2.50) can be substantially improved for $(\Delta J_x)^2 < 1$, if we assume bosonic symmetry for the system, or we measure an additional quantity, such as $\langle J_x^4 \rangle$ as shown in Figure ?? [TD: Ask Geza for data].

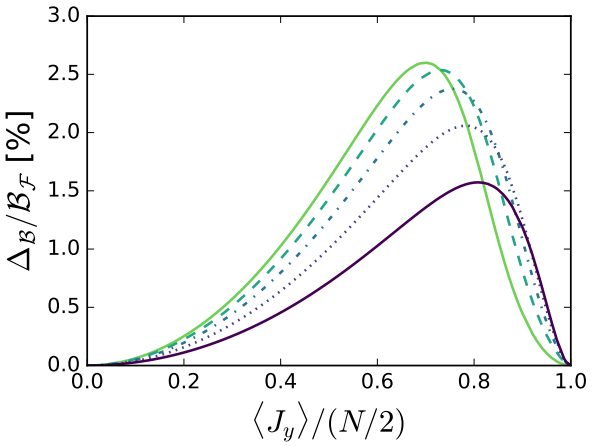

Figure 4.3: Difference between the bound of Pezze-Smerzi and the optimal bound for the quantum Fisher information normalized by the value of the optimal bound itself for the bosonic ground states of $H = J_x^2 - \lambda J_y$ for $\forall \lambda \in [0, \infty)$. From dark to lighter colors (line, point, dash-point, dashed, pointed, line), results for different particle numbers, $N = 4, 6, 10, 20, 1000$ respectively. Heuristically speaking, one can say that for large particle number the difference is biggest when the polarisation is around two thirds of the maximal polarisation and that this difference is about 2.6%.

4.2.4 Dicke states

In this section, we use our method to find lower bounds on the QFI for states characterized to be close to the Dicke states (4.19), based on collective measurements. We discuss what operators have to be measured to estimate the metrological usefulness of the state. In Section ??, we will test our approach fo a realistic system with very many particles.

In order to estimate the metrological usefulness of states created in such experiments, we choose to measure $W_1 = J_x^2$, $W_2 = J_y^2$ and $W_3 = J_z^2$ since the expectation values of these operators uniquely define the ideal Dicke state, and they have been already used for entanglement detection [?]. In cold gas experiments of nowadays, the state created is invariant under transformations of the type $U_x(\phi) = \exp(-iJ_x\phi)$ [98]. For such states $\langle J_y^2 \rangle = \langle J_z^2 \rangle$, which we also use as a constraint in our optimization.

Let us demonstrate how our method works in an example for small systems. Figure 4.4 shows the

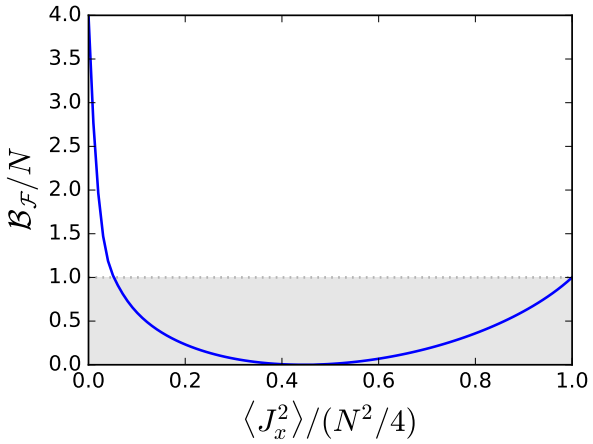

Figure 4.4: Optimal lower bound on the quantum Fisher Information for symmetric states with $\langle J_y^2 \rangle = \langle J_z^2 \rangle$. Even if it is metrologicaly useful for a wide range of $\langle J_x^2 \rangle$, the numerics shows us a tiny region where the metrological gain is surpassing the shot-noise limit.

result for 6 qubits for symmetric states for which

$$\langle J_x^2 + J_y^2 + J_z^2 \rangle = \frac{N(N+2)}{4} =: \mathcal{J}_N. \tag{4.24}$$

It can be seen that the lower bound on quantum Fisher Information is the largest for $\langle J_x^2 \rangle = 0$. It reaches the value corresponding to the ideal Dicke state, $\mathcal{F}_Q[\rho, J_z]/N = (N+2)/2 = 4$. It is remarcable that the state is also useful for metrology if $\langle J_x^2 \rangle$ is very large. In this case $\langle J_y^2 \rangle$ and $\langle J_z^2 \rangle$ are smaller than $\langle J_x^2 \rangle$.

4.3 Calculations for experimental data

In this section, we use our method to find tight lower bound on the QFI based on experimental data. In particular, we will determine the bound for several experiments in photons and trapped ions creating GHZ states and Dicke states, in which the fidelity has been measured [50, 52–54, 58, 99**?** –102], which is much easier than obtaining the quantum Fisher Information from the density matrix [73], or estimation it from a metrological procedure [20]. We will obtain a bound on the QFI for a spin-squeezing experiment with thousand of particles [19]. Based on numerical examples, we see that the bound Eq. (2.50) is close to the optimal even for not completely polarized states. Assuming symmetry or knowing additional expectation values can improve the bound Eq. (2.50). Finally, we will also obtain the bound for the QFI for a recent experiment with Dicke states [**?**]. The estimate of the

Physical system	Target quantum state	Fidelity	$\mathcal{B}_{\mathcal{F}}/N$	Ref.
photons	$\|D_4\rangle$	0.844 ± 0.008	1.432 ± 0.044	[?]
		0.78 ± 0.008	1.124 ± 0.236	[102]
		0.8872 ± 0.0055	1.680 ± 0.036	[58]
		0.873 ± 0.005	1.44 ± 0.024	[12]
	$\|D_6\rangle$	0.654 ± 0.024	0.564 ± 0.076	[100]
		0.56 ± 0.02	0.304 ± 0.048	[101]
photons	$\|GHZ_4\rangle$	0.840 ± 0.007	1.848 ± 0.076	[50]
	$\|GHZ_5\rangle$	0.68	0.65	[?]
	$\|GHZ_8\rangle$	0.59 ± 0.02	0.256 ± 0.128	[?]
	$\|GHZ_8\rangle$	0.776 ± 0.06	2.4376 ± 0.1072	[52]
	$\|GHZ_{10}\rangle$	0.561 ± 0.019	0.15 ± 0.11	[52]
trapped-ions	$\|GHZ_3\rangle$	0.89 ± 0.03	1.824 ± 0.291	[47]
	$\|GHZ_4\rangle$	0.57 ± 0.02	0.08 ± 0.052	[?]
	$\|GHZ_6\rangle$	0.509 ± 0.004	0.0018 ± 0.0018	[?]
	$\|GHZ_8\rangle$	0.817 ± 0.004	3.21 ± 0.08	[54]
	$\|GHZ_{10}\rangle$	0.626 ± 0.006	0.64 ± 0.06	[54]

Table 4.1: Fidelity values and the corresponding bound for the QFI for several experiments with Dicke states and GHZ states. Bounds normalized with N are shown. The ones surpassing the value one, they show quantum entanglement enhanced metrological usefulness. For Dicke states the maximum is achieved at $(N+2)/2$, i.e., 3 for the $|D_4\rangle$ case and 4 for the $|D_6\rangle$ case. For the case on which GHZ states are used the limit for the normalized bound is N, the particle number.

precision based on considering the particular case when $\langle J_x^2 \rangle$ is measured for parameter estimation [98] is close to the optimal bound computed by our method.

4.3.1 Few-particle experiments

Now, we will estimate the quantum Fisher information based on the fidelity with respect to Dicke states and GHZ states for several experiments with photons and trapped cold ions, following the ideas of Section ??.

Our results are summarized in Table 4.1. The expoeriments in [52, 102] are with hyperentangled qubits, while in the rest of experiments a single qubit is stored in a particle. Ref. [54] describes experiments with 2–14 ions, we presented only results of 2 of them. Finally, for the experiment of Ref. [?] we used the fidelity estimated using reasonable assumptions discussed in that paper, while the worst case fidelity is lower.

We can compare our estimate to the quantum Fisher information of the state for the experiment of

Ref. [58], where the QFI for the density matrix was obtained as $\mathcal{F}_Q[\rho, J_z]/N = (10.326 \pm 0.093)/N = (2.5816 \pm 0.02325)$. As can be seen in Table 4.1, this value is larger than we obtained, however, it was calculated by knowing the entire matrixm, while our bound is obtained from the fidelity alone.

4.3.2 Many-particle experiments

In this section, we will estimate the quantum Fisher information based on collective measurements for experiments aiming to create spin-squeezing states and Dicke states.

Spin-squeezing experiment

We turn our attention to a recent many-particle spin-squeezing experiment in cold gases to use our method to find lower bounds on the quantum Fisher information, following the ideas of the Section ??. With that we show that the lower bound given in Eq. (2.50) is close to the optimal. We also demonstrate that we carry out calculations for real systems.

In particular, for our calculations we use the data from spin-squeezing experiments of Ref. [19]. The particle number is $N = 2300$, and the spin squeezing parameter defined as

$$\xi_s^2 = N\frac{(\Delta J_x)^2}{\langle J_y\rangle^2} \tag{4.25}$$

has the value $\xi_s^2 = -8.2\text{dB} = 10^{-8.2/10} = 0.1514$. The spin length $\langle J_y\rangle$ has been close to maximal. In our calculations, we choose

$$\langle J_y\rangle = \alpha\frac{N}{2}, \tag{4.26}$$

where we will test our method with various values for α. For each α we use $(\Delta J_x)^2$ will be given such that we get the experimentally obtained spin-squeezing parameter Eq. (4.25). Moreover, we assume $\langle J_x\rangle = 0$, as the y-direction was the direction of the mean spin in the experiment. Based on Eq. (2.50), the bound for the quantum Fisher information is obtained as

$$\frac{\mathcal{F}_Q[\rho, J_z]}{N} \geqslant \frac{1}{\xi_s^2} = 6.605. \tag{4.27}$$

For our computations we need a tool to handle large systems. We will carry out the calculations for symmetric states. this way we obtain a lower bound on the QFI that we will denote by $\mathcal{B}_{\text{sym}}$. As already mentioned, we could obtain a bound for the QFI that is valid even for general case, not necessarily symmetric states if the matrix from which compute the maximum eigenvalue Eq. (4.9) has a

non-degenerated largest eigenvalue. This is not the case in general for the spin-squeezing problem. However, we still know that our bound obtained with our calculations on the symmetric subspace cannot be smaller than the optimal bound $\mathcal{B}_{\mathcal{F}}$, which must be bigger or equal to the Eq. (2.50) since it cannot be larger than the optimal bound for general states. These relations can be summarized as

$$\mathcal{B}_{\text{sym}} \geqslant \mathcal{B}_{\mathcal{F}} \geqslant \frac{\langle J_y \rangle^2}{(\Delta J_x)^2}, \tag{4.28}$$

where on the right-hand side we just used the bound in Eq. (2.50).

Our calculations lead to

$$\frac{\mathcal{B}_{\text{sym}}(\langle J_y \rangle, (\Delta J_x)^2)}{N} = 6.605 \tag{4.29}$$

for a wide range of values of α. That is, based on numerics, the left-hand side and the right-hand side of Eq. (4.29) seem to be equal. This implies that the lower bound Eq. (2.50) is optimal for estimating the QFI for the system.

We follow giving the details of our calculations for $\alpha = 0.5, 0.85$ and we show examples on which we can improve the bound Eq. (2.50) with our approach, if symmetry is assumed. We present simple scheme that we need to handle large systems, and make calculations for larger particle number. Thus, we need fewer steps for the numerical optimization for large system sizes, which makes our computations faster. Second, while we will be able to carry out the calculation for the particle number of the experiment, we will also see that we could even extrapolate the results from the results obtained for lower particle numbers. This is useful for future application of our method for very large systems.

The basic idea is that we transform the collective quantities from N to a smaller particle number using the scaling relation

$$\langle J_y \rangle = \frac{N'}{2}\alpha, \tag{4.30}$$

$$(\Delta J_x)^2 = \xi_s^2 \frac{N'}{4}\alpha^2. \tag{4.31}$$

We see that for the scaling we consider, for all N' the bound in Eq. (2.50) is valid, i.e., is obtained as

$$\frac{\mathcal{F}_{\text{Q}}[\rho_{N'}, J_z]}{N'} \geqslant \frac{1}{\xi_s^2} = 6.605. \tag{4.32}$$

Let us first take $\alpha = 0.85$, which is somewhat smaller than the experimental value, however, it helps us to see various characteristics of the method. At the end of the section we will also discuss the results for other values of α. Based on these ideas, we compute the bound $\mathcal{B}_{\text{sym}}$ for the quantum

Fisher information for an increasing system size N'.

The results can be seen in Figure 4.5.a. The bound obtained this way is close to the bound in

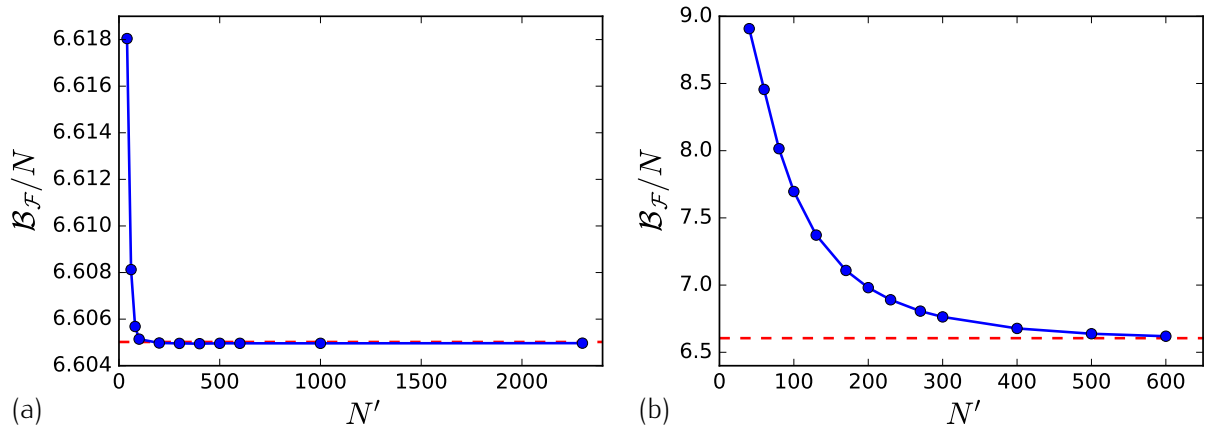

Figure 4.5: [TD: Change vertical label to $\mathcal{B}_{\text{sym}}$] (Color line) Lower bound on the QFI based on $\langle J_y \rangle$ and $(\Delta J_x)^2$ obtainde for the symmetric subspace for different particle numbers N'.

Eq. (4.27) even for small N'. For larger particle number it is constant and coincides with the bound in Eq. (4.27) This also strongly supports the idea that we could used the result for small particle numbers to extrapolate the bound for N. Since for the experimental particle number we obtain that $\mathcal{B}_{\text{sym}}$ equals the bound in Eq. (4.27), we find that all three lower bounds in Eq. (4.29) must be equal. Hence, Eq. (2.50) is optimal for the experimental system and α considered before in this section. BEsides, these results present also a strong argument for the correctness of our approach.

We now give more details of the calculation. We were able to carry out the optimizations up to $N' = 2300$ with a usual laptop computer using MATLAB programing language. We started the calculation for each given particle number with the r_k parameters obtained for the previous simulation with a smaller particle number. This allows for faster finding of the solution than if we would start the r_k parameters arbitrarily.

Let us consider a spin-squeezing state that is not fully polarized and $\alpha = 0.5$. In Figure 4.5.b, we can see that for small particle numbers we have a larger bound on $\mathcal{F}_{\text{Q}}[\rho, J_z]$ than the one obtained from Eq (2.50). Thus for the case on which the particle number would be smaller we could improve the bound Eq. (2.50) by assuming symmetry. On the other hand, for large particle number we recover the bound Eq. (2.50).

Finally, we add a note on the technical detail. We carried out our calculations with the constraints on $(\Delta J_x)^2$ and $\langle J_y \rangle$, with the additional constraint $\langle J_x \rangle = 0$. For the experimental particle numbers, one

For MATLAB R2015a, see `http://www.mathworks.com`.

can show that our results are calid even if we constrained only $(\Delta J_x)^2$ and $\langle J_y \rangle$, and did not use the $\langle J_x \rangle = 0$ constraint. This way, in principle, we could only get a lower bound that is equal to the one we obtained before or lower. However, we obtained before a value identical to the analytical bound Eq. (2.50). The optimal bound cannot be below the analytic bound, since then the analytic bound would overestimate the quantum Fisher information, and it would not be a valid bound. Hence, even an optimization without the $\langle J_x \rangle = 0$ constraint could not obtain a smaller value than our results.

Experiment creating Dicke states

In this section, we present our calculations for an experiment aiming at creating Dicke states in cold gases [92]. The basic ideas are similar to the ones explained in Section 4.2.4 for small systems. The experimental data, as in previous Section **??**, are $N = 7900$, $\langle J_y^2 \rangle = 112 \pm 31$, $\langle J_x^2 \rangle = \langle J_z^2 \rangle = 6 \times 10^6 \pm 0.6 \times 10^6$ [98]. Applying some simple transformations, we can make calculations for a very large numbers of particles, and obtain results even for general, non-symmetric systems.

In the general, non-symmetric case, we can handle only small problems. Thus, we have to transform the collective quantities such that the corresponding quantum state, i.e., it has to fulfill

$$\langle J_x^2 \rangle_{\text{sym}} + \langle J_x^2 \rangle_{\text{sym}} + \langle J_x^2 \rangle_{\text{sym}} = \mathcal{J}_N, \tag{4.33}$$

where $\mathcal{J}_N$ is defined on Eq. (4.24). A mapping of this type can be realized equally scaling all second moments of the angular momentum projections as

$$\langle J_l^2 \rangle_{\text{sym},N} = \gamma \langle J_l^2 \rangle_N, \tag{4.34}$$

where we now added the label N to avoid confusions in upcoming equations, $l = x, y, z$ and where we used the coefficient γ to be

$$\gamma = \frac{\mathcal{J}_N}{\langle J_x^2 \rangle_N + \langle J_y^2 \rangle_N + \langle J_z^2 \rangle_N}. \tag{4.35}$$

Note that $\gamma = 1$ if the original state is symmetric.

Next, based on the ideas of this chapter, we calculate the lower bound on the quantum Fisher information for symmetric systems, which we denote it by $\mathcal{B}_{\text{sym},N}$. Then, to obtain the results for the original non-symmetric case, notice the convex nature of the $\mathcal{B}_N$, which is the bound to be computed for the general case, implies

$$\mathcal{B}_N \leqslant \frac{1}{N} \mathcal{B}_{\text{sym},N}, \tag{4.36}$$

where $\mathcal{B}_{\text{sym},N}$ corresponds to the bound one would obtain on the symmetric subspace for expectation values given using the Eq. (4.34). This can be seen using an auxiliary state $\tilde{\rho}$ that mixes the symmetric state that in principle has the expectation values appearing on Eq. (4.34) and the singlet state that has zero value for all those expectation values Hence, if we construct a mixture of this type as follows

$$\tilde{\rho}_N = (1-\gamma^{-1})\rho_{\text{singlet},N} + \gamma^{-1}\rho_{\text{sym},N}, \tag{4.37}$$

we have that $\tilde{\rho}$ has the same expectation values as the original non-symmetric case. This way, we can relate the bound for general systems to the quantum Fisher information for symmetric cases as

$$\mathcal{B}_N \leqslant \mathcal{F}_{\text{Q}}[\tilde{\rho}_N, J_z] = \frac{1}{\gamma}\mathcal{F}_{\text{Q}}[\rho_{\text{sym,N}}, J_z]. \tag{4.38}$$

Here, the inequality comes due to that our bound cannot be larger than the QFI of any state having the given set of expectation values. On the other hand, the equality holds due to the fact that both $\tilde{\rho}$ and J_z can be written as block-diagonal matrix of blocks corresponding to different eigenvalues of $\boldsymbol{J}^2$. In particular, $\rho_{\text{singlet},N}$ has non-zero elements only in the blocks for which $\langle \boldsymbol{J}^2 \rangle = 0$, while $\rho_{\text{sym},N}$ has nonzero elements only in the blocks in which $\langle \boldsymbol{J}^2 \rangle$ is maximal. Notice that $\boldsymbol{J}^2$ is a shorthand of $J_x^2 + J_y^2 + J_z^2$. Then we can use the general formula [64]

$$\mathcal{F}_{\text{Q}}[\bigoplus_k p_k\rho_k, \bigoplus_k A_k] = \sum_k p_k \mathcal{F}_{\text{Q}}[\rho_k, A_k], \tag{4.39}$$

where ρ_k are density matrices with unit trace, $\sum_k p_k = 1$ and the k index represent the block subspaces of the system and the operators A_k.

Extensive numerics for small systems show that the inequality in Eq. (4.38) is very close to an equality within the numerical precision

$$\mathcal{B}_N \approx \frac{1}{\gamma}\mathcal{B}_{\text{sym},N}. \tag{4.40}$$

To obtain the lower bound $\mathcal{B}_N$ we also use an increasing system size N' as we have done in at the beginning of this section. However, in this case we will not be able to do the calculation for the experimental particle number, and we will use extrapolation from the results obtained for smaller particle numbers.

First, we transform the measured second moments to values corresponding to a symmetric system

using Eqs. (4.34) and (4.35). For our case, $\gamma = 1.301$. This way, we obtain

$$\begin{aligned} \langle J_y^2 \rangle_{\mathrm{sym},N} &= 145.69, \\ \langle J_x^2 \rangle_{\mathrm{sym},N} &= \langle J_z^2 \rangle_{\mathrm{sym},N} = 7.8 \times 10^6. \end{aligned} \tag{4.41}$$

Next, we will carry out calculations for symmetric systems. We will consider a smaller system N' that keeps expectation values such that the corresponding quantum state must be symmetric. Hence, we will use the following relation to find the target expectation values for smaller systems

$$\begin{aligned} \langle J_y^2 \rangle_{\mathrm{sym},N'} &= \langle J_y^2 \rangle_{\mathrm{sym},N}, \\ \langle J_x^2 \rangle_{\mathrm{sym},N'} &= \langle J_z^2 \rangle_{\mathrm{sym},N'} = \frac{1}{2}(\mathcal{J}_{N'}) - \langle J_y^2 \rangle_{\mathrm{sym},N'}), \end{aligned} \tag{4.42}$$

where $\mathcal{J}_{N'}$ is defined in Eq. (4.24). Note that with Eq. (4.24) holds for all N', hence the state must be symmetric. Hence, the main characteristics of the scaling relation can be summarized as follows, $\langle J_y^2 \rangle_{\mathrm{sym},N'}$ remains equal for all N' while $\langle J_x^2 \rangle_{\mathrm{sym},N'}$ and $\langle J_z^2 \rangle_{\mathrm{sym},N'}$ are chosen such that they are equal to each other and the state is symmetric. For large N, this implies a scaling of $\langle J_y^2 \rangle_{\mathrm{sym},N}$ constant and $\langle J_x^2 \rangle_{\mathrm{sym},N} = \langle J_z^2 \rangle_{\mathrm{sym},N} \sim N(N+2)/8$.

Let us now turn to central quantities of our chapter, the lower bounds on the quantum Fisher information. A central point in our scheme is that due to the scaling properties of the system, we can obtain the value for the particle number N from the values of a smaller particle number N' as [91]

$$\mathcal{B}_{\mathrm{sym},N} \approx \frac{\mathcal{J}_N}{\mathcal{J}_{N'}} \mathcal{B}_{\mathrm{sym},N'}, \tag{4.43}$$

which we will verify numerically. Note that for large N, we have $\mathcal{J}_N/\mathcal{J}_{N'} \sim N^2/(N')^2$.

As last step, we have to return from the symmetric system to our real system, not fully symmetric one. Based on Eq. (4.43) and assuming Eq. (4.40), a relation for the lower bound for the original problem can be obtained from the bound on the symmetric problem with N' particles as

$$\mathcal{B}_N \approx \frac{1}{\gamma} \frac{\mathcal{J}_N}{\mathcal{J}_{N'}} \mathcal{B}_{\mathrm{sym},N'} = \frac{\langle J_x^2 \rangle_N + \langle J_y^2 \rangle_N + \langle J_z^2 \rangle_N}{\mathcal{J}'_N} \mathcal{B}_{\mathrm{sym},N'}. \tag{4.44}$$

In Figure 4.6, we plotted the right-hand side of Eq. (4.44) as the function of N' divided by N. We can see that $\mathcal{B}_{N'}/N$ is constant or slightly increasing for $N' > 400$. This is a strong evidence that Eq. (4.43) is valid for relatively large particle numbers. With this, we arrive at the result for the

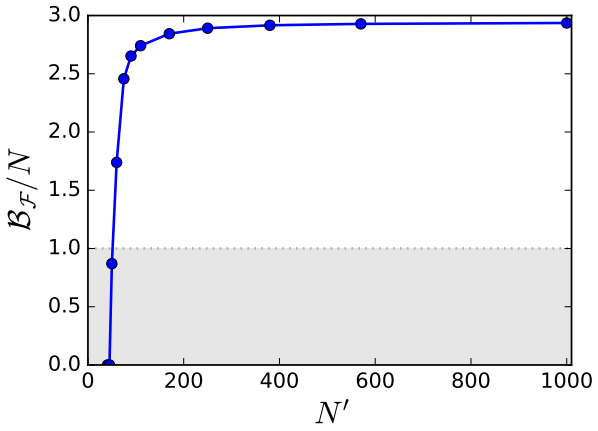

Figure 4.6: Secuence of the evolution of an unpolarized Dicke state of 16 qubits for $\theta = \{i\pi/6\}_{i=0}^{4}$. Bloch spheres representing the Hirusi distribution of the state, and below PDF of the J_x POVM for each step of the secuence

experimental system

$$\frac{\mathcal{B}_N(\langle J_y^2\rangle, \langle J_x^2\rangle = \langle J_z^2\rangle)}{N} \approx 2.94. \tag{4.45}$$

The $\approx$ sign is used referring to the fact that we assume that the inequality in Eq. (4.38) is close to be saturated and that we did sufficient numerics for an increasing system size N' to have a good asymptotic approach to the real value Eq. (4.43).

It is instructive to compare the value of Eq. (4.45) to the one obtained in Chapter **??**, where the same system was characterized base on its metrological usefulness. Such result implies $\mathcal{F}_Q[\rho, J_z]/N \geqslant 3.3$ which is somewhat bigger than our recent result as we did not use the knowledge of the fourth moments, only the second moments. The closeness of the two results is a strong argument for the correctness of our calculations.

4.4 Scaling for $\mathcal{F}_Q[\rho, J_z]$ with N

Recent important works examine the scaling of the quantum Fisher information with the particle number for metrology under the presence of decoherence [59**?**]. They consider the QFI defined now for the non-unitary, noisy evolution. They find that for small N it is close to the value obtainded by considering coherent dynamics. Hence, even the Heisenberg scaling, $\mathcal{O}(N^2)$, can be reached. However, if N is sufficiently large, then, due to the decoherence during the parameter estimation, the QFI scales as $\mathcal{O}(N)$.

We have to stress that the findings of [59**?**] are not applicable to our case. Our methods estimates

the quantum Fisher information assuming a perfect unitary dynamics. The quantum Fisher information can be smaller that what we expect ideally only due to the imperfect preparation of the state**. We can even find simple conditions on the state preparation that lead to a Heisenberg scaling. Based on Eq. (4.17), if we could realize quantum states ρ_N such that $F_{\mathrm{GHZ}}(\rho_N) \geqslant 0.5 + \epsilon$ for $N \to \infty$ for some $\epsilon > 0$, then we would reach $\mathcal{B}_{\mathcal{F}}(F_{\mathrm{GHZ}}) = \mathcal{O}(N^2)$. Strong numerical evidence suggest that a similar relation holds for fidelity F_{Dicke} and $\mathcal{B}_{\mathcal{F}}(F_{\mathrm{GHZ}})$, see Section ??. [TD: Decide if remove the following sentence. It is very strong] From another point of view, our method can estimate $\mathcal{F}_{\mathrm{Q}}[\rho, J_z]$ for large particle numbers, while a direct measurement of the metrological sensitivity considerably underestimates it.

** This is also relevant for [?], where $\mathcal{F}_{\mathrm{Q}} = \mathcal{O}(N^2)$ is reached with weakly entangled states.

5 Accuracy bound for gradient field estimation with atomic ensembles

"To consult the statistician after an experiment is finished is often merely to ask him to conduct a post mortem examination. He can perhaps say what the experiment died of."
Ronald Fisher

In this chapter, one of the most fundamental two-parameter estimation tasks in magnetometry is considered, namely gradient magnetometry. We will add the gradient of the magnetic field as the second parameter beside the constant (homogeneous) part of the field. While most works in magnetometry with a single ensemble focus only on the determination of the strength and direction of magnetic field, certain measurement schemes for the gradient have already been proposed and tested experimentally. We study gradient magnetometry with an ensemble of atoms described by a very general probability distribution function for the position of the atoms, and considering atoms with an arbitrary spin. Some schemes use an imaging of the ensemble with a high spatial resolution, however, they do not count as single-ensemble methods in the sense we use this expression in our paper, since in this case not only collective observables are measured [29–31]. There is a method based on collective measurements of the spin length of a fully polarized ensemble [35]. Finally, there is a scheme where they use as a prove state a many-body singlet states, which is described in Ref. [55].

We calculate precision bounds for estimating the gradient of the magnetic field based on the

quantum Fisher information. For quantum states that are invariant under the homogeneous magnetic field, a single parameter estimation is sufficient. In contrast for states that are sensitive to the homogeneous fields, a two-parameter estimation problem must be solved to obtain the gradient parameter, since the homogeneous field must be also taken into account. We use our method to calculate precision bounds for gradient estimation with a chain of atoms and even with two spatially separated atomic ensembles which feel different magnetic fields. As we said, we also consider a single atomic ensemble with an arbitrary density profile, in which atoms cannot be addressed individually, which is a very relevant case for experiments. Our model can take into account even correlations between particle positions.

The atoms will be distributed along the x-axis, so $y = z = 0$, and in principle they will be able to feel differences on the magnetic field at different points of the axis. The magnetic field at the atoms will be given by a linear function on the position x

$$\boldsymbol{B}(x, 0, 0) = \boldsymbol{B}_0 + x\boldsymbol{B}_1 + O(x^2), \tag{5.1}$$

where we will neglect the terms of order two or higher. We will consider the magnetic field pointing along the z-direction direction only, $\boldsymbol{B}_0 = B_0\boldsymbol{k}$ and $\boldsymbol{B}_1 = B_1\boldsymbol{k}$, where $\boldsymbol{k}$ is the unitary vector pointing on the z-direction. For this configuration, due to the Maxwell equations, with no currents or changing electric fields, we have

$$\begin{aligned} \nabla \cdot \boldsymbol{B} &= 0, \\ \nabla \times \boldsymbol{B} &= \boldsymbol{0}, \end{aligned} \tag{5.2}$$

where $\boldsymbol{0} \equiv (0, 0, 0)$ is the null 3-dimensional vector. This implies $\sum_{l=x,y,z} \partial_l B_l = 0$ and $\partial_m B_l - \partial_l B_m = 0$ for $\forall l \neq m$, where $\partial_m \equiv \partial/\partial_m$ stands for the partial derivative over the variable m. Thus, the spatial derivatives of the field components are not independent of each other. However, in the case of a linear arranged particle ensemble only the derivative along the x-axis has an influence on the quantum dynamics of the atoms.

We will determine the precision bounds for the estimation of the magnetic field gradient B_1 based on the quantum Fisher information [4, 9, 11, 72, 83, 103]. In this context the Heisenberg and shot-noise scaling are defined as usual. The achievable precision in terms of the number of particles scale as $(\Delta\theta)^{-2} \sim N$ and $(\Delta\theta)^{-2} \sim N^2$ for SNS and HS respectively. Sometimes, one must take care of adding more particles to the system, which may increase the effective length of it, and it becomes more sensitive to the gradient field merely because the system reaches further away. We will show that with spin chains or two ensembles at different positions the Heisenberg scaling is possible,

even after the normalization of the effective size of the system. Concerning the case of a single ensemble, we will show the following. Since in such systems the atoms cannot be be individually addressed, we will assume that the quantum state is permutationally invariant. We will show that for states insensitive to the homogeneous magnetic field, one can reduce the problem to a one-parameter estimation scenario. Such states can arise in a single-ensemble scheme, however, it will be shown the Heisenberg limit cannot be reached in this case. When the state is sensitive to the homogeneous field the spatial correlation between the atoms must be taken into account in order to show whether the system can overcome the shot-noise scaling and achieve the Heisenberg scaling. Nevertheless, single-ensemble measurements have certain advantages since the spatial resolution can be higher and the experimental requirements are smaller since only a single ensemble must be prepared.

On the other hand, for states sensitive to the homogeneous field, the classical limit can be overcome only if the particle positions are highly correlated with each other. Our calculations are generally valid for any measurement, thus they are relevant to many recent experiments [25–31, 35]. We note that in the case of the singlet, our precision bounds are saturated by the metrological scheme presented in Ref. [55].

We can also connect our results to entanglement theory [13, 14, 104]. We find that even in the case of gradient magnetometry the shot-noise scaling cannot be surpassed with separable states, while the Heisenberg scaling can be reached with entangled states. However, in the single-ensemble scenario, the shot-noise scaling can be surpassed only if the particle positions are correlated, which is the case if the particles attract each other. We will go into the details in Section 5.3.

Next, we will present characteristics of our setup. For simplicity, as well as following recent experiments (e.g., Ref. [29]), we will consider an ensemble of spin-j particles placed in a one-dimensional setup, x being the spatial coordinate. Furthermore, we assume that we have that we have particles that behave classically with respect to their spatial state. That is, they cannot be in a superposition of being in two different positions. On the other hand, they have internal degrees of freedom, their spin, that is quantum. This is a very good description to many of the cold gas experiments.

Based on these considerations, we assume that the state is factorizable into a spatial and a spin part as

$$\rho = \rho_{\mathrm{x}} \otimes \rho_{\mathrm{s}}, \tag{5.3}$$

and that the spatial part can be characterized as an incoherent mixture of point-like particles that can be written as

$$\rho_{\mathrm{x}} = \int \frac{\Pr(\boldsymbol{x})}{\delta(\mathbf{0})} |\boldsymbol{x}\rangle\langle\boldsymbol{x}| \, \mathrm{d}^N \boldsymbol{x}. \tag{5.4}$$

where $\boldsymbol{x} = (x_1, x_2, \ldots, x_N)$ is a vector of the particle coordinates, and $\Pr(\boldsymbol{x})$ is the spatial PDF of the

atoms. Note that the spatial part Eq. (5.4) is diagonal on the position eigenbasis, where the entry x_n of $\boldsymbol{x} = (x_1, \ldots, x_N)$ is the coordinate of the n^{th} particle, which simplifies considerably our calculations. Note also that we normalize the density matrix by $\delta(\mathbf{0})$, the N-dimensional Dirac delta, so to obtain $\mathrm{tr}(\rho_x) = 1$, where the trace of any operator O in the continuous position Hilbert space is defined by $\mathrm{tr}(O) = \int \langle \boldsymbol{x}|O|\boldsymbol{x}\rangle \, \mathrm{d}^N\boldsymbol{x}$. During the evolution of the state, correlations might arise between the two inner and spatial parts and the product form Eq. (5.3) might be not valid to describe the evolution of the system. Besides, the states of the form Eqs. (5.3) and (5.4) are written altogether as

$$\rho = \int \sum_{\lambda} \frac{\Pr(\boldsymbol{x})}{\delta(\mathbf{0})} p_\lambda |\boldsymbol{x}, \lambda\rangle\langle \boldsymbol{x}, \lambda| \, \mathrm{d}^N\boldsymbol{x}, \tag{5.5}$$

where the internal state has is decomposed as $\rho_s = \sum_\lambda p_\lambda |\lambda\rangle\langle\lambda|$, so the eigenvalues of the whole state are $\frac{\Pr(\boldsymbol{x})}{\delta(\mathbf{0})} p_\lambda$ and the corresponding eigenstates $|\boldsymbol{x}, \lambda\rangle$.

We note that our method could be easily extended to the case of Bose-Einstein condensates, not considered in this paper. In that case, the spatial state of the particles would be a pure state, and we would have $\rho_x = (|\Psi\rangle\langle\Psi|)^{\otimes N}$, where $|\Psi\rangle$ is a spatial single-particle state.

Although in our case the parameter to be estimated is B_1, the time-evolution of the state is usually also affected by the second unknown parameter, the homogeneous field B_0, which means that we generally have to consider a two-parameter estimation problem. The angular momentum of an individual atom is coupled to the magnetic field, yielding the following interaction term

$$h^{(n)} = \gamma B_z^{(n)} \otimes j_z^{(n)}, \tag{5.6}$$

where the operator $B_z^{(n)} = B_0 + B_1 x^{(n)}$ acts on the spatial part of the Hilbert space. The sum of all one particle interactions with the magnetic field provide the total Hamiltonian

$$H = \gamma \sum_{n=1}^{N} B_z^{(n)} \otimes j_z^{(n)}, \tag{5.7}$$

which will generate the time evolution of the system.

We will calculate lower bounds on the precision of estimating B_1 based on measurements on the state after it passed through the unitary dynamics $U = \exp(-i\frac{H}{\hbar}t)$, where t is the time spent by the system under the influence of the magnetic field. The unitary operator can be rewritten in the following way

$$U = e^{-i(b_0 H_0 + b_1 H_1)}, \tag{5.8}$$

where the $b_i = \gamma B_i t/\hbar$ and therefore b_1 encodes the gradient of the magnetic field B_1. Here, the generator describing the effect of the homogeneous field is given as

$$H_0 = \sum_{n=1}^{N} j_z^{(n)} = J_z, \tag{5.9}$$

while the generator describing the effect of the gradient is

$$H_1 = \sum_{n=1}^{N} x^{(n)} j_z^{(n)}. \tag{5.10}$$

As in Eq. (5.10), we will usually omit $\otimes$ for simplicity, and will use it only if it is necessary to make our explanation clearer.

Note that the operators H_0 and H_1 commute with each other. These two commuting dynamics are the two simplest in an atomic ensemble as they are based on collective operators not requiring an individual access to the particles. This is mainly because the spatial part in Eq. (5.6) is represented by a single particle operator and not by a scalar depending on the position of the particle. The second approach, where the position of the particle is encoded in a scalar, would require to know in advance the location of the particle making the Hamiltonian H_1 Eq. (5.10) non-collective. This approach is widely adopted by the community, since its the most easy to understand and makes the initial calculations on gradient metrology easier [].

Note also that it is not necessarily true that the operators we have to measure in order to estimate b_0 and b_1 must commute with each other. The reason for that is that both operators to be measured act on the same single atomic ensemble. On the other hand, in schemes in which the gradient is calculated based on measurements in two separate atomic ensembles or different atoms in a chain, the measuring operators can always commute with each other [25, 26, 91].

The following sections are organized as follows. In Section 5.1, the basic concepts used in the paper are presented. In Section 5.2, we will show the results for the chain of ions and for when two distant ensembles are considered In Section 5.3, we restrict our calculations to single PI atomic ensembles and we develop some particular cases, such as the singlet spin state or the totally polarized state.

5.1 Cramér-Rao precision bounds

In this section, we show how the Cramér-Rao bound and the QFI help us to obtain the precision bound that is valid for any measurement scenario. We will discuss gradient magnetometry using quantum states that are insensitive to homogeneous fields, which is a single-parameter estimation task. Then, we discuss the case of quantum states sensitive to homogeneous fields, which is a two-parameter estimation problem. Note that we require the state to be sensitive to the gradient parameter, which is a reasonable requirement when we are trying to characterize the precision bounds for the gradient estimation. We show that the precision bound obtained does not change under spatial translation, which is one of the main tools to derive our bounds. For the two-parameter estimation task, we will introduce the two-parameter Cramér-Rao bound and the corresponding two-parameter QFI matrix, and we adapt those expressions to our problem.

For clarity we present our main tools in subsequent paragraphs before going onto details. Here we define a functional very similar to the QFI Eq. 2.51. This expression will be used along this chapter and it will be useful for the transition to the multi-parameter problem, i.e, it is equivalent to the QFI for the single parameter estimation problem but still it gives the chance to switch to the multi-parameter case easily. The function is defined as follows. For two arbitrary operators A and B, it is written as

$$\mathcal{F}_{\mathrm{Q}}[\rho, A, B] := 2\sum_{\lambda,\nu} \frac{(p_\lambda - p_\nu)^2}{p_\lambda + p_\nu} A_{\lambda,\nu} B_{\nu,\lambda}, \tag{5.11}$$

where the subscript for A and B stand for the matrix elements on the eigenbasis of the initial state $\rho = \sum_\lambda p_\lambda |\lambda\rangle\langle\lambda|$. If the two operators are the same, the usual form of the QFI Eq. (2.51) is recovered [4, 9, 11, 72, 83, 103],

$$\mathcal{F}_{\mathrm{Q}}[\rho, A, A] := \mathcal{F}_{\mathrm{Q}}[\rho, A] = 2\sum_{\lambda,\nu} \frac{(p_\lambda - p_\nu)^2}{p_\lambda + p_\nu} |A_{\lambda,\nu}|^2. \tag{5.12}$$

We mention that in our case the operators A and B will commute on all situations, making some computations easier. We also make use of the fact that the QFI as written as in Eq. (5.11) is linear on the second and last arguments,

$$\mathcal{F}_{\mathrm{Q}}[\rho, A, \textstyle\sum_i b_i] = \displaystyle\sum_i \mathcal{F}_{\mathrm{Q}}[\rho, A, b_i]. \tag{5.13}$$

It also holds for commuting A and B, that the last two arguments can be exchanged without affecting the outcome, $\mathcal{F}_{\mathrm{Q}}[\rho, A, B] = \mathcal{F}_{\mathrm{Q}}[\rho, B, A]$.

Similar to Eq. (2.54), Eq. (5.11) can be rewritten as

$$\mathcal{F}_{\mathrm{Q}}[\rho, A, B] = 4\langle AB\rangle - 8\sum_{\lambda,\nu}\frac{(p_\lambda - p_\nu)^2}{p_\lambda + p_\nu}A_{\lambda,\nu}B_{\nu,\lambda}, \tag{5.14}$$

when the operators A and B commute. This form leads to simpler arguments in our derivations through the following sections. For pure states it simplifies also to

$$\mathcal{F}_{\mathrm{Q}}[|\psi\rangle, A, B] = 4\left(\langle AB\rangle_\psi - \langle A\rangle_\psi\langle B\rangle_\psi\right). \tag{5.15}$$

Note that we recover $\mathcal{F}_{\mathrm{Q}}[\rho, A, A] = 4(\Delta A)^2_\rho$ as can be found in the Eq. (2.54) for single-parameter estimation with pure states [4, 84]. Another important feature of the function Eq. (5.11) is that it is convex on the states. This property is written as follows

$$\mathcal{F}_{\mathrm{Q}}[q\rho_1+(1-p)\rho_2] \leqslant p\mathcal{F}_{\mathrm{Q}}[\rho_1]+(1-p)\mathcal{F}_{\mathrm{Q}}[\rho_2], \tag{5.16}$$

where we omit in writing the last two arguments for simplicity.

In the following subsections we show the general form for the precision bounds for states insensitive to the homogeneous fields and for states sensitive to them. We also show that both bounds are invariant under spatial translation of the system which makes the computing for particular cases much easier.

5.1.1 Precision bound for states insensitive to homogeneous fields: Single-parameter dependence

Let us consider quantum states that are insensitive to the homogeneous field. For these states, $[\rho, H_0] = 0$ and hence the evolved state is a function of a single unknown parameter, b_1. For the unitary dynamics we consider, the QFI for single-parameter estimation problem can be expressed in terms of the eigenstates and eigenvalues of the density matrix, as usual, [4, 9, 11, 72, 83, 103],

$$\mathcal{F}_{\mathrm{Q}}[\rho, H_1] = 2\sum_{\lambda,\nu}\frac{(p_\lambda - p_\nu)^2}{p_\lambda + p_\nu}|\langle\lambda|H_1|\nu\rangle|^2. \tag{5.17}$$

Note that here the eigenvalues λ and ν and eigenstates $|\lambda\rangle$ and $|\nu\rangle$ represent the external and internal Hilbert spaces and therefore this expression must be taken carefully. Due to the Cramér-Rao formula,

it gives us an upper bound for the precision

$$(\Delta b_1)^{-2}|_{\max} = \mathcal{F}_{\mathrm{Q}}[\rho, H_1]. \tag{5.18}$$

Note that it is *always* possible to find a measurement that saturates the precision bound above. Hence, we denote it using the "$|_{\max}$ =" notation. Here, $\mathcal{F}_{\mathrm{Q}}[\rho, H_1]$ denotes the QFI that depends, in the case of unitary transformation of the form Eq. (5.8), on the state ρ and on the generator of the evolution H_1.

For the particular case on which the states has the form of Eqs. (5.3) and (5.4), the Eq. (5.17) can be simplified in the following way. Note that we have to compute the matrix elements of H_1 which is already diagonal on the spatial subspace. Therefore, the following holds for the matrix elements of H_1

$$\begin{aligned}(H_1)_{\boldsymbol{x},\lambda;\boldsymbol{y},\nu} &= \langle \boldsymbol{x}, \lambda | H_1 | \boldsymbol{y}, \nu \rangle \\ &= \langle \boldsymbol{x}, \lambda | \sum_{n=1}^{N} x^{(n)} j^{(n)} | \boldsymbol{y}, \nu \rangle \\ &= \delta(\boldsymbol{x} - \boldsymbol{y}) \sum_{n=1}^{N} x_n \langle \lambda | j^{(n)} | \mu \rangle,\end{aligned} \tag{5.19}$$

where $|\lambda\rangle$ and $|\mu\rangle$ refer now to eigenstates of the internal state ρ_{s} and we use $\langle \boldsymbol{x}|x^{(n)}|\boldsymbol{y}\rangle = \delta(\boldsymbol{x}-\boldsymbol{y})x_n$. We will use the Dirac delta function appearing in Eq. (5.19) to further simplify the Eq. (5.17).

We show now how translated systems have unchanged the sensitivity over the gradient estimation. The translation operator U_d grabs the state to a new position at a distance d from its previous location, and it is written as

$$U_d = e^{-idP_x/\hbar}, \tag{5.20}$$

where P_x is the sum of all single-particle linear momentum operators $p_x^{(n)}$ in the x-direction and it only acts on the external degrees of freedom of the state, i.e., the external Hilbert space. To show that the precision is unchanged, we use the Heisenberg picture on which the operators are transformed

instead of the states. Thus, we compute the transformation of H_1 in the following way,

$$\begin{aligned} U_d : H_1 \to H_1(d) &= U_d^\dagger H_1 U_d \\ &= \sum_{n=1}^{N} U_d^\dagger x^{(n)} U_d \otimes j_z^{(n)} \\ &= \sum_{n=1}^{N} (x^{(n)} - d) j_z^{(n)} \\ &= H_1 - d H_0. \end{aligned} \tag{5.21}$$

Hence, the new unitary evolution operator to represent the translated system, instead of Eq. (5.8), is

$$U = e^{-i(b_0 H_0 + b_1 H_1(d))} = e^{-i((b_0 - b_1 d) H_0 + b_1 H_1)}, \tag{5.22}$$

which is equivalent to Eq. (5.8) for states insensitive to the homogeneous fields, since $[\rho, H_0] = 0$.

We leave some computations for the Appendix I. Note that for the simplification for the QFI, we use the Dirac delta appearing in Eq. (5.19), and the state defined by Eq. (5.5). The following bound in the precision of the estimation of the gradient parameter b_1 holds for states insensitive to the homogeneous magnetic fields

$$(\Delta b_1)^{-2}|_{\max} = \sum_{n,m}^{N} \int \Pr(\boldsymbol{x}) x_n x_m \, \mathrm{d}^N \boldsymbol{x} \, \mathcal{F}_{\mathrm{Q}}[\rho_{\mathrm{s}}, j_z^{(n)}, j_z^{(m)}], \tag{5.23}$$

where the integral has the form of a two-point correlation function of the spatial state.

5.1.2 Precision bound for states sensitive to homogeneous fields: Two-parameter dependence

In order to obtain the precision bound for states sensitive to the homogeneous field, one has to consider the effect on the state of a second unknown parameter, in this case b_0, which represents the homogeneous magnetic field. The homogeneous field will rotate all the spins in the same way, while the field gradient rotates the spins differently depending on the position of the particles. Now, instead to the Cramér-Rao bound Eq. (5.18), we have a matrix inequality [4]. For the matrix inequality, we have the inverse of QFI matrix $\boldsymbol{\mathcal{F}}$ on one hand, which depends on ρ and the two generators H_0 and H_1, and the covariance matrix on the other hand. In this section, we are only interested on the variance of the gradient parameter, $(\Delta b_1)^2$. Since we have to compute the inverse of the QFI matrix and then look at the element corresponding to the $(\Delta b_1)^2$, the determinant of $\boldsymbol{\mathcal{F}}$ cannot be zero. H_0

and H_1 are Hermitian operators and commute with each other. For unitary dynamics of the type Eq. (5.8), the QFI matrix elements are computed as $\boldsymbol{\mathcal{F}}_{ij} \equiv \mathcal{F}_{\mathrm{Q}}[\rho, H_i, H_j]$, following the definition of Eq. (5.11).

In the two-parameter estimation problem, $\boldsymbol{\mathcal{F}}$ is a 2×2 matrix and the precision bound for the estimation of the gradient is

$$(\Delta b_1)^{-2} \leqslant \boldsymbol{\mathcal{F}}_{11} - \frac{\boldsymbol{\mathcal{F}}_{01}\boldsymbol{\mathcal{F}}_{10}}{\boldsymbol{\mathcal{F}}_{00}}, \tag{5.24}$$

where the inequality is saturated only if there exists a set of compatible measurements to determine both parameters b_0 and b_1, which is not true in general and must be studied for each particular case [4, 105]. We distinguish this case from the Eq. (5.18), in which the bound is surely saturated by some measurement, using an inequality "$\leqslant$" instead of "$|_{\max} =$".

To compute the bound Eq. (5.24), we will need to simplify the matrix elements of H_0 and H_1 written in the eigenbasis of the state Eq. (5.5), see Eq. (5.11). Note that the matrix elements for H_1 were already computed in Eq. (5.19). Hence, we now calculate $(H_0)_{\boldsymbol{x},\lambda;\boldsymbol{y},\nu}$ in a similar way as we did for Eq. (5.19)

$$\begin{aligned}(H_0)_{\boldsymbol{x},\lambda,\boldsymbol{y},\nu} &= \langle \boldsymbol{x}, \lambda | H_0 | \boldsymbol{y}, \nu \rangle \\ &= \langle \boldsymbol{x}, \lambda | J_z | \boldsymbol{y}, \nu \rangle \\ &= \delta(\boldsymbol{x} - \boldsymbol{y}) \langle \lambda | J_z | \nu \rangle.\end{aligned} \tag{5.25}$$

With this we are now in a position to compute the missing matrix elements of $\boldsymbol{\mathcal{F}}$. One can find most of the computations of the matrix elements of $\boldsymbol{\mathcal{F}}$ in the Appendix I. First of all, we compute $\boldsymbol{\mathcal{F}}_{11} = \mathcal{F}_{\mathrm{Q}}[\rho, H_1, H_1]$ which turns to be equal to Eq. (5.23) for obvious reasons,

$$\boldsymbol{\mathcal{F}}_{11} = \sum_{n,m}^{N} \int x_n x_m \Pr(\boldsymbol{x}) \, \mathrm{d}^N \boldsymbol{x} \, \mathcal{F}_{\mathrm{Q}}[\rho_{\mathrm{s}}, j_z^{(n)}, j_z^{(m)}]. \tag{5.26}$$

Second, the most trivial matrix element is $\boldsymbol{\mathcal{F}}_{00}$ which turns to depend only on the internal state ρ_{s},

$$\boldsymbol{\mathcal{F}}_{00} = \mathcal{F}_{\mathrm{Q}}[\rho_{\mathrm{s}}, J_z]. \tag{5.27}$$

Finally, we compute both $\boldsymbol{\mathcal{F}}_{01}$ and $\boldsymbol{\mathcal{F}}_{10}$. To compute this, note that both matrix elements are equal $\boldsymbol{\mathcal{F}}_{01} = \boldsymbol{\mathcal{F}}_{01}$, due to the properties of Eq. (5.11) for commuting H_0 and H_1. Therefore, we have to

compute only one of them

$$\boldsymbol{\mathcal{F}}_{01} = \sum_{n=1}^{N} \int x_n \Pr(\boldsymbol{x})\, \mathrm{d}^N \boldsymbol{x}\, \mathcal{F}_{\mathrm{Q}}[\rho_{\mathrm{s}}, j_z^{(n)}, J_z]. \tag{5.28}$$

With those results the bound for the precision for states sensitive to the homogeneous field which have the for of Eq. (5.5) is

$$(\Delta b_1)^{-2} \leqslant \sum_{n,m}^{N} \int x_n x_m \Pr(\boldsymbol{x})\, \mathrm{d}^N \boldsymbol{x}\, \mathcal{F}_{\mathrm{Q}}[\rho_{\mathrm{s}}, j_z^{(n)}, j_z^{(m)}] - \frac{\left(\sum_{n=1}^{N} \int x_n \Pr(\boldsymbol{x})\, \mathrm{d}^N \boldsymbol{x}\, \mathcal{F}_{\mathrm{Q}}[\rho_{\mathrm{s}}, j_z^{(n)}, J_z]\right)^2}{\mathcal{F}_{\mathrm{Q}}[\rho_{\mathrm{s}}, J_z]}. \tag{5.29}$$

We show now that this bound is invariant under displacements of the system as it is the Eq. (5.23). To compute this, we use the linearity of the last two arguments of $\mathcal{F}_{\mathrm{Q}}[\rho, A, B]$, Eq. (5.13), the fact that H_0 remains unchanged on the Heisenberg picture, and we also use the shifted H_1 operator, Eq. (5.21). Hence, the translated QFI matrix elements are written as

$$\boldsymbol{\mathcal{F}}_{00}(d) = \mathcal{F}_{\mathrm{Q}}[\rho, H_0(d)] = \mathcal{F}_{\mathrm{Q}}[\rho, H_0], \tag{5.30}$$

$$\begin{aligned} \boldsymbol{\mathcal{F}}_{01}(d) &= \mathcal{F}_{\mathrm{Q}}[\rho, H_0(d), H_1(d)] \\ &= \mathcal{F}_{\mathrm{Q}}[\rho, H_0, H_1 - dH_0] = \boldsymbol{\mathcal{F}}_{01} - d\boldsymbol{\mathcal{F}}_{00}, \end{aligned} \tag{5.31}$$

$$\begin{aligned} \boldsymbol{\mathcal{F}}_{11}(d) &= \mathcal{F}_{\mathrm{Q}}[\rho, H_1(d), H_1(d)] \\ &= \mathcal{F}_{\mathrm{Q}}[\rho, H_1 - dH_0, H_1 - dH_0] \\ &= \boldsymbol{\mathcal{F}}_{11} - 2d\boldsymbol{\mathcal{F}}_{01} + d^2\boldsymbol{\mathcal{F}}_{00}. \end{aligned} \tag{5.32}$$

Simple algebra shows that the bound for a displaced system is the same bound as is it would not be displaced,

$$\begin{aligned} (\Delta b_1)_d^{-2} &\leqslant \boldsymbol{\mathcal{F}}_{11}(d) - \frac{(\boldsymbol{\mathcal{F}}_{01}(d))^2}{\boldsymbol{\mathcal{F}}_{00}(d)} \\ &= \boldsymbol{\mathcal{F}}_{11} - 2d\boldsymbol{\mathcal{F}}_{01} + d^2\boldsymbol{\mathcal{F}}_{00} \\ &\quad - \frac{\boldsymbol{\mathcal{F}}_{01}^2 - 2d\boldsymbol{\mathcal{F}}_{01}\boldsymbol{\mathcal{F}}_{00} + d^2\boldsymbol{\mathcal{F}}_{00}^2}{\boldsymbol{\mathcal{F}}_{00}} \\ &= \boldsymbol{\mathcal{F}}_{11} - \frac{\boldsymbol{\mathcal{F}}_{01}^2}{\boldsymbol{\mathcal{F}}_{00}}. \end{aligned} \tag{5.33}$$

Note that this is equal to the Eq. (5.24).

This observations make the computations to compute the precision bounds in the next sections easier, since the now we can place the system arbitrarily wherever we choose. It also allows us, for example, to place the origin of our coordinate system as well as the system itself where the magnetic field is null. So, we can write the linear magnetic field simply as $\boldsymbol{B}(x) = xB_1\boldsymbol{k}$ where $\boldsymbol{k}$ is the unitary vector pointing on the z-direction perpendicular to x- and y-axis. The discourse we have had on the preceding section has a vital importance to understand properly the our results.

5.2 Chain of distinguishable atoms and two separated ensembles for magnetometry

Despite the generality of the tools we developed in Section 5.1, it is always useful to start with simple but concise examples. For this, we choose two state-of-the-art systems for the external state ρ_x which we know that behave well for estimating the gradient parameter. We will study the chain of atoms, where the atoms are placed one-by-one in a 1-dimensional grid of constant separation of a, and the two-ensembles of atoms, where half of the atoms are in $x = -a$ and the rest in $x = +a$.

5.2.1 Chain of distinguishable atoms

As we have said, the first spatial state will be given by N particles all placed equidistantly from each other on a one-dimensional spin chain, i.e., a chain of atoms in a 1-dimensional lattice [106], see Figure 5.1. We have that for that matter the probability density function describing the system is

$$\Pr(\boldsymbol{x}) = \prod_{n=1}^{N} \delta(x_n - na). \tag{5.34}$$

With this at hand we compute the single point averages and the two point averages corresponding to the ion-chain. For the single-point average, one of the integrals appearing in Eq. (5.29), we have that

$$\int x_n \Pr(\boldsymbol{x})\, \mathrm{d}^N\boldsymbol{x} = na, \tag{5.35}$$

and for the two-point correlation, which appears in Eqs. (5.23) and (5.29), we have the following for the case of the chain of atoms,

$$\int x_n x_m \Pr(\boldsymbol{x})\, \mathrm{d}^N\boldsymbol{x} = nma^2. \tag{5.36}$$

On the other hand, we use first a totally polarized state in the y-direction for the internal

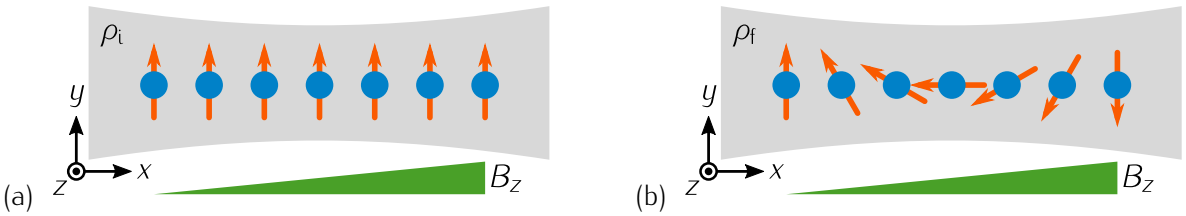

Figure 5.1: (blue-circles) A system of N-atoms of spin-j trapped (a) The ensemble is initially totally polarised along a perpendicular direction of the magnetic field B_z and the direction of the chain. The internal state can be written as $|+j\rangle_y^{\otimes N}$, the number represents m_y the eigenvalue of the one particle operator $j_y^{(n)}$. (b) One can see how the gradient field affects with a varying field strength the different spins when they are placed in different positions.

degrees of freedom, $\rho_s = (|+j\rangle_y\langle+j|_y)^{\otimes N}$ appeared in Eq. (2.33). This state is a state sensitive to the homogeneous field, so using that the state is pure and separable

$$\mathcal{F}_Q[|+j\rangle_y^{\otimes}, j_z^{(n)}, j_z^{(m)}] = 4(\langle j_z^{(n)}, j_z^{(m)}\rangle - \langle j_z^{(n)}\rangle\langle j_z^{(m)}\rangle) = 2j\delta_{n,m}. \tag{5.37}$$

Since this function is linear in the second and third arguments, $\mathcal{F}_Q[|+j\rangle_y^{\otimes}, j_z^{(n)}, J_z] = 2j$ and $\mathcal{F}_Q[|+j\rangle_y^{\otimes}, J_z] = 2jN$. With this, we can now write the precision bound for a chain of atoms when the internal state is totally polarized along the y-axis as

$$\begin{aligned}(\Delta b_1)^{-2}_{\text{ch,tp}} &\leqslant a^2\left\{\sum_{n=1}^{N} n^2 2j - \frac{(\sum_{n=1}^{N} n2j)^2}{N2j}\right\} \\ &= a^2\frac{N^2-1}{12}2jN.\end{aligned} \tag{5.38}$$

Despite that Equation (5.38) is a third order function of the particle number N and that it seems to overcome the ultimate scaling HS, on should notice that the length of the chain increases as we introduce more particles into the system. As we discussed before, one must normalize the effective size of the system to avoid false positives.

In our case we decide to use on all cases the standard deviation of the averaged particle position as the standard length measure of the system. We also include in our next definitions the averaged correlation of two different particle positions, since it will appear in the following sections and for

completeness. They are computed as follows respectively,

$$\mu = \int \frac{\sum_{n=1}^{N} x_n}{N} \Pr(\boldsymbol{x})\, \mathrm{d}^N \boldsymbol{x}, \tag{5.39}$$

$$\sigma^2 = \int \frac{\sum_{n=1}^{N} x_n^2}{N} \Pr(\boldsymbol{x})\, \mathrm{d}^N \boldsymbol{x} - \mu^2, \tag{5.40}$$

$$\eta = \int \frac{\sum_{n\neq m} x_n x_m}{N(N-1)} \Pr(\boldsymbol{x})\, \mathrm{d}^N \boldsymbol{x} - \mu^2. \tag{5.41}$$

So, the system effective width for the chain of atoms, computed by the variance Eq. (5.40), is given as

$$\sigma_{\mathrm{ch}}^2 = a^2 \frac{N^2 - 1}{12}. \tag{5.42}$$

It turns out that this exactly coincides with one of the factors we have in Eq. (5.38). Substituting this into the Eq. (5.38) we have that, for ion-chains where their constituents are separated by a constant distance and where the spin-state ρ_{s} is the totally polarized state along the y-direction, the precision bound is given by

$$(\Delta b_1)^{-2}_{\mathrm{ch,tp}} \leqslant \sigma_{\mathrm{ch}}^2 2jN, \tag{5.43}$$

in terms of σ_{ch}, the spin-number of each particle j and the particle number N.

5.2.2 Differential magnetometry with two ensembles

We now turn our attention to a state which is constituted by two distinguishable ensembles of atoms. Two ensembles of spin-j atoms spatially separated from each other have been realized in cold gases (e.g., Ref. [39]), and can be used for differential interferometry [26, 107]. We will also use an internal state such the maximal QFI is achieved so the reader gets familiar with our approach and sees how the best state to measure the gradient parameter looks like in our framework.

The spatial part is described by the following probability density function, where for an even number of particles half of the particles are at one position and the rest at another, both places at a distance of a from the origin

$$\Pr(\boldsymbol{x}) = \prod_{n=1}^{N/2} \delta(x_n + a) \prod_{n=N/2+1}^{N} \delta(x_n - a). \tag{5.44}$$

This could be realized in a double-well trap, where the width of the wells is negligible compared to the distance of the wells. To distinguish the two wells we will use the labels "L" and "R" for the

left and right wells respectively. With this we are able to compute the single-point and two-point correlation functions as

$$\int x_n \Pr(\boldsymbol{x})\, \mathrm{d}^N \boldsymbol{x} = \begin{cases} -a & \text{if} \quad n \leq N/2, \\ +a & \text{if} \quad n > N/2, \end{cases} \tag{5.45}$$

$$\int x_n x_m \Pr(\boldsymbol{x})\, \mathrm{d}^N \boldsymbol{x} = \begin{cases} -a^2 & \text{if} \quad (n,m) = (\mathrm{L},\mathrm{L}) \text{ or } (\mathrm{R},\mathrm{R}), \\ +a^2 & \text{if} \quad (n,m) = (\mathrm{L},\mathrm{R}) \text{ or } (\mathrm{L},\mathrm{R}). \end{cases} \tag{5.46}$$

For pure states insensitive to the homogeneous magnetic field we have that the QFI is computed directly as four times the variance of the gradient Hamiltonian, $\mathcal{F}_{\mathrm{Q}}[\rho, H_1, H_1] = 4(\Delta H_1)^2$. So, we just choose a state that having the spatial part defined by Eq. (5.44) and it is written as

$$|\Psi\rangle = \frac{1}{\sqrt{2}}(|{+}j\cdots{+}j\rangle^{(\mathrm{L})}|{-}j\cdots{-}j\rangle^{(\mathrm{R})} + |{-}j\cdots{-}j\rangle^{(\mathrm{L})}|{+}j\cdots{+}j\rangle^{(\mathrm{R})}), \tag{5.47}$$

where it can be seen as the superposition of the state fewest energy and the state with the greatest energy under the Hamiltonian H_1, see Figure 5.2.

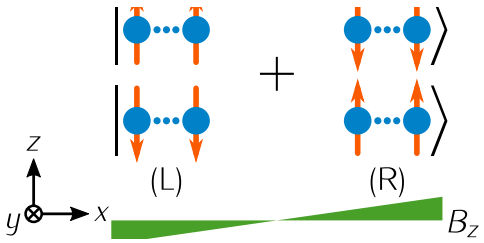

Figure 5.2: (blue-circles)

The state $|\Psi\rangle$ is indeed insensitive to the homogeneous field since both constituents are eigenstates of H_0 with the same eigenvalue. So we have that

$$\begin{aligned} (\Delta b_1)^{-2}|_{\max} &= \sum_{n,m}^{N} (-1)^{n+m} a^2 \mathcal{F}_{\mathrm{Q}}[|\psi\rangle, j_z^{(n)}, j_z^{(m)}] \\ &= a^2 \sum_{n,m}^{N} (-1)^{n+m} 4(-1)^{n+m} j^2 \\ &= 4a^2 j^2 N^2, \end{aligned} \tag{5.48}$$

where we have used the definition for pure states of QFI, $4(\langle j_z^{(n)} j_z^{(m)}\rangle - \langle j_z^{(n)}\rangle\langle j_z^{(m)}\rangle)$.

On the other hand if we compute now the standard deviation as we did before for the case of the

chain, Eqs. (5.39-5.42), we have that in this case $\mu = 0$ and the standard deviation

$$\sigma_{\text{dw}}^2 = \int d^N \boldsymbol{x} \Pr(\boldsymbol{x}) = a^2, \tag{5.49}$$

with which the proof follows. Before concluding the proof we want to show another more usual approach to the same problem.

It is as follows, given that the QFI is convex on states and having already fixed the external spatial state to be Equation (??), the inner state that maximises the QFI is the one that maximises $(\Delta H_1)^2$. In this case, taking into account the particle locations and that we have zero magnetic field at the origin,

$$H_{1,\text{eff}} = b_1 a(\mathbb{I}_{\text{od}} \otimes J_{z,\text{ev}} - J_{z,\text{od}} \otimes \mathbb{I}_{\text{ev}}), \tag{5.50}$$

where we write the effective Hamiltonian that the particles feel and "od" and "ev" stand for odd and even particle index respectively. From here it is easy to show that the state maximising such variance is the following,

, (5.51)

which is equivalent to the state in Equation (5.52). This proofs that we have use the right state, and with this we can compute the QFI as in the literature as $\mathcal{F}_{\text{Q}}[|\psi\rangle, H_1] = 4(\Delta H_1)^2 = 4a^2 j^2 N^2$. With this we finally conclude the proof.

The maximally entangled internal state that maximized the QFI too is

$$|\psi\rangle = \tfrac{1}{\sqrt{2}}(|0101\cdots01\rangle + |1010\cdots10\rangle). \tag{5.52}$$

Notice that this is a coherent state of all particles on the left "up" and all on the right "down" plus all on the left "down" and all on the right "up". We will choose without loosing of generality the particles to be spin-j particles. For this state insensitive to the homogeneous field and in the double-well spatial configuration, Eq. (??), the maximal achievable precision is

$$(\Delta b_1)^{-2}|_{\text{max}} = 4\sigma_{\text{dw}}^2 j^2 N^2 \tag{5.53}$$

In this section we have shown to the reader how one should handle the spatial width of the system for classifying it for gradient metrology as well as a state-of-the-art system on which the Heisenberg limit is achieved. Moreover, we have sown how to use the tools developed on previous section to compute simple bounds. In the next section we will focus on single cold-atoms ensembles since the play an important role on todays quantum technology and experiments and many groups are trying

to realize them whit great success but with few theoretical support from our point of view.

5.3 Magnetometry with an atomic ensemble

In this section, we discuss magnetometry with a single atomic ensemble in a more deep way than in the previous section. For that, we present precision bounds for the estimation of the magnetic field gradient, for states that are insensitive to the homogeneous field. We also present precision bounds for states that are sensitive to the the homogeneous field. We consider a one-dimensional cloud of spin-j atoms placed in a one dimensional trap, which is elongated in the $x-$direction. The magnetic field points in the $z-$direction, and has a constant gradient along the $x-$direction. The setup is depicted in Fig. **??**. In the last part of this section, we calculate precision bounds for the gradient estimation for some important multi-particle quantum states, for instance, Dicke states [] or GHZ states [46]. Note that all these states are permutationally invariant, since we assume a PI procedure to prepare the states.

5.3.1 Precision bound for an atomic ensemble

An atomic ensemble is defined as a finite number of atoms where they cannot be labeled individually. Thus, the initial quantum state is assumed to be PI. Hence apart from ρ_s, the probability distribution function $\Pr(\boldsymbol{x})$, appearing in Equation (**??**), must also be PI. The permutational invariance of $\Pr(\boldsymbol{x})$ implies that

$$\Pr(\boldsymbol{x}) = \tfrac{1}{N!}\sum_k \Pi_k[\Pr(\boldsymbol{x})], \tag{5.54}$$

where the summation is over all the possible permutations of the variables x_n denoted by Π_k.

As we have shown on Observations XXX and XXX, the precision bound is invariant under translations on the spatial Hilbert space. This allows us to place the "center of mass" of the system at the origin of the coordinates. With this simplifying assumptions the single-point average of the whole ensemble is

$$\mu = \int d^N\boldsymbol{x}\Pr(\boldsymbol{x})x_n = 0, \tag{5.55}$$

where we used the PI nature of $\Pr(\boldsymbol{x})$ to eliminate the sum and the N from the Equation (5.39). We will do the same with the second moments appearing on the variance, Eq. (5.40). Because of this, the size of the system can be related with the single variable, x_n, variance

$$\sigma^2 = \int \Pr(\boldsymbol{x})x_n^2\, d^N\boldsymbol{x}, \tag{5.56}$$

for any n, which is simplified due to the fact that the system is placed at the origin. In the same way, and due again to the PI nature of $\Pr(\boldsymbol{x})$ we write the covariance of two particle positions as

$$\eta = \int \Pr(\boldsymbol{x}) x_n x_m \, d^N\boldsymbol{x} \tag{5.57}$$

for any $n \neq m$. With this we have characterised all two-points correlations that potentially will appear on our calculations. An interesting property of the covariance of this type is that it is a value bounded from below and from above by the variance itself and the particle number N in the following way,

$$\frac{-\sigma^2}{N-1} \leqslant \eta \leqslant \sigma^2. \tag{5.58}$$

So it cannot contribute for a better scaling on the precision than since it scales as much as σ^2 with the particle number. Notice that the lower bound scales worse.

First of all we show an important property of states insensitive to the homogeneous field and we do so using the fact that the QFI for the homogeneous field generator, i.e, J_z, on those states is zero, $\mathcal{F}_{\mathrm{Q}}[\rho, J_z] = 0$. The identity follows,

$$\begin{aligned} \mathcal{F}_{\mathrm{Q}}[\rho, J_z] &= 0 \\ \sum_{n,m}^{N} \mathcal{F}_{\mathrm{Q}}[\rho, j_z^{(n)}, j_z^{(m)}] &= 0 \\ \sum_{n=1}^{N} \mathcal{F}_{\mathrm{Q}}[\rho, j_z^{(n)}] &= -\sum_{n\neq m}^{N} \mathcal{F}_{\mathrm{Q}}[\rho, j_z^{(n)}, j_z^{(m)}] \end{aligned} \tag{5.59}$$

where we use the linearity on the second and third arguments of $\mathcal{F}_{\mathrm{Q}}[\rho, \cdot, \cdot]$ to jump to the second line and subsequently the last line follows.

From the definition of the QFI for states insensitive to the homogeneous field, Eq. (5.23), we compute the bound for single ensembles in the following way,

$$\begin{aligned} (\Delta b_1)^{-2}|_{\max} &= \sum_{n,m}^{N} \int d^N\boldsymbol{x} \Pr(\boldsymbol{x}) x_n x_m \mathcal{F}_{\mathrm{Q}}[\rho_{\mathrm{s}}, j_z^{(n)}, j_z^{(m)}] \\ &= \sum_{n=1}^{N} \sigma^2 \mathcal{F}_{\mathrm{Q}}[\rho, j_z^{(n)}] + \sum_{n\neq m}^{N} \eta \mathcal{F}_{\mathrm{Q}}[\rho, j_z^{(n)}, j_z^{(m)}]. \end{aligned} \tag{5.60}$$

Together with Equation (5.59) the Observation **??** follows.

The precision is bounded from below for a single atomic ensemble insensitive to homogeneous field with the following quantity

$$(\Delta b_1)^{-2}|_{\max} = (\sigma^2 - \eta)\sum_{n=1}^{N} \mathcal{F}_{\mathrm{Q}}[\rho_{\mathrm{s}}, j_z^{(n)}]. \tag{5.61}$$

The bound in Eq. (5.61) can be saturated by an optimal measurement. Nevertheless, it is worth to notice that it cannot surpass the shot-noise scaling, $\sim N$, because $\mathcal{F}_{\mathrm{Q}}[\rho_{\mathrm{s}}, j_z^{(n)}]$, the QFI for the single-particle operator $j_z^{(n)}$, cannot be larger than j^2.

First of all, notice that the second term appearing on Equation (5.29) is proportional to the single-point average $\int d^N\boldsymbol{x}\mathrm{Pr}(\boldsymbol{x})x_n$ which by definition is the same for any x_n and by decision is chosen to be zero, since we placed the system at the origin. So, we only have to compute the first term of the Equation (5.29),

$$\begin{aligned}(\Delta b_1)^{-2} \leqslant& \sum_{n,m}^{N} \int d^N\boldsymbol{x}\mathrm{Pr}(\boldsymbol{x})x_n x_m \mathcal{F}_{\mathrm{Q}}[\rho_{\mathrm{s}}, j_z^{(n)}, j_z^{(m)}] \\ =& \sum_{n=1}^{N} \sigma^2 \mathcal{F}_{\mathrm{Q}}[\rho, j_z^{(n)}] + \sum_{n\neq m}^{N} \eta \mathcal{F}_{\mathrm{Q}}[\rho, j_z^{(n)}, j_z^{(m)}] \\ =&(\sigma^2 - \eta)\sum_{n=1}^{N} \mathcal{F}_{\mathrm{Q}}[\rho, j_z^{(n)}] + \eta \sum_{n,m}^{N} \mathcal{F}_{\mathrm{Q}}[\rho, j_z^{(n)}, j_z^{(m)}],\end{aligned} \tag{5.62}$$

where we add to the last term $\eta\sum_{n=1}^{N}\mathcal{F}_{\mathrm{Q}}[\rho, j_z^{(n)}]$ and subtract it from the first term. From this, using the fact that the QFI is linear on the second and third arguments again, the proof holds.

For states sensitive to homogeneous fields, the precision of estimating the gradient is bounded from above as

$$(\Delta b_1)^{-2} \leqslant (\sigma^2 - \eta)\sum_{n=1}^{N} \mathcal{F}_{\mathrm{Q}}[\rho_{\mathrm{s}}, j_z^{(n)}] + \eta\mathcal{F}_{\mathrm{Q}}[\rho_{\mathrm{s}}, J_z]. \tag{5.63}$$

The second term on the right-hand side of Eq. (5.63) is new in the sense that it did not appear on the bound for states insensitive to homogeneous fields. Note that the bound in Eq. (5.63) is not necessarily saturable if the optimal measurements to estimate the gradient parameter and the homogeneous parameter do not commute with each other. This question will be discussed in Appendix **??**. Note that even if the first term cannot overcome the SL, in the second term the covariance is multiplied by QFI for estimating the homogeneous field and therefore this concrete term can make the bound, for extremely correlated particle positions, to scale as HL.

5.3.2 Precision limit for various spin-states

In this section, we present the precision limits for different classes of important quantum states such as the totally polarised state, the state having the largest precision among separable state, or the singlet state. We see how the precision bounds presented before, Eqs. (5.61, 5.63), are implemented. We show first the results for singlet that are insensitive to homogeneous fields. In this case, the bounds can be achieved by choosing the appropriate magnitude to measure. The rest of the results are for states sensitive to homogeneous fields which in general are not necessarily achievable bounds.

Singlet states

We consider now the singlet state, which is invariant under the influence of a homogeneous field along any direction. So we have to compute the formula for the bound of the precision Eq. (5.61), and we already know that it can be saturated for a certain optimal measurement.

A singlet state is an eigenstate of the collective J_z and J^2 operators, with an eigenvalue zero in both cases. Since this subspace is degenerate we have to take care in order to compute the precision bound. There are many different singlet states for an ensemble of N spin-j particles, and still a great amount of them are PI. Surprisingly the precision bound we compute is the same for any PI singlet. Atomic ensembles in a singlet state have been experimentally created with cold gases [12, 56].

In an N-particle system, there are several singlets pairwise orthogonal to each other. The number of such singlets, D_0, depends on the particle spin j and the number of particles N.

The most general singlet state can be written in the total angular momentum basis, using D to label the degenerate states, $|J, M_z, D\rangle$, in the following diagonal way

$$\rho_s = \sum_{D=1}^{D_0} \lambda_D |0,0,D\rangle\langle 0,0,D|, \tag{5.64}$$

where $\sum_D \lambda_D = 1$. In its complete form the eigenvalues of the spin density matrix are $\lambda_{J,M_z,D} = \delta_{0,J}\lambda_D$.

Looking at Eq. (5.61), we must compute the generalized QFI for the one-particle operator $j_z^{(n)}$ in order to compute the precision bound for PI singlet states. For that purpose we use the fact that when $j_z^{(n)}$ acts on a singlet state, it produces a state outside of the singlet subspace. This can be proved by noting that

$$e^{i\pi J_x} j_z^{(n)} e^{-i\pi J_x} = -j_z^{(n)} \tag{5.65}$$

and that $e^{-i\pi J_x}|0,0,D\rangle = |0,0,D\rangle$ holds for any pure singlet state. Employing these equalities, we

can arbitrarily flip the sign of $j_z^{(n)}$ so

$$\langle 0,0,D|j_z^{(n)}|0,0,D'\rangle = -\langle 0,0,D|j_z^{(n)}|0,0,D'\rangle, \tag{5.66}$$

which implies

$$\langle 0,0,D|j_z^{(n)}|0,0,D'\rangle = 0, \tag{5.67}$$

for any pair of pure singlet singlet states.

In order to compute the QFI for the singlet state we use Eq. (5.14). Hence we can write the following for the second term on Eq. (5.14),

$$8\sum_{D,D'} \frac{\lambda_D \lambda_{D'}}{\lambda_D+\lambda_{D'}} |\langle 0,0,D|j_z^{(n)}|0,0,D'\rangle|^2 = 0. \tag{5.68}$$

It follows that the QFI for any singlet is indeed simply

$$\mathcal{F}_{\mathrm{Q}}[\rho_{\mathrm{s}}, j_z^{(n)}] = 4\,\mathrm{tr}(\rho_{\mathrm{s}}(j_z^{(n)})^2). \tag{5.69}$$

For the last part of the proof, we must compute the expectation value of the operator $(j_z^{(n)})^2$. For that we have that

$$\mathrm{tr}(\rho_{\mathrm{s}}(j_k^{(n)})^2) = \mathrm{tr}(\rho_{\mathrm{s}}(j_l^{(n)})^2), \tag{5.70}$$

for any pair $k, l \in x, y, z$ due to the rotationally invariance of the singlet, i.e, all the singlets remain invariant under a $SU(2)$ transformation of the kind $U = e^{i\phi J_{\vec{n}}}$, where $\vec{n}$ is an unitary vector belonging to the positional space. We also have that

$$\langle (j_x^{(n)})^2 + (j_y^{(n)})^2 + (j_z^{(n)})^2\rangle = j(j+1), \tag{5.71}$$

for any state, since it represent the spin number of the particle, which is fixed. Hence, the expectation value of $(j_z^{(n)})^2$ on the singlet is

$$\mathrm{tr}(\rho_{\mathrm{s}}(j_z^{(n)})^2) = \tfrac{j(j+1)}{3}, \tag{5.72}$$

for all the singlets. Inserting this into Eq. (5.69), we obtain $\mathcal{F}_{\mathrm{Q}}[\rho_{\mathrm{s}}, j_z^{(n)}] = \frac{4j(j+1)}{3}$; and by Eq. (5.61) the statement is proved.

For PI spin states living in the singlet subspace, i.e., states composed of vectors that have zero eigenvalues for J_z and J^2 and all their possible statistical mixtures, the precision of the magnetic

gradient parameter is bounded from above as

$$(\Delta b_1)^{-2}_{\max} = \tfrac{4Nj(j+1)}{3}\left(\sigma^2 - \eta\right). \tag{5.73}$$

As mentioned earlier, singlet states are insensitive to homogeneous magnetic fields, hence determining the gradient leads to a single-parameter estimation problem. This implies that there is an optimal operator that saturates the precision bound given by Eq. (5.73). However, it is usually very hard to find this optimal measurement, although a formal procedure for this exists [4]. In Ref. [55], a particular set-up for determining the magnetic gradient with PI singlet states was suggested by the measurement of the J_x^2 collective operator. For this scenario the precision is given by

$$(\Delta b_1)^{-2} = \frac{|\partial_{b_1}\langle J_x^2\rangle|^2}{\langle J_x^4\rangle - \langle J_x^2\rangle^2}. \tag{5.74}$$

In Appedix **??**, we show that this measurement actually provides, in the short-time limit, an optimal precision for gradient metrology.

Totally polarised state

The totally polarised state can easily be prepared experimentally. It has already been used for gradient magnetometry with a single atomic ensemble [29, 30]. For the gradient measurement as for the measurement of the homogeneous field, the polarisation must be perpendicular to the field we want to measure in order to take advantage of the interaction between the particles and the field. Here we chose as before the totally polarized state along the y-axis which is written as $|j\rangle_y^{\otimes N}$. Notice that this state is a state sensitive to the homogeneous field, hence, we must use the Equation (5.63) to compute the bound.

For the pure product states we have that $\mathcal{F}_{\mathrm{Q}}[|\psi\rangle, A] = 4(\Delta A)^2$. Together with, $(\Delta j_z^{(n)})^2 = j/2$ and $(\Delta J_z)^2 = Nj/2$, when the polarisation is perpendicular to the z-direction, the precision will be computed straightforward from Equation (5.63).

Before to do so, let us comment on the heuristics description of the evolution of the system. The homogeneous field rotates all spins by the same angle, while the gradient rotates the spin at different position by a different angle. Due to that, the homogeneous field rotates the collective spin, but does not change its absolute value. On the other hand, the field gradient decreases the absolute value of the spin, which has been used in Ref. [35] for gradient magnetometry, see Fig. 5.1.

Therefore, the Cramér-Rao bound fixes the highest value for the precision of the totaly polarised

state as follows,

$$(\Delta b_1)^{-2} \leqslant 2Nj\sigma^2. \tag{5.75}$$

Note that the precision bound for the totally polarised state is smaller than that of the optimal separable state we present later on. We can see clearly that the precision scales as $\mathcal{O}(N)$.

The best separable state

We will now turn our attention to the precision bound for all separable spin states. It is useful to obtain this value so we have a direct comparison of what is the best classically achievable precision. It will turn out that for $j > \frac{1}{2}$, it is possible to achieve a precision higher than with the fully polarised state. We use the Equation (5.55) and substituting it onto the the low-level definitions of the precision bounds for the gradient magnetometry, Eqs. (5.23, 5.29). We see that if the state is sensitive to the homogeneous field only affects on the implications of the bound, one can be saturated for sure and on the other case it depends on the measurements compatibility as we discussed before. What we have is that the bound is the same $\mathcal{F}_Q[\rho, H_1]$ for both cases. Thus, it is easy to argue that the precision bound is a convex function on the states, even when the external state ρ_x is fixed. Therefore, the separable inner state that maximizes the precision must be a pure product state that maximises all possible $\mathcal{F}_Q[\rho_s, j_z^{(n)}, j_z^{(m)}]$.For pure product states we have first that $\mathcal{F}_Q[\rho_s, j_z^{(n)}, j_z^{(m)}]$ is four times the correlation between the single particle spin operators, which using the well known properties of the pure product states is zero when $n \neq m$. Finally, we have to maximise each $4(\Delta j_z^{(n)})^2$.

As we mentioned before, the best possible precision bound will be reached for a pure product state that maximises all $(\Delta j_z^{(n)})^2$. From the definition of the variance,

$$(\Delta j_z^{(n)})^2 = \langle (j_z^{(n)})^2 \rangle - \langle j_z^{(n)} \rangle^2. \tag{5.76}$$

Hence, We try a state that approaches to zero its polarisation on the z-direction and maximises $\langle (j_z^{(n)})^2 \rangle$. We have that $|\psi\rangle = (|+j\rangle + |-j\rangle)/\sqrt{2}$ is ideal for this. The inner state for all particles is just the product state $\rho_s = |\psi\rangle\langle\psi|^{\otimes N}$. Notice that this state is permutationally invariant, hence it is a tight bound for what can be achieved with PI separable states. The variance of a single particle operator is $(\Delta j_z^{(n)})^2 = j^2$ so the proof holds.

After this discussion we make the following observation. The best achievable precision for separable states is written as

$$(\Delta b_1)^{-2} \leqslant 4Nj^2\sigma^2, \tag{5.77}$$

where the state itself is sensitive to homogeneous fields. This bound coincides with the totally polarized state studied before when the spin number j is equal to half.

In the following we try to find a better precision bound making use of presumably better entangled states. Note that the bound for the singlet state, even if it is entangled, is above the bound for the totally polarised state but below of the bound defined for the best separable state. Nevertheless, when the singlet state is used effect of the homogeneous magnetic field has not to be compensated since it is insensitive to it and thus the bound can be saturated with an optimal estimator for the gradient field.

The unpolarised Dicke states $|Nj,0\rangle$ and $|Nj,0\rangle_x$

Unpolarised Dicke states play an important role in quantum opticsand quantum information science. The Dicke state $|Nj,0\rangle_l$ with a maximal $\langle J_x^2+J_y^2+J_z^2\rangle$ and $\langle J_l\rangle=0$ for any $l\in x,y,z$ is particularly interesting due to its entanglement properties and its metrological usefulness. This state has been created in photonic experiments [99, 100, 102] and in cold atoms [20, 57], while a Dicke state with $\langle J_z\rangle>0$ has been created with cold trapped ions [108].

The Dicke state $|Nj,0\rangle$ is an eigenstate of J_z so insensitive to homogeneous magnetic field pointing into the z-direction, thus the precision can be saturate by some measurement. Whereas, The Dicke state $|Nj,0\rangle_x$ is sensitive to the homogeneous field. Moreover it is very useful for homogeneous magnetometry as it has been shown in Ref. [XXX]. Here we consider large particle numbers, to make the results simpler.

Since both Dicke states are pure, we have that the QFI appearing on Equations (5.61, 5.63) are simply four times the following variances of $j_z^{(n)}$ and J_z. Since both Dicke states are unpolarized, all the first moments $\langle J_l\rangle$ are equal to zero and due to they are PI all $\langle j_l^{(n)}\rangle$ are also zero for all $l\in x,y,z$. Therefore, we only need to compute the second moments to compute the variances.

We will compute all the second moments on all directions of single particle operators $j_l^{(n)}$ as well as the global operators J_l for $|Nj,0\rangle$. Later on, we will map those result to the Dicke state for the x-direction. We have the following characteristic identities for $|Nj,0\rangle$, $\langle J_z^2\rangle=0$ and $\langle J_{\perp z}^2\rangle=\frac{Nj(Nj+1)}{2}$ where "$\perp z$" can be seen as x or y. From the global second moments we can write for the single particle the following,

$$\langle (j_z^{(n)})^2\rangle=-(N-1)\langle j_z^{(n)}j_z^{(m)}\rangle \tag{5.78}$$

$$\langle (j_{\perp z}^{(n)})^2\rangle=\tfrac{j(Nj+1)}{2}-(N-1)\langle j_{\perp z}^{(n)}j_{\perp z}^{(m)}\rangle \tag{5.79}$$

for all $\forall n\neq m$ due to the PI nature of the state. Together with $\langle (j_z^{(n)})^2+2(j_{\perp z}^{(n)})^2\rangle=j(j+1)$ due to the rotational symmetry along the z-axis, we have three independent equations relating all the four moments. In Ref. [55], a mapping between the Dicke states of spin-j ensembles and of spin-$\frac{1}{2}$

ensembles was provided, by which the expectation value

$$\langle (j_z^{(n)})^2 \rangle = \tfrac{(N-1)j^2}{2jN-1} \tag{5.80}$$

was derived. With this we are able to obtain all the rest unknown values we are searching for. In the large N limit, this gives

$$\lim_{N\to\infty} \langle (j_z^{(n)})^2 \rangle = \tfrac{j}{2}. \tag{5.81}$$

From Eq. (5.61) we can conclude that $\mathcal{F}_Q[\rho_s, j_z^{(1)}] = 2j$, hence the proof for homogeneous insensitive $|Nj, 0\rangle$ holds.

Now we have only to apply a mapping between the x- and z-axis to obtain the respective second moments for $|Nj, 0\rangle_x$. We do that on the large N limit,

$$\lim_{N\to\infty} \langle (j_z^{(n)})^2 \rangle = \tfrac{j(2j+1)}{4}. \tag{5.82}$$

Finally, we have all the ingredients to go forward on writing the precision bound.

For large N, the precision bound for the Dicke $|Nj, 0\rangle$ state is

$$(\Delta b_1)^{-2}_{\max} = 2Nj\left(\sigma^2 - \eta\right), \tag{5.83}$$

whereas for the homogeneous sensitive Dicke state $|Nj, 0\rangle_x$ the precision is bounded from above by

$$(\Delta b_1)^{-2} \leqslant Nj(2j+1)(\sigma^2 - \eta) + 2Nj(Nj+1)\eta, \tag{5.84}$$

which shows in principle a Heisenberg behavior in the second term on the right-hand side.

The GHZ state

The GHZ states are also highly entangled states that play an important role in quantum physics [46]. They have been created experimentally in photonic systems [49, 51, 109] and trapped ions [53, 54].

The GHZ state is defined for qubits in the following way

$$|\mathrm{GHZ}\rangle = \tfrac{1}{\sqrt{2}}(|0\cdots 0\rangle + |1\cdots 1\rangle). \tag{5.85}$$

This state is very sensitive to the homogeneous field. On the other hand, as shown in Appendix **??**, for this state the optimal estimators for the homogeneous field and the gradient field are compatible.

Singlet states	$(\Delta b_1)^{-2}\big\|_{\max} = \frac{4Nj(j+1)}{3}\left(\sigma^2 - \eta\right)$
Totally polarised state	$(\Delta b_1)^{-2} \leqslant 2N\sigma^2 j$
Best separable state	$(\Delta b_1)^{-2} \leqslant 4N\sigma^2 j^2$
$\|Nj, 0\rangle$ Dicke state	$(\Delta b_1)^{-2}\big\|_{\max} = \frac{Nj}{2}\left(\sigma^2 - \eta\right)$
$\|Nj, 0\rangle_x$ Dicke state	$(\Delta b_1)^{-2} \leqslant N(\sigma^2 - \eta)(2j^2 + j) + 2\eta Nj(Nj + 1)$
GHZ state	$(\Delta b_1)^{-2}\big\|_{\max} = 4Nj^2(\sigma^2 + (N-1)\eta)$

Table 5.1: Precision bounds for differential magnetometry for various quantum states. For the definition of the states, see the text. If the bound are proved to be saturable then the m̈axs̈ubscript is used instead of an inequality.

It means that both parameters can be estimated at once. Hence, in this case, the bound given in Eq. (5.63) can be saturated by some measurement set-up. In order to calculate this bound explicitly, let us recall that for pure states the QFI is simplified to Eq. (5.15). In the GHZ state the expectation value of $j_z^{(n)}$ and J_z is equal to zero, as it was for the Dicke state, and $\langle (j_z^{(n)})^2 \rangle = j^2$ and $\langle J_z^2 \rangle = N^2 j^2$, hence we obtain the following result

$$(\Delta b_1)^{-2}_{\max} = 4Nj^2\sigma^2 + 4N(N-1)j^2\eta. \tag{5.86}$$

This means that we can reach the Heisenberg-limit with such states, but only in cases where η is positive, i.e, that the particles stay spatially correlated.

Summary of results

Finally, we summarise the precision bounds obtained for various quantum states in Table 5.1.

6 Conclusions

HELLO it's me again

Appendices

A Discussion on angular momentum subspaces for different spins

As we mentioned in the Section 2.2.1, when dealing with many particle systems their Hilbert spaces are represented by tensor product of the individuals. So, the final dimension is the product of all single-particle dimensions which lead to an exponentially large Hilbert space. In order to simplify many of the computations we work with, it is worth to notice that some interesting structures arise from this kind of tensor product construction.

Let us name some basic assumptions with which the problem of adding angular momentum subspaces is even further simplified. First of all, the single particle Hilbert space must be discrete and finite, so we have that it can be represented by d-level system or qudit, where d is the dimension of the single-particle system. When d equals to two, we have the well known 2-level system or qubit. We assume as well, that all the particles have the same dimension. The basis of such systems is composed by d different eigenstates of the spin operator $j_z^{(n)}$, where n denotes the Hilbert space in which the operator is defined. We also assume that all parties have the same dimension d, so the total dimension is d^N. The spin-number j is defined as $j = (d-1)/2$. It is usual to use the single-particle angular momentum projector operator in the z-direction to completely characterize the basis

$$j_z^{(n)}|m\rangle = m|m\rangle, \tag{A.1}$$

where $m = -j, -j+1, \ldots, +j-1, +j$ and this way the necessary d different pure states are defined.

In quantum information, the two eigenstates $|-1/2\rangle$ and $|+1/2\rangle$ of 2-level systems, or qubits, are

usually identified with $|0\rangle$ and $|1\rangle$ respectively, since the qubit case is the most studied case on which the dichotomized representation of classic *bit*s, ones and zeros, is directly related with. It is also usual to make use of a more simplified notation $|-1/2\rangle \equiv |-\rangle$ and $|+1/2\rangle \equiv= |+\rangle$ for this particular case. Besides, one can map directly the $m = -j, -j+1, \ldots, +j-1, +j$ to $\tilde{m} = 0, 1, \ldots, d-1$, where $\tilde{m}$ is normally used in the quantum information framework, whereas the m gives directly the eigenvalue of the state when $j_z^{(n)}$ is applied.

A first approach to write a concise eigenbasis for the whole Hilbert space is to multiply by tensor product all the eigenstates of each single party. This way, and permuting all the states from right to left, we construct a well defined basis as

$$\begin{aligned}
&|-j, -j, \ldots, -j, -j\rangle, \\
&|-j, -j, \ldots, -j, -j+1\rangle, \\
&\vdots \\
&|-j, -j, \ldots, -j+1, -j\rangle, \\
&|-j, -j, \ldots, -j+1, -j+1\rangle, \\
&\vdots \\
&|+j, +j, \ldots, +j, +j\rangle,
\end{aligned} \tag{A.2}$$

where we have used the notation $|m_1, m_2, \ldots, m_{N-1}, m_N\rangle \equiv |m_1\rangle \otimes |m_2\rangle \cdots \otimes |m_N\rangle$. This basis is yet an eigenbasis of $J_z = \sum_n j_z^{(n)}$. On the other hand, it is not a eigenbasis of the total angular momentum $\boldsymbol{J}^2 = J_x^2 + J_y^2 + J_z^2$, neither all the eigenstates are permutationally invariant, which is useful for dealing with symmetric subspaces.

We will explain shortly how to write a basis in which all members are eigenstates of the total angular momentum $\boldsymbol{J}^2$ as well as of the J_z operator. This is a usual procedure when adding angular momentum operators, see Ref. [65, 66] for more details. For that, we have the ladder $J_\pm := J_x \pm iJ_y$ operators which increase or decrease the eigenvalue of the state when J_z is applied without changing the eigenvalue for $\boldsymbol{J}^2$. Therefore, if we start from $|-j, -j, \ldots, -j\rangle$, which is an eigenstate of $\boldsymbol{J}^2$ with the maximal eigenvalue $Nj(Nj+1)$, and we apply J_+ subsequently we obtain all the states belonging to that subspace on which $\boldsymbol{J}^2$ is maximal. We use the following notation for the maximal eigenvalue of the $\boldsymbol{J}^2$ operator

$$\mathcal{J}_{Nj} \equiv Nj(Nj+1), \tag{A.3}$$

since it appears many times throughout the thesis. Then, we use orthogonal states and we keep doing this until we have all the subspaces characterized.

Hence, the eigenstates are characterized with only three simple numbers $|J, M, D\rangle$ instead of Eq. (A.2), First of all, we have the total angular momentum number J, where $J = 0, 1, \ldots, Nj$ for this particular case in which we are adding together N spin-j particles (we also assume that if the spin number j equals we have even number of particles for simplicity), and defined the eigenvalue of the $\boldsymbol{J}$ operator as $J(J+1)$. Then, we have the quantum number of the angular momentum projection into the z-direction, $M = -J, -J+1, \ldots, +J-1, +J$, which corresponds to the eigenvalue of the J_z operator. And finally, the degeneracy number of the J subspaces, $D = 1, 2, \ldots, D_J$, that is always one for the $J = Nj$ subspace and for the rest it depends in general in the number of particles as well as in the spin-number j.

We now show the definition of some of the most used states throughout this thesis. For the spin-$\frac{1}{2}$ particles, i.e., qubits, several states appear. For instance, the symmetric states, i.e., the states that interchanging any pair of particles remain the same, are all confined into the subspace where $J = \frac{N}{2}$ is maximal. They can be constructed taking n particles in the $|-1/2\rangle$ or $|0\rangle$ state and $N - n$ in the $|+1/2\rangle$ or $|1\rangle$ state and making them symmetric in the following way

$$|J = N/2, M\rangle \equiv \binom{N}{N/2+M}^{-1/2} \sum_k \mathcal{P}_k(|0\rangle^{\otimes N/2-M} \otimes |1\rangle^{\otimes N/2+M}) \tag{A.4}$$

where the sum is over all possible different permutations of the state denoted by $\mathcal{P}_k$. Note that the Dicke states, called like this after R. H. Dicke use them to explain the coherent superradiance effect [90], or the two-mode Fock states for a constant particle number (note also that we have two modes, the two level of each particle, and that the whole state is symmetric), are equivalent to the states in Eq. (A.4). Therefore apart from Eq. (A.4), we use the following notation for these states

$$|\mathrm{D}_{N,n}\rangle \equiv |J = N/2, M = N/2 - n\rangle, \tag{A.5}$$

where where n gives the number of particles that are in $|-1/2\rangle$ or . One particularly interesting case of these states is the unpolarized Dicke state

$$|\mathrm{D}_N\rangle \equiv |\mathrm{D}_{N,\frac{N}{2}}\rangle, \tag{A.6}$$

where because it appears many times in this thesis, we skip writing the second subscript for simplicity.

Finally, we present another state before the conclusion of this appendix. It is the permutationally invariant singlet state for spin-$\frac{1}{2}$ particles. This is a uniquely defined state that can be constructed in several different ways. One can start by the product state of pairwise singlets $|\Psi^-\rangle = \frac{1}{\sqrt{2}}(|01\rangle - 10)$ and later impose the permutational invariance for the density matrix. Or one can find the thermal

ground states of the Hamiltonian $H = \boldsymbol{J}^2$. Finally, either it can be constructed as the completely mixed state of the subspace where $J = 0$. All these alternative constructions are collected in the following equation respectively

$$\left(\frac{N!}{2^{N/2}(N/2)!}\right)^{-\frac{1}{2}} \sum_{k\in\sigma_s} \mathcal{P}_k(|\Psi^-\rangle\langle\Psi^-|^{\otimes N/2}) \equiv \lim_{\beta\to\infty} \frac{\exp(-\boldsymbol{J}^2\beta)}{\mathrm{tr}(\exp(-\boldsymbol{J}^2\beta))} \equiv \frac{1}{D_0}\sum_{D=1}^{D_0} |0,0,D\rangle\langle 0,0,D|, \tag{A.7}$$

where β is the inverse of the Boltzman constant k_B times the temperature T, and σ_s is the set of all possible unique permutations, in this case $\frac{N!}{2^{N/2}(N/2)!}$.

B Proof of Equation (??)

To compute the Eq. (??), we start by the expectation value of $\boldsymbol{J}^4$ for the pure Dicke state $|D_N\rangle$. In one hand we have that it is simply equal to square $\langle \boldsymbol{J}^2\rangle$

$$\langle \boldsymbol{J}^4\rangle = \left(\frac{N(N+2)}{4}\right)^2. \tag{B.1}$$

On the other hand this must be equal to

$$\langle (J_y^2 + J_z^2 + J_x^2)\boldsymbol{J}^2\rangle = \langle J_y^4\rangle + \langle J_z^4\rangle + \langle \{J_y^2, J_z^2\}\rangle, \tag{B.2}$$

where we omitted the terms that contain J_x^2 since we obtain zero from them. Next, due to the rotational symmetry along the x-axis, we can swap the index y and z inside each expectation value to obtain

$$\langle J_y^4\rangle + \langle J_y^2 J_z^2\rangle = \frac{1}{2}\left(\frac{N(N+2)}{4}\right)^2. \tag{B.3}$$

Now we focus on computing $\langle J_y^2 J_z^2\rangle$.

C Simplification of $\langle \{J_x^2, J_y^2\} + \{J_x, J_y\}^2\rangle$

The expectation value appearing on Eq. (3.15) which we want to simplify has 6 different terms, all with two J_x and another two J_y,

$$\langle J_x^2 J_y^2\rangle + \langle J_x J_y J_x J_y\rangle + \langle J_x J_y^2 J_x\rangle + \langle J_y J_x^2 J_y\rangle + \langle J_y J_x J_y J_x\rangle + \langle J_y^2 J_x^2\rangle. \tag{C.1}$$

From all those terms the third is somehow referent, since the pure unpolarized Dicke state used as reference is align with the x-axis, so $J_x|\mathrm{D}_{N,N/2}\rangle_x = 0$.

We use the commutation relations of the angular momentum operators $[J_k, J_l] = \epsilon_{klm} i J_m$, where ϵ_{klm} is the Levi-Civita symbol, to rearrange all operators,

$$\langle J_x^2 J_y^2\rangle = i\langle J_x J_z J_y\rangle + \langle J_x J_y J_x J_y\rangle, \tag{C.2a}$$
$$\langle J_x J_y J_x J_y\rangle = i\langle J_x J_y J_z\rangle + \langle J_x J_y^2 J_x\rangle, \tag{C.2b}$$
$$\langle J_x J_y^2 J_x\rangle = \langle J_x J_y^2 J_x\rangle, \tag{C.2c}$$
$$\langle J_y J_x^2 J_y\rangle = i\langle J_y J_x J_z\rangle + \langle J_y J_x J_y J_x\rangle, \tag{C.2d}$$
$$\langle J_y J_x J_y J_x\rangle = -i\langle J_z J_y J_x\rangle + \langle J_x J_y^2 J_x\rangle, \tag{C.2e}$$
$$\langle J_y^2 J_x^2\rangle = -i\langle J_y J_z J_x\rangle + \langle J_y J_x J_y J_x\rangle. \tag{C.2f}$$

One may notice that with those relations is enough to see that we have six $\langle J_x J_y^2 J_x\rangle$, for instance, Equation (C.2a) is $i\langle J_x J_z J_y\rangle$ plus Equation (C.2b) which at the same time is $i\langle J_x J_y J_z\rangle$ plus Equation (C.3c). So each equation has at the end one $\langle J_x J_y^2 J_x\rangle$ plus or minus some expectation value of the product of three operators.

For the three terms operators and again using the commutation relations we can further simplify this expression. Trying to get one $\langle J_x J_y J_z\rangle$ on each term, we obtain the following,

$$i\langle J_x J_z J_y\rangle = \langle J_x^2\rangle + i\langle J_x J_y J_z\rangle, \tag{C.3a}$$
$$2i\langle J_x J_y J_z\rangle = 2i\langle J_x J_y J_z\rangle, \tag{C.3b}$$
$$i\langle J_y J_x J_z\rangle = \langle J_z^2\rangle + i\langle J_x J_y J_z\rangle, \tag{C.3c}$$
$$-i\langle J_y J_z J_x\rangle = \langle J_y^2\rangle - \langle J_z\rangle - i\langle J_x J_y J_z\rangle \tag{C.3d}$$
$$\begin{aligned} -3i\langle J_z J_y J_x\rangle &= -3\langle J_x^2\rangle - 3i\langle J_y J_z J_x\rangle \\ &= -3\langle J_x^2\rangle + 3\langle J_y^2\rangle - 3i\langle J_y J_x J_z\rangle \\ &, = -3\langle J_x^2\rangle + 3\langle J_y^2\rangle - 3\langle J_z^2\rangle - 3i\langle J_x J_y J_z\rangle. \end{aligned} \tag{C.3e}$$

Now if we sum it all, note that the all 3 operators terms simplify, and if we take into account $6\langle J_x J_y^2 J_x\rangle$ the resulting expression is the following,

$$4\langle J_y^2\rangle - 3\langle J_z^2\rangle - 2\langle J_x^2\rangle + 6\langle J_x J_y^2 J_x\rangle \tag{C.4}$$

D Calculation of $|\langle D_{N,m}|_z|D_{N,N/2}\rangle_x|^2$

The Dicke state is defined in Eq: (??), for more details on algular momentu subspaces see Appendix ?? Hello this is the appendix to write about ...

E Spin-squeezing Hamiltonian

F Husimi Q-representation and the Bloch sphere

To represent states with angular momentum bigger than $J = \frac{1}{2}$ is convinient to use the so-called Husimi Q-representation [] on the Bloch-sphere. In fact it is straightforward to represent in a 3D-sphere all the possible states as it is done for qubits.

The Husimi Q-representation must be normalized to 1. Hence,

$$\int Q_\rho(\Omega)\,\mathrm{d}\Omega = 1, \tag{F.1}$$

where Ω represents the solid angle of the sphere, i.e., the function is a function of φ and θ, the azimuth angle and the polar angle respectivelly, and $\mathrm{d}\Omega = \sin(\theta)\mathrm{d}\varphi\mathrm{d}\theta$. We will use it to describe states belonging to the symmetric subspace or for states belonging to the maximum angular momentum. Therefore, the $Q_\rho(\Omega)$ function will be proportional to the fidelities of totally polarized states that point to different directions represented by Ω.

In the case of many qubits such totally polarized states can be written as

$$|N/2, N/2\rangle_\Omega \equiv |\Omega\rangle := |1\rangle_\Omega \otimes |1\rangle_\Omega \otimes |1\rangle_\Omega \otimes \ldots |1\rangle_\Omega, \tag{F.2}$$

where can be reformulated as the eigenstate with the maximum eigenvalue for $J_\Omega = \cos(\varphi)\sin(\theta)J_x + \sin(\varphi)\sin(\theta)\,J_y + \cos(\theta)J_z$ operator. An alternative way to obtain such totally polarized states $|\Omega\rangle$ is to rotate a totally polarized state along the z-direction by θ angle along the y-axis and then applying a rotation of φ angle along the z-axis. Hence,

$$\begin{aligned} |\Omega\rangle &= e^{-i\varphi J_z} e^{-i\theta J_y} |11\ldots1\rangle \\ J_\Omega|\Omega\rangle &= \frac{N}{2}|\Omega\rangle \end{aligned} \tag{F.3}$$

We write the quasi-probability $Q(\Omega)$ proportional to the fidelity with respect to $|\Omega\rangle$ of the state

$$Q_\rho(\Omega) \propto \mathrm{tr}(\rho|\Omega\rangle\langle\Omega|). \tag{F.4}$$

The normalization constant comes from Eq. (F.1), where a prove state such as the totally mixed state on the symmetric subspace can be used for which $\mathrm{tr}(\frac{\mathbb{I}}{N+1}|\Omega\rangle\langle\Omega|) = \frac{1}{N+1}$. Integrating the Eq. (F.1) we obtain the proportionality factor and it is shown in the following equation

$$Q_\rho(\Omega) = \frac{1}{4\pi(N+1)}\,\mathrm{tr}(\rho|\Omega\rangle\langle\Omega|), \tag{F.5}$$

which must be true for N qubits in the symmetric subspace. Similar definitions could be acompleased for different subspaces or even for different spin number of the constituents.

G Legendre transform

The Legendre transform of a convex function, say $f : x \to f(x)$, is defined as the maximum distance between the function the line rx and $f(x)$ at same x. In can be written as follows,

$$\hat{f}(r) := \max_x\{rx - f(x)\}, \tag{G.1}$$

where $\hat{f}(r)$ represents the transformed function [96]. A geometric representation of the transform is given on the Figure .1.

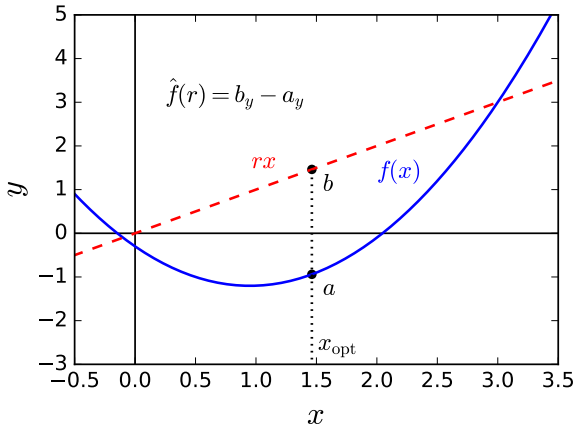

Figure .1: Graphical representation of the Legendre transform. (blue-line) Convex function, $f(x) = x^2 - 1.9x - 0.3$, to be transformed. (red-dashed) Constant slope line passing by the coordinate system origin, rx. The Legendre transform is the maximal difference between rx and $f(x)$ at the same x. In this case, the vertical distance between a and b.

The inverse transformation is simply obtained by applying again the same technique. One fully recovers the

$$f(x) = \max_r\{rx - \hat{f}(r)\}. \tag{G.2}$$

Let us develop the example shown in the Figure .1, where the function is $f(x) = x^2 - 1.9x - 0.3$. In this case the problem is well defined on the complete real axis. Now, one has to find the maximum of $g(r, x) = rx - f(x)$ for all $\forall r$. This maximum is easily obtained in this particular case with usual techniques. On has to solve for x the following equation $\partial_x g(r, x) = 0$. Thus, the maximum is at $x_{\text{opt}} = \frac{r+1.9}{2}$ and hence, the Legendre transform is the following,

$$\hat{f}(r) = \frac{r^2}{4} + 0.95r + 1.2025. \tag{G.3}$$

If one applies again the transformation the resulting function is again the original one.

H Binomial identities

I Calculation of the QFI matrix elements

Starting first for states insensitive to the homogeneous fields and later on for states sensitive to it, we must compute the matrix elements of the quantum Fisher information defined for the generators H_0 and H_1. We use the functional defined in Eq. (5.11) to compute the matrix elements. We also use thermal states with respect to the spatial degrees of freedom Eq. (5.5), since it is one of the most common situations in the experiments.

First of all, we compute the $\boldsymbol{\mathcal{F}}_{11} \equiv \mathcal{F}_{\text{Q}}[\rho, H_1, H_1] \equiv \mathcal{F}_{\text{Q}}[\rho, H_1]$, since it is valid for states that are insensitive to the homogeneous field as well as for states that are sensitive to it. We have the following for the QFI

$$\begin{aligned}\mathcal{F}_{\text{Q}}[\rho, H_1] &= 2\iint \sum_{\lambda,\nu} \frac{1}{\delta(\mathbf{0})} \frac{(\Pr(\boldsymbol{x})p_\lambda - \Pr(\boldsymbol{y})p_\nu)^2}{\Pr(\boldsymbol{x})p_\lambda + \Pr(\boldsymbol{y})p_\nu} |(H_1)_{\boldsymbol{x},\lambda;\boldsymbol{y},\nu}|^2 \,\mathrm{d}^N\boldsymbol{x}\mathrm{d}^N\boldsymbol{y} \\ &= 2\iint \sum_{\lambda,\nu} \frac{1}{\delta(\mathbf{0})} \frac{(\Pr(\boldsymbol{x})p_\lambda - \Pr(\boldsymbol{y})p_\nu)^2}{\Pr(\boldsymbol{x})p_\lambda + \Pr(\boldsymbol{y})p_\nu} (\delta(\boldsymbol{x} - \boldsymbol{y}))^2 \sum_{n,m}^{N} x_n x_m \langle\lambda|j_z^{(n)}|\nu\rangle\langle\nu|j_z^{(m)}|\lambda\rangle \,\mathrm{d}^N\boldsymbol{x}\mathrm{d}^N\boldsymbol{y}\end{aligned} \tag{I.1}$$

Using the definition of the Dirac delta inside one of the integrals we have that

$$\begin{aligned}\mathcal{F}_{\mathrm{Q}}[\rho, H_1] &= 2\int \sum_{\lambda,\nu} \frac{\Pr(\boldsymbol{x})}{\delta(\boldsymbol{0})} \frac{(p_\lambda - p_\nu)^2}{p_\lambda + p_\nu} \delta(\boldsymbol{x}-\boldsymbol{x}) \sum_{n,m}^{N} x_n x_m \langle\lambda|j_z^{(n)}|\nu\rangle\langle\nu|j_z^{(m)}|\lambda\rangle \,\mathrm{d}^N\boldsymbol{x} \\ &= 2\int \Pr(\boldsymbol{x}) \sum_{\lambda,\nu} \frac{(p_\lambda - p_\nu)^2}{p_\lambda + p_\nu} \sum_{n,m}^{N} x_n x_m \langle\lambda|j_z^{(n)}|\nu\rangle\langle\nu|j_z^{(m)}|\lambda\rangle \,\mathrm{d}^N\boldsymbol{x} \\ &= \sum_{n,m}^{N} \int x_n x_m \Pr(\boldsymbol{x})\,\mathrm{d}^N\boldsymbol{x}\, \mathcal{F}_{\mathrm{Q}}[\rho_{\mathrm{s}}, j_z^{(n)}, j_z^{(m)}],\end{aligned} \tag{I.2}$$

where we used the Eq. (5.19) for the simplification of the matrix elements of H_1, where in the third line we used on of the Dirac deltas to eliminate $\boldsymbol{y}$ from the equation, and where in the fourth line we toke the 2 factor in front, the sum over λ and ν and the matrix elements of $j_z^{(n)}$ and $j_z^{(m)}$ and we reconstructed $\mathcal{F}_{\mathrm{Q}}[\rho_{\mathrm{s}}, j_z^{(n)}, j_z^{(m)}]$ using its definition Eq. (5.11). We finally reordered all the terms in order to group what it has to be integrated together between "$\int$" and "$\mathrm{d}^N\boldsymbol{x}$", which in this case represents a two-point correlation function of x_n and x_m over the PDF $\Pr(\boldsymbol{x})$.

We now similarly do for $\boldsymbol{\mathcal{F}}_{01}$ and $\boldsymbol{\mathcal{F}}_{00}$. We use again a state of the form Eq. (5.5) to compute these matrix elements of the QFI. We also use the simplified expression for the matrix elements of H_0 for this case Eq. (5.25). For $\boldsymbol{\mathcal{F}}_{01}$, the computation looks like

$$\begin{aligned}\boldsymbol{\mathcal{F}}_{01} &= 2\iint \sum_{\lambda,\nu} \frac{1}{\delta(\boldsymbol{0})} \frac{(\Pr(\boldsymbol{x})p_\lambda - \Pr(\boldsymbol{y})p_\nu)^2}{\Pr(\boldsymbol{x})p_\lambda + \Pr(\boldsymbol{y})p_\nu} (H_0)_{\boldsymbol{x},\lambda;\boldsymbol{y},\nu} (H_1)_{\boldsymbol{y},\nu;\boldsymbol{x},\lambda} \,\mathrm{d}^N\boldsymbol{x}\mathrm{d}^N\boldsymbol{y} \\ &= 2\iint \sum_{\lambda,\nu} \frac{1}{\delta(\boldsymbol{0})} \frac{(\Pr(\boldsymbol{x})p_\lambda - \Pr(\boldsymbol{y})p_\nu)^2}{\Pr(\boldsymbol{x})p_\lambda + \Pr(\boldsymbol{y})p_\nu} (\delta(\boldsymbol{x}-\boldsymbol{y}))^2 \sum_{n,m}^{N} x_m \langle\lambda|j_z^{(n)}|\nu\rangle\langle\nu|j_z^{(m)}|\lambda\rangle \,\mathrm{d}^N\boldsymbol{x}\mathrm{d}^N\boldsymbol{y}.\end{aligned} \tag{I.3}$$

Using the definition of the Dirac delta inside one of the integrals we have that

$$\begin{aligned}\boldsymbol{\mathcal{F}}_{01} &= 2\int \sum_{\lambda,\nu} \frac{\Pr(\boldsymbol{x})}{\delta(\boldsymbol{0})} \frac{(p_\lambda - p_\nu)^2}{p_\lambda + p_\nu} \delta(\boldsymbol{x}-\boldsymbol{x}) \sum_{n,m}^{N} x_m \langle\lambda|j_z^{(n)}|\nu\rangle\langle\nu|j_z^{(m)}|\lambda\rangle \,\mathrm{d}^N\boldsymbol{x} \\ &= 2\int \Pr(\boldsymbol{x}) \sum_{\lambda,\nu} \frac{(p_\lambda - p_\nu)^2}{p_\lambda + p_\nu} \sum_{n,m}^{N} x_m \langle\lambda|j_z^{(n)}|\nu\rangle\langle\nu|j_z^{(m)}|\lambda\rangle \,\mathrm{d}^N\boldsymbol{x}.\end{aligned} \tag{I.4}$$

Which follows from the definition of Eq. (5.11)

$$\begin{aligned}\boldsymbol{\mathcal{F}}_{01} &= \sum_{n,m}^{N} \int x_m \mathrm{Pr}(\boldsymbol{x})\, \mathrm{d}^N\boldsymbol{x}\, \mathcal{F}_{\mathrm{Q}}[\rho_{\mathrm{s}}, j_z^{(n)}, j_z^{(m)}] \\ &= \sum_{n=1}^{N} \int x_n \mathrm{Pr}(\boldsymbol{x})\, \mathrm{d}^N\boldsymbol{x}\, \mathcal{F}_{\mathrm{Q}}[\rho_{\mathrm{s}}, j_z^{(n)}, J_z],\end{aligned} \tag{I.5}$$

where we used the same arguments as when computing Eq. (I.2), and we use the linearity on the second and third arguments of the functional Eq. (5.11) in the last line to remove the one of the summation indexes. Note that the main difference with respect to $\boldsymbol{\mathcal{F}}_{11}$ is that in this case the integral represents a single-point average instead of a two-point correlation function. Finally, for the matrix element $\boldsymbol{\mathcal{F}}_{00}$ we have that

$$\begin{aligned}\boldsymbol{\mathcal{F}}_{00} &= 2 \iint \sum_{\lambda,\nu} \frac{1}{\delta(\mathbf{0})} \frac{(\mathrm{Pr}(\boldsymbol{x})p_\lambda - \mathrm{Pr}(\boldsymbol{y})p_\nu)^2}{\mathrm{Pr}(\boldsymbol{x})p_\lambda + \mathrm{Pr}(\boldsymbol{y})p_\nu} |(H_0)_{\boldsymbol{x},\lambda;\boldsymbol{y},\nu}|^2\, \mathrm{d}^N\boldsymbol{x}\mathrm{d}^N\boldsymbol{y} \\ &= 2 \iint \sum_{\lambda,\nu} \frac{1}{\delta(\mathbf{0})} \frac{(\mathrm{Pr}(\boldsymbol{x})p_\lambda - \mathrm{Pr}(\boldsymbol{y})p_\nu)^2}{\mathrm{Pr}(\boldsymbol{x})p_\lambda + \mathrm{Pr}(\boldsymbol{y})p_\nu} (\delta(\boldsymbol{x}-\boldsymbol{y}))^2 \sum_{n,m}^{N} \langle\lambda|j_z^{(n)}|\nu\rangle\langle\nu|j_z^{(m)}|\lambda\rangle\, \mathrm{d}^N\boldsymbol{x}\mathrm{d}^N\boldsymbol{y}.\end{aligned} \tag{I.6}$$

We use now the definition of the Dirac delta such that

$$\begin{aligned}\boldsymbol{\mathcal{F}}_{00} &= 2 \int \sum_{\lambda,\nu} \frac{\mathrm{Pr}(\boldsymbol{x})}{\delta(\mathbf{0})} \frac{(p_\lambda - p_\nu)^2}{p_\lambda + p_\nu} \delta(\boldsymbol{x}-\boldsymbol{x}) \sum_{n,m}^{N} \langle\lambda|j_z^{(n)}|\nu\rangle\langle\nu|j_z^{(m)}|\lambda\rangle\, \mathrm{d}^N\boldsymbol{x} \\ &= 2 \int \mathrm{Pr}(\boldsymbol{x}) \sum_{\lambda,\nu} \frac{(p_\lambda - p_\nu)^2}{p_\lambda + p_\nu} \sum_{n,m}^{N} \langle\lambda|j_z^{(n)}|\nu\rangle\langle\nu|j_z^{(m)}|\lambda\rangle\, \mathrm{d}^N\boldsymbol{x}.\end{aligned} \tag{I.7}$$

We apply the definition of Eq. (5.11) and we reorder terms as

$$\begin{aligned}\boldsymbol{\mathcal{F}}_{00} &= \sum_{n,m}^{N} \int \mathrm{Pr}(\boldsymbol{x})\, \mathrm{d}^N\boldsymbol{x}\, \mathcal{F}_{\mathrm{Q}}[\rho_{\mathrm{s}}, j_z^{(n)}, j_z^{(m)}] \\ &= \sum_{n,m}^{N} \mathcal{F}_{\mathrm{Q}}[\rho_{\mathrm{s}}, j_z^{(n)}, j_z^{(m)}] \\ &= \mathcal{F}_{\mathrm{Q}}[\rho_{\mathrm{s}}, J_z, J_z] = \mathcal{F}_{\mathrm{Q}}[\rho_{\mathrm{s}}, J_z],\end{aligned} \tag{I.8}$$

where we simplify the integral using the normalization of the PDF which is equal to 1. Note that we obtain the QFI for the homogeneous field as expected.

Bibliography

[1] M. Glaser and M. Kochsiek. *Handbook of Metrology*. Wiley, New York, 2010.

[2] V. Giovannetti, S. Lloyd, and L. Maccone. *Quantum-enhanced measurements: Beating the standard quantum limit*. Science, **306** 1330–1336, 2004.

[3] V. Giovannetti, S. Lloyd, and L. Maccone. *Quantum metrology*. Phys. Rev. Lett, **96** 010401, 2006.

[4] M. G. A. Paris. *Quantum estimation for quantum technology*. International Journal of Quantum Information, **7** 125–137, 2009.

[5] C. Gross. *Spin squeezing, entanglement and quantum metrology with bose–einstein condensates*. Journal of Physics B: Atomic, Molecular and Optical Physics, **45** 103001, 2012.

[6] R. Demkowicz-Dobrzański, M. Jarzyna, and J. Kołodyński. *Quantum limits in optical interferometry*. Progress in Optics, **60** 345, May 2015.

[7] L. Pezze and A. Smerzi. *Quantum theory of phase estimation*. Preprint, arXiv:1411.5164, 2014.

[8] C. W. Helstrom. *Quantum detection and estimation theory*. Journal of Statistical Physics, **1** 231–252, 1969.

[9] A. Holevo. *Probabilistic and Statistical Aspects of Quantum Theory*. North-Holland, Amsterdam, 1982.

[10] S. L. Braunstein, C. M. Caves, and G. Milburn. *Generalized uncertainty relations: Theory, examples, and lorentz invariance*. Annals of Physics, **247** 135–173, April 1996.

[11] D. Petz. *Quantum information theory and quantum statistics*. Springer, Berlin, Heilderberg, 2008.

[12] G. Tóth and M. W. Mitchell. *Generation of macroscopic singlet states in atomic ensembles*. New Journal of Physics, **12** 053007, 2010.

[13] R. Horodecki, P. Horodecki, M. Horodecki, and K. Horodecki. *Quantum entanglement*. Reviews of Modern Physics, **81** 865–942, June 2009.

[14] O. Gühne and G. Tóth. *Entanglement detection*. Physics Reports, **474** 1–75, 2009.

[15] L. Pezzé and A. Smerzi. *Entanglement, nonlinear dynamics, and the heisenberg limit*. Physical Review Letters, **102** 100401, March 2009.

[16] A. Louchet-Chauvet, J. Appel, J. J. Renema, D. Oblak, N. Kjaergaard, and E. S. Polzik. *Entanglement-assisted atomic clock beyond the projection noise limit*. New Journal of Physics, **12** 065032, 2010.

[17] J. Appel, P. J. Windpassinger, D. Oblak, U. B. Hoff, N. Kjaergaard, and E. S. Polzik. *Mesoscopic atomic entanglement for precision measurements beyond the standard quantum limit*. Proceedings of the National Academy of Sciences, **106** 10960–10965, June 2009.

[18] M. F. Riedel, P. Böhi, Y. Li, T. W. Hänsch, A. Sinatra, and P. Treutlein. *Atom-chip-based generation of entanglement for quantum metrology*. Nature, **464** 1170–1173, 2010.

[19] C. Gross, T. Zibold, E. Nicklas, J. Esteve, and M. K. Oberthaler. *Nonlinear atom interferometer surpasses classical precision limit*. Nature, **464** 1165–1169, 2010.

[20] B. Lücke, M. Scherer, J. Kruse, L. Pezzé, F. Deuretzbacher, P. Hyllus, J. Peise, W. Ertmer, J. Arlt, L. Santos, A. Smerzi, and C. Klempt. *Twin matter waves for interferometry beyond the classical limit*. Science, **334** 773–776, November 2011.

[21] H. Strobel, W. Muessel, D. Linnemann, T. Zibold, D. B. Hume, L. Pezzé, A. Smerzi, and M. K. Oberthaler. *Fisher information and entanglement of non-gaussian spin states*. Science, **345** 424–427, 2014.

[22] P. Hyllus, O. Gühne, and A. Smerzi. *Not all pure entangled states are useful for sub-shot-noise interferometry*. Physical Review A, **82** 012337, July 2010.

[23] J. Borregaard and A. S. Sørensen. *Near-heisenberg-limited atomic clocks in the presence of decoherence*. Physical Review Letters, **111**, August 2013.

[24] E. M. Kessler, P. Kómár, M. Bishof, L. Jiang, A. S. Sørensen, J. Ye, and M. D. Lukin. *Heisenberg-limited atom clocks based on entangled qubits*. Physical Review Letters, **112**, May 2014.

[25] W. Wasilewski, K. Jensen, H. Krauter, J. J. Renema, M. V. Balabas, and E. S. Polzik. *Quantum noise limited and entanglement-assisted magnetometry*. Physical Review Letters, **104** 133601, March 2010.

[26] K. Eckert, P. Hyllus, D. Bruss, U. V. Poulsen, M. Lewenstein, C. Jentsch, T. Müller, E. Rasel, and W. Ertmer. *Differential atom interferometry beyond the standard quantum limit*. Physical Review A, **73** 013814, 2006.

[27] S. Wildermuth, S. Hofferberth, I. Lesanovsky, S. Groth, P. Krüger, J. Schmiedmayer, and I. Bar-Joseph. *Sensing electric and magnetic fields with bose-einstein condensates*. Applied Physics Letters, **88** 264103, 2006.

[28] F. Wolfgramm, A. Cere, F. A. Beduini, A. Predojević, M. Koschorreck, and M. W. Mitchell. *Squeezed-light optical magnetometry*. Physical Review Letters, **105** 053601, 2010.

[29] M. Koschorreck, M. Napolitano, B. Dubost, and M. W. Mitchell. *High resolution magnetic vector-field imaging with cold atomic ensembles*. Applied Physics Letters, **98** 074101, 2011.

[30] M. Vengalattore, J. M. Higbie, S. R. Leslie, J. Guzman, L. E. Sadler, and D. M. Stamper-Kurn. *High-resolution magnetometry with a spinor bose-einstein condensate*. Physical Review Letters, **98** 200801, May 2007.

[31] M.-K. Zhou, Z.-K. Hu, X.-C. Duan, B.-L. Sun, J.-B. Zhao, and J. Luo. *Precisely mapping the magnetic field gradient in vacuum with an atom interferometer*. Physical Review A, **82** 061602, December 2010.

[32] R. Schnabel, N. Mavalvala, D. E. McClelland, and P. K. Lam. *Quantum metrology for gravitational wave astronomy*. Nature Communications, **1** 121, November 2010.

[33] The LIGO Scientific Collaboration et al. *A gravitational wave observatory operating beyond the quantum shot-noise limit*. Nature Physics, **7** 962–965, 2011.

[34] R. Demkowicz-Dobrzański, K. Banaszek, and R. Schnabel. *Fundamental quantum interferometry bound for the squeezed-light-enhanced gravitational wave detector geo 600*. Physical Review A, **88** 041802, October 2013.

[35] N. Behbood, F. Martin Ciurana, G. Colangelo, M. Napolitano, M. W. Mitchell, and R. J. Sewell. *Real-time vector field tracking with a cold-atom magnetometer*. Applied Physics Letters, **102** 173504, 2013.

[36] W. Muessel, H. Strobel, D. Linnemann, D. B. Hume, and M. K. Oberthaler. *Scalable spin squeezing for quantum-enhanced magnetometry with bose-einstein condensates*. Physical Review Letters, **113** 103004, September 2014.

[37] T. Fernholz, H. Krauter, K. Jensen, J. F. Sherson, A. S. Sørensen, and E. S. Polzik. *Spin squeezing of atomic ensembles via nuclear-electronic spin entanglement*. Physical Review Letters, **101** 073601, August 2008.

[38] J. Hald, J. L. Sørensen, C. Schori, and E. S. Polzik. *Spin squeezed atoms: A macroscopic entangled ensemble created by light*. Physical Review Letters, **83** 1319–1322, August 1999.

[39] B. Julsgaard, A. Kozhekin, and E. S. Polzik. *Experimental long-lived entanglement of two macroscopic objects*. Nature, **413** 400–403, 2001.

[40] K. Hammerer, A. S. Sørensen, and E. S. Polzik. *Quantum interface between light and atomic ensembles*. Reviews of Modern Physics, **82** 1041–1093, April 2010.

[41] J. Esteve, C. Gross, A. Weller, S. Giovanazzi, and M. Oberthaler. *Squeezing and entanglement in a bose–einstein condensate*. Nature, **455** 1216–1219, 2008.

[42] M. Kitagawa and M. Ueda. *Squeezed spin states*. Physical Review A, **47** 5138–5143, June 1993.

[43] D. J. Wineland, J. J. Bollinger, W. M. Itano, and D. J. Heinzen. *Squeezed atomic states and projection noise in spectroscopy*. Physical Review A, **50** 67–88, July 1994.

[44] A. Sørensen, L.-M. Duan, J. I. Cirac, and P. Zoller. *Many-particle entanglement with bose–einstein condensates*. Nature, **409** 63–66, January 2001.

[45] J. Ma, X. Wang, C. P. Sun, and F. Nori. *Quantum spin squeezing*. Physics Reports, **509** 89–165, December 2011.

[46] D. M. Greenberger, M. A. Horne, A. Shimony, and A. Zeilinger. *Bell's theorem without inequalities*. **58** 1131–1143, 1990.

[47] D. Leibfried, M. Barrett, T. Schaetz, J. Britton, J. Chiaverini, W. Itano, J. Jost, C. Langer, and D. Wineland. *Toward heisenberg-limited spectroscopy with multiparticle entangled states*. Science, **304** 1476–1478, 2004.

[48] D. Bouwmeester, J.-W. Pan, M. Daniell, H. Weinfurter, and A. Zeilinger. *Observation of three-photon Greenberger-Horne-Zeilinger entanglement*. Physical Review Letters, **82** 1345, February 1999.

[49] J.-W. Pan, D. Bouwmeester, M. Daniell, H. Weinfurter, and A. Zeilinger. *Experimental test of quantum nonlocality in three-photon Greenberger-Horne-Zeilinger entanglement*. Nature, **403** 515, February 2000.

[50] Z. Zhao, T. Yang, Y.-A. Chen, A.-N. Zhang, M. Żukowski, and J.-W. Pan. *Experimental violation of local realism by four-photon Greenberger-Horne-Zeilinger entanglement*. Physical Review Letters, **91** 180401, October 2003.

[51] C.-Y. Lu, X.-Q. Zhou, O. Gühne, W.-B. Gao, J. Zhang, Z.-S. Yuan, A. Goebel, T. Yang, and J.-W. Pan. *Experimental entanglement of six photons in graph states*. Nature Physics, **3** 91–95, 2007.

[52] W.-B. Gao, C.-Y. Lu, X.-C. Yao, P. Xu, O. Gühne, A. Goebel, Y.-A. Chen, C.-Z. Peng, Z.-B. Chen, and J.-W. Pan. *Experimental demonstration of a hyper-entangled ten-qubit schrödinger cat state*. Nature Physics, **6** 331–335, 2010.

[53] C. Sackett, D. Kielpinski, B. King, C. Langer, V. Meyer, C. Myatt, M. Rowe, Q. Turchette, W. Itano, D. Wineland, and C. Monroe. *Experimental entanglement of four particles*. Nature, **404** 256–259, 2000.

[54] T. Monz, P. Schindler, J. T. Barreiro, M. Chwalla, D. Nigg, W. A. Coish, M. Harlander, W. Hänsel, M. Hennrich, and R. Blatt. *14-qubit entanglement: Creation and coherence*. Physical Review Letters, **106** 130506, March 2011.

[55] I. Urizar-Lanz, P. Hyllus, I. L. Egusquiza, M. W. Mitchell, and G. Tóth. *Macroscopic singlet states for gradient magnetometry*. Physical Review A, **88** 013626, July 2013.

[56] N. Behbood, F. Martin Ciurana, G. Colangelo, M. Napolitano, G. Tóth, R. J. Sewell, and M. W. Mitchell. *Generation of macroscopic singlet states in a cold atomic ensemble*. Physical Review Letters, **113** 093601, August 2014.

[57] C. Hamley, C. Gerving, T. Hoang, E. Bookjans, and M. Chapman. *Spin-nematic squeezed vacuum in a quantum gas*. Nature Physics, **8** 305–308, 2012.

[58] R. Krischek, C. Schwemmer, W. Wieczorek, H. Weinfurter, P. Hyllus, L. Pezzé, and A. Smerzi. *Useful multiparticle entanglement and sub-shot-noise sensitivity in experimental phase estimation*. Physical Review Letters, **107** 080504, August 2011.

[59] B. Escher, R. de Matos Filho, and L. Davidovich. *General framework for estimating the ultimate precision limit in noisy quantum-enhanced metrology*. Nature Physics, **7** 406–411, 2011.

[60] R. Demkowicz-Dobrzański, J. Kołodyński, and M. Guţă. *The elusive heisenberg limit in quantum-enhanced metrology*. Nature Communications, **3** 1063, 2012.

[61] K. F. Riley, M. P. Hobson, and S. J. Bence. *Mathematical methods for physics and engineering: a comprehensive guide*. Cambridge University Press, 2006.

[62] R. J. Barlow. *Statistics: a guide to the use of statistical methods in the physical sciences*. John Wiley & Sons, 1989.

[63] A. Luis. *Nonlinear transformations and the heisenberg limit*. Physics Letters A, **329** 8–13, 2004.

[64] G. Tóth and I. Apellaniz. *Quantum metrology from a quantum information science perspective*. Journal of Physics A: Mathematical and Theoretical, **47** 424006, 2014.

[65] C. Cohen-Tannoudji, B. Diu, and F. Laloë. *Quantum mechanics*. Wiley, New York, 1977.

[66] J. J. Sakurai and J. J. Napolitano. *Modern quantum mechanics*. Pearson Higher Ed, 2014.

[67] G. Lindblad. *On the generators of quantum dynamical semigroups*. Communications in Mathematical Physics, **48** 119–130, 1976.

[68] M. A. Nielsen and I. L. Chuang. *Quantum information and quantum computation*. Cambridge: Cambridge University Press, **2** 23, 2000.

[69] H.-P. Breuer and F. Petruccione. *The theory of open quantum systems*. Oxford University Press on Demand, 2002.

[70] W. K. Wootters. *Statistical distance and hilbert space*. Physical Review D, **23** 357, 1981.

[71] S. L. Braunstein. *Quantum limits on precision measurements of phase*. Physical Review Letters, **69** 3598–3601, December 1992.

[72] S. L. Braunstein and C. M. Caves. *Statistical distance and the geometry of quantum states*. Physical Review Letters, **72** 3439–3443, May 1994.

[73] P. Hyllus, W. Laskowski, R. Krischek, C. Schwemmer, W. Wieczorek, H. Weinfurter, L. Pezzé, and A. Smerzi. *Fisher information and multiparticle entanglement*. Physical Review A, **85** 022321, February 2012.

[74] P. Hyllus, L. Pezzé, and A. Smerzi. *Entanglement and sensitivity in precision measurements with states of a fluctuating number of particles*. Physical Review Letters, **105** 120501, September 2010.

[75] J. Kołodyński and R. Demkowicz-Dobrzański. *Phase estimation without a priori knowledge in the presence of loss*. Physical Review A, **82** 053804, November 2010.

[76] J. Kołodyński and R. Demkowicz-Dobrzański. *Efficient tools for quantum metrology with uncorrelated noise*. New Journal of Physics, **15** 073043, 2013.

[77] M. Napolitano, M. Koschorreck, B. Dubost, N. Behbood, R. J. Sewell, and M. W. W. Mitchell. *Interaction-based quantum metrology showing scaling beyond the heisenberg limit*. Nature, **471** 486–489, March 2011.

[78] S. Boixo, S. T. Flammia, C. M. Caves, and J. Geremia. *Generalized limits for single-parameter quantum estimation*. Physical Review Letters, **98** 090401, February 2007.

[79] D. Braun and J. Martin. *Heisenberg-limited sensitivity with decoherence-enhanced measurements*. Nature Communications, **2** 223, March 2011.

[80] S. M. Roy and S. L. Braunstein. *Exponentially enhanced quantum metrology*. Physical Review Letters, **100** 220501, June 2008.

[81] S. Choi and B. Sundaram. *Bose-einstein condensate as a nonlinear ramsey interferometer operating beyond the heisenberg limit*. Physical Review A, **77** 053613, May 2008.

[82] A. M. Rey, L. Jiang, and M. D. Lukin. *Quantum-limited measurements of atomic scattering properties*. Physical Review A, **76** 053617, November 2007.

[83] C. Helstrom. *Quantum Detection and Estimation Theory*. Academic Press, New York, 1976.

[84] G. Tóth and D. Petz. *Extremal properties of the variance and the quantum fisher information*. Physical Review A, **87** 032324, March 2013.

[85] S. Yu. *Quantum fisher information as the convex roof of variance*. Preprint, arXiv:1302.5311, 2013.

[86] J. Liu, X.-X. Jing, W. Zhong, and X.-G. Wang. *Quantum Fisher Information for Density Matrices with Arbitrary Ranks*. Communications in Theoretical Physics, **61** 45–50, January 2014.

[87] S. Boixo and A. Monras. *Operational interpretation for global multipartite entanglement*. Physical Review Letters, **100** 100503, March 2008.

[88] G. Tóth. *Multipartite entanglement and high-precision metrology*. Physical Review A, **85** 022322, February 2012.

[89] Ł. Czekaj, A. Przysiężna, M. Horodecki, and P. Horodecki. *Quantum metrology: Heisenberg limit with bound entanglement*. Physical Review A, **92** 062303, December 2015.

[90] R. H. Dicke. *Coherence in spontaneous radiation processes*. Physical Review, **93** 99–110, January 1954.

[91] Y.-L. Zhang, H. Wang, L. Jing, L.-Z. Mu, and H. Fan. *Fitting magnetic field gradient with heisenberg-scaling accuracy*. Scientific Reports, **4** 7390, December 2014.

[92] B. Lücke, J. Peise, G. Vitagliano, J. Arlt, L. Santos, G. Tóth, and C. Klempt. *Detecting multiparticle entanglement of dicke states*. Physical Review Letters, **112** 155304, April 2014.

[93] P. Hyllus, L. Pezzé, A. Smerzi, and G. Tóth. *Entanglement and extreme spin squeezing for a fluctuating number of indistinguishable particles*. Physical Review A, **86** 012337, July 2012.

[94] O. Gühne, M. Reimpell, and R. F. Werner. *Estimating entanglement measures in experiments*. Phys. Rev. Lett., **98**, March 2007.

[95] J. Eisert, F. G. S. L. Brandão, and K. M. R. Audenaert. *Quantitative entanglement witnesses*. New Journal of Physics, **9** 46–46, March 2007.

[96] R. Rockafellar. *Convex Analysis*. Princeton University Press, 1996.

[97] G. Tóth. *Detection of multipartite entanglement in the vicinity of symmetric dicke states*. Journal of the Optical Society of America B: Optical Physics, **24** 275–282, February 2007.

[98] I. Apellaniz, B. Lücke, J. Peise, C. Klempt, and G. Tóth. *Detecting metrologically useful entanglement in the vicinity of dicke states*. New Journal of Physics, **17** 083027, August 2015.

[99] N. Kiesel, C. Schmid, G. Tóth, E. Solano, and H. Weinfurter. *Experimental observation of four-photon entangled dicke state with high fidelity*. Physical Review Letters, **98** 063604, February 2007.

[100] W. Wieczorek, R. Krischek, N. Kiesel, P. Michelberger, G. Tóth, and H. Weinfurter. *Experimental entanglement of a six-photon symmetric dicke state*. Physical Review Letters, **103** 020504, July 2009.

[101] R. Prevedel, G. Cronenberg, M. S. Tame, M. Paternostro, P. Walther, M. S. Kim, and A. Zeilinger. *Experimental realization of dicke states of up to six qubits for multiparty quantum networking*. Physical Review Letters, **103** 020503, July 2009.

[102] A. Chiuri, C. Greganti, M. Paternostro, G. Vallone, and P. Mataloni. *Experimental quantum networking protocols via four-qubit hyperentangled dicke states*. Physical Review Letters, **109** 173604, October 2012.

[103] D. Petz. *Covariance and fisher information in quantum mechanics*. Journal of Physics A: Mathematical and General, **35** 929, 2002.

[104] R. F. Werner. *Quantum states with einstein-podolsky-rosen correlations admitting a hidden-variable model*. Physical Review A, **40** 4277–4281, October 1989.

[105] S. Ragy, M. Jarzyna, and R. Demkowicz-Dobrzański. *Compatibility in multiparameter quantum metrology*. Physical Review A, **94**, November 2016.

[106] S. Altenburg, S. Wölk, G. Tóth, and O. Gühne. *Optimized parameter estimation in the presence of collective phase noise*. Physical Review A, **94**, November 2016.

[107] M. Landini, M. Fattori, L. Pezzè, and A. Smerzi. *Phase-noise protection in quantum-enhanced differential interferometry*. New Journal of Physics, **16** 113074, November 2014.

[108] H. Häffner, W. Hänsel, C. Roos, J. Benhelm, M. Chwalla, T. Körber, U. Rapol, M. Riebe, P. Schmidt, C. Becher, O. Gühne, W. Dür, and R. Blatt. *Scalable multiparticle entanglement of trapped ions*. Nature, **438** 643–646, 2005.

[109] X.-C. Yao, T.-X. Wang, P. Xu, H. Lu, G.-S. Pan, X.-H. Bao, C.-Z. Peng, C.-Y. Lu, Y.-A. Chen, and J.-W. Pan. *Observation of eight-photon entanglement*. Nature Photonics, **6** 225–228, February 2012.